Revised April 2006

Development of experimental setups for earthquake engineering education

Final Report

Submitted to

National Program on Earthquake Engineering Education
MHRD, Government of India

by

C S Manohar and S Venkatesha

Department of Civil Engineering
Indian Institute of Science
Bangalore 560 012

Acknowledgements

This work has been supported by the National Programme on Earthquake Engineering Education, Ministry of Human Resources Development, Government of India. Mr Somayya Ammanagi and Mr M R Karthik served as project assistants in this project. The project has also been benefited by contributions from Mr Ashutosh Srivastava (BTech student from BHU) and Mr P Dharma Teja Reddy (BTech student from IIT Guwahati) who underwent summer training at IISc. Ashutosh worked on the problem of dynamics of liquid storage tanks under base motion and Dharma Teja designed the frames with a weak and/or soft ground floor. We have had useful discussions with Professors R N Iyengar, D Roy and B K Raghu Prasad during the course of this work. Finally, we would like to thank Professor Sudhir K Jain of IIT Kanpur who enthused us to take up this work.

The manuals were used as course material during the NPEEE short term course on "Earthquake engineering education through laboratory experiments" held at IISc during 16-21 January 2006. The course participants provided a detailed feedback on the manuals, based on which, the present revised version has been produced. Mr M R Karthik has contributed significantly in affecting the revisions.

CONTENTS

Summary

0.0 Background

The study of structural dynamics in civil engineering curriculum is commonly perceived to be a difficult exercise, more so in India, especially at the undergraduate level, and, even at the graduate level, because of the mathematical nature of the subject. This difficulty is felt, not only by the students, but also, by the teachers, who may not have had formal advanced level training in the subjects of earthquake engineering and structural dynamics. Thus, there exists a need to develop suitable teaching and learning aids to augment the classroom teaching of these subjects. One of the most effective ways to achieve this would be to develop a suite of simple experimental setups which would enable the study of basic issues related to vibration behavior, such as, damping, dynamic response magnification, resonance, structural vibration under support motions, normal modes, vibration isolation, vibration absorption, dynamics with soft and/or weak first/intermediate stories, role of structural ductility in resisting dynamic loads, liquefaction of soils under dynamic loads, seismic wave amplification through soil layer, and rocking and up throw of rigid objects under dynamic base motions. These setups would provide valuable physical insights into the basic vibration behavior of structures in general, and, structural dynamic responses under base motions, in particular. The work reported in this document contains the work done at the Department of Civil Engineering, Indian Institute of Science, as a part of a development project funded by the National Program on Earthquake Engineering Education, MHRD, Government of India.

0.1 Deliverables from the Project

1. Development and installation of one set of working models at IISc. This also includes details of measurement layout, data acquisition and post processing of acquired data.
2. Documents detailing the design of the experimental setups including details of material required and cost estimation. Requirements on transducers, data acquisition hardware and data processing software will also be provided.
3. Documents detailing the laboratory exercises to be carried out by students and the layout of laboratory reports to be submitted by students.
4. A set of additional notes for the instructors that contains details of experiments performed on setups developed at IISc and the development of simple to advanced analytical and experimental models for the vibrating systems developed. Questions on mutual agreement/disagreement between predictions of experimental and analytical models would also be discussed in this document.

0.2 List of experimental setups developed

1. Dynamics of a three storied building frame subjected to harmonic base motion. The frame possesses planar symmetry. Here the students learn the phenomenon of vibration of structures under base motions, occurrence of resonances in multi degree-of-freedom (dof) systems, normal modes and their visualization, and the nature of the

frequency response functions in mdof systems. The study also enables the students to appreciate the value of shear beam models in earthquake engineering.

2. Dynamics of a one-storied building frame with planar asymmetry subjected to harmonic base motions. The frame is configured such that it can be well modeled by a three dof system with two translations dofs and one rotation dof. The study enables the student to appreciate how horizontal base motion can induce torsional responses in frame structures.
3. This experiment is a variation on the experiments 1 and 2 listed above, in which the base motion is made to impinge on the structure at an arbitrary angle. The student would learn about the importance of angle of incidence of base motions in computing structural responses.
4. Dynamics of a secondary system mounted on the frame mentioned in experiment 1 with and without a vibration isolator. The student here would learn about the concept of displacement transmissibility and conditions under which, an isolation device would be effective.
5. Dynamics one span clamped beam subjected to harmonic motion and passive vibration control using the principle of dynamic vibration absorber.
6. Dynamics of one/two span simply supported beams subjected to harmonic excitations. The student would learn about modes of a two span simply supported beam and their relation to modes of single span simply supported and propped cantilever beams.
7. This experiment is a variation of experiments 1,2 and 3 mentioned above in which the frames would be subjected to nonharmonic periodic base motions. The student would learn about the use of Fourier series representations in analysis of structures under periodic base motions.
8. Dynamics of freestanding rigid objects subjected to base motions. Questions on minimum ground acceleration levels needed to initiate rocking and accelerations required for the toppling of such blocks are also addressed.
9. Dynamics of four-storied building frames with and without a soft first/intermediate story.
10. Setups that mimic seismic wave motion through soil layers, liquefaction in soil layers subjected to dynamic base motions and dynamic soil structure interactions.
11. Behavior of water tanks under base motions. The focus of the study is on understanding the nature of earthquake induced waves in rectangular water tanks with rigid walls.

0.3 Shake tables developed

As a part of this work we have developed three electro-mechanical shake tables. Two of these provide horizontal base motions. Both these tables have the capabilities for applying harmonic base motions with one of the tables having additional capability to apply nonharmonic but periodic base motions. Furthermore, these tables have the provision to mount the test structure at any desired angle with respect to the direction of applied base motion. The third table has capability to apply harmonic vertical base motions.

0.4 Format of the activities and the format of this report

In conducting each of the experiments listed above, the following activities are performed:

- The conduct of the experiment as we would expect the student to do.
- Development of approximate mathematical model for the system under study as we would expect the student to achieve.
- The conduct of the experiment using advanced techniques of experimental modal analysis, such as, impulse hammer tests for measurement of frequency response functions, to be followed by modal extraction using inverse procedures. This activity is limited to only those experiments in which the structure under study can be taken to behave linearly.
- Development of a sophisticated finite element models for the systems under study.

The first two activities are to be pursued by students who perform the experiments, while, results of the last two activities are provided to the laboratory instructors for gaining deeper understanding of the behavior of the structural systems under study.

Accordingly, this document is divided into three parts and the following is a summary of these parts.

Part I: Students manual:

This document is to be provided to the students prior to the conduct of the experiment. This describes the requisite preparation that the student needs to make before he/she conducts the experiment. It also provides the format for writing the report, recording the experimental observations, and lists a few questions that the students need to answer at the time of submitting the laboratory report.

Part II: Additional notes for the instructors:

This contains the outcome of detailed studies conducted on the setups developed at IISc. This typically includes the details of the conduct of the experiment as the student would do, more sophisticated experimental studies involving EMA and also outcome of detailed finite element analysis of the models developed. It is hoped that these details would provide deeper insights to the instructors on the behavior of models.

Part III: Inventory of items and cost estimation

The details of all the models, sensors, signal conditioners, data acquisition system, oscilloscope and shake tables that are used in conducting the experiments are provided. This Part also contains two commercial quotes from two vendors for the fabrication of all models and shake table needed for conducting the ten experiments.

0.5 Conclusions

1. The experimental setups developed are reasonably simple, cost-effective and, yet the same time, demonstrate a wide range of dynamic phenomena of relevance to earthquake engineering problems. This range covers issues such as damping, dynamic response magnification, resonance in multi-degree of freedom systems, structural vibration under support motions, normal modes, vibration isolation, vibration absorption, dynamics with soft first/intermediate stories, liquefaction of soils under dynamic loads, seismic wave amplification through soil layer, soil-structure interactions, and rocking and up throw of rigid objects under dynamic base motions.
2. Detailed documents suitable for use by students and instructors have been developed. The students' manual contains specification of experimental procedure, methods for developing simplified mathematical models, and preparation of laboratory report. A set of questions are also provided for each of the experiments with a hope that they might trigger interest in the mind of students to undertake further studies possibly leading to BE project work. The notes for the instructors' are aimed at providing insights into the system behavior and possible limitations in the setups developed. A detailed inventory of items and equipment and cost estimation has also been provided to facilitate educational institutes in India to fashion developments of setups similar to those described in this document.
3. Detailed studies using advanced tools such as experimental modal analysis and finite element modeling have also been conducted and documented on these setups with a view to understand the scope and limitations of the setups developed. These detailed studies have enabled the recommendation of appropriate simplified procedures that students can use in a laboratory class to conduct experiments as a part of a laboratory curriculum.
4. It is estimated that, for a laboratory equipped with accelerometers (at least two), signal conditioners (at least two channels), and the computer based data acquisition system, the cost of acquiring the models, shake tables and oscilloscope is estimated to be about Rs 2.3 lakhs. If the laboratory is not equipped as above, the cost is estimated to be about Rs 4.0 to 6.5 lakhs depending upon the specifications and make of signal conditioners, accelerometers and data acquisition system.

PART I

STUDENTS' MANUAL

Experiment 1

Dynamics of a three storied building frame subjected to harmonic base motion.

1.1 Background

We study in this experiment the behavior of a three storied building frame model subjected to harmonic base motions. This experiment also enables the understanding of occurrence of resonance phenomenon in simple multi-degree of freedom (MDOF) systems. The frame is rectangular in plan with stiffness and mass properties distributed uniformly in plan as well as in elevation. The frame is designed to facilitate the visualization of the first three mode shapes with bare eyes. Also, the frame is so configured such that a three degrees of freedom model would serve as a reasonable model, at least to a first approximation. See, for instance, the book by Paz (1984) for the details of mathematical modeling. A brief description of normal modes and their use in vibration analysis is also provided in Appendix A of this manual. The model shown in figure 1.1 can be thought of as a model for a building frame with three floors which suffers earthquake like base motions. The model however is an idealized demonstration of this phenomenon since the building can only be subjected to harmonic base motions. The frequency of the base motion can be varied by changing the RPM of the electric motor; it is also possible to vary the amplitude of the base motion by adjusting the stroke- this adjustment, however, requires somewhat involved manipulations. By changing the motor RPM it would be possible to set the frame into resonant motions, which would enable you to visualize the first three normal modes of the frame.

1.2 Experimental setup

Figures 1.1 and 1.5 show the experimental setup. This consists of four aluminum columns and four aluminum slabs each attached to the four columns at an interval of 400 mm. The entire structure assembly (figure 1.4) is placed on a shake table driven by an electric motor. The RPM of the motor can be varied to achieve harmonic base motions at different frequencies. In the set-up at IISc, the amplitude of base motion can also be varied but this aspect is not crucial in the conduct of the present experiment.

1.3 Mathematical model

The frame in figure 1.1 can be approximately modeled as a three degree of freedom shear beam as shown in figure 1.2a. Following the free body diagram shown in figure 1.2b, we can set up the equation of motion for the total displacement of the three masses as follows:

$$\begin{aligned} &M_1\ddot{x}_1 + C_1(\dot{x}_1 - \dot{y}) + C_2(\dot{x}_1 - \dot{x}_2) + K_1(x_1 - y) + K_2(x_1 - x_2) = 0 \\ &M_2\ddot{x}_2 + C_2(\dot{x}_2 - \dot{x}_1) + C_3(\dot{x}_2 - x_3) + K_2(x_2 - x_1) + K_3(x_2 - x_3) = 0 \\ &M_3\ddot{x}_3 + C_3(\dot{x}_3 - \dot{x}_2) + K_3(x_3 - x_2) = 0 \end{aligned} \qquad \ldots 1.1$$

This can be re-cast into the matrix form as

$$\begin{bmatrix} M_1 & 0 & 0 \\ 0 & M_2 & 0 \\ 0 & 0 & M_3 \end{bmatrix}\begin{Bmatrix} \ddot{x}_1 \\ \ddot{x}_2 \\ \ddot{x}_3 \end{Bmatrix}+\begin{bmatrix} C_1+C_2 & -C_2 & 0 \\ -C_2 & C_2+C_3 & -C_3 \\ 0 & -C_3 & C_3 \end{bmatrix}\begin{Bmatrix} \dot{x}_1 \\ \dot{x}_2 \\ \dot{x}_3 \end{Bmatrix}+\begin{bmatrix} K_1+K_2 & -K_2 & 0 \\ -K_2 & K_2+K_3 & -K_3 \\ 0 & -K_3 & K_3 \end{bmatrix}\begin{Bmatrix} x_1 \\ x_2 \\ x_3 \end{Bmatrix}=$$
$$\begin{bmatrix} C_1+C_2 & -C_2 & 0 \\ -C_2 & C_2+C_3 & -C_3 \\ 0 & -C_3 & C_3 \end{bmatrix}\begin{Bmatrix} 1 \\ 1 \\ 1 \end{Bmatrix}\dot{y}+\begin{bmatrix} K_1+K_2 & -K_2 & 0 \\ -K_2 & K_2+K_3 & -K_3 \\ 0 & -K_3 & K_3 \end{bmatrix}\begin{Bmatrix} 1 \\ 1 \\ 1 \end{Bmatrix}y \qquad \ldots 1.2$$

In a more compact form the equation reads

$$[M]\{\ddot{x}\}+[C]\{\dot{x}\}+[K]\{x\}=[C]\{\Gamma\}\dot{y}+[K]\{\Gamma\}y \qquad \ldots 1.3$$

In these equations a dot represents differentiation with respect to the time, $\{x\}=3\times 1$ vector of total displacement, *{y(t)}* is the applied harmonic base motion, *M,C* and *K*, are respectively the 3×3 structural mass, damping and stiffness matrices, $\{\Gamma\}=3\times 1$ vector of ones. In deriving this model it is assumed that slabs are very rigid with the columns supplying all the stiffness for the system. The inertia is manly contributed by the slabs; allowance can be made for taking into mass of the columns and screws at the joints. The undamped natural frequencies and modal vectors can be computed for the mathematical model by solving the eigenvalue problem $K\phi=\omega^2 M\phi$. These solutions, in turn, can be used to evaluate the forced response analysis by assuming that the undamped modal matrix would diagonalize the damping matrix also. Alternatively, solution to equation 1.3 can also be constructed by noting that, under harmonic excitations, the system would respond harmonically at the driving frequency as time becomes large. Accordingly, when $y(t)=Y\exp[i\omega t]$ we can take the solution to be of the form $x(t)=X(\omega)\exp[i\omega t]$ as $t\to\infty$. This leads to

$$\{X(\omega)\}=\left[-\omega^2 M+i\omega C+K\right]^{-1}[i\omega C+K]\{\Gamma\}Y \qquad \ldots 1.4$$

The matrix $\left[-\omega^2 M+i\omega C+K\right]$ can be thought of as the stiffness matrix of the structure that includes the effects of mass and damping and therefore, is referred to as the dynamic stiffness matrix. Refer to Appendix A for details on response analysis using normal mode expansion. Figure 1.3 shows typical plots of amplitude and phase spectra for a three-dof system.

The parameters of the above model can be arrived at by following the usual assumptions made in construction of shear beam models (Paz 1984). Thus one gets

$$\begin{aligned} &K_c=\frac{12EI}{L^3{}_A};\ I=\frac{B_A D_A^3}{12} \\ &K_1=K_2=K_3=4K_c \\ &M_1=M_2=M_s+4M_c+8M_{sc} \\ &M_3=M_s+(4*0.5*M_c)+8M_{sc} \end{aligned} \qquad \ldots 1.5$$

Here E= Young's modulus, I=moment of inertia, B_A=breadth of column cross-section, D_A=depth of the column cross-section, L_A= length of column, M_c=mass of individual column, and M_{sc}=mass of screws at the joints. The damping properties of the structure need to be established based on experimentation.

1.4.0 Experimental procedure

1.4.1 Instruments and sensors

Table 1.1 provides the details of instruments to be used in the experimental study.

1.4.2 Preliminary measurements

a) Collect the data pertaining to geometric and material properties of the vibrating system (tables 1.2 and 1.3). Parts of data in table 1.2 have to be obtained from the instructor/handbooks.
b) Using the three-degrees of freedom model, form the mass and stiffness matrices of the structure. Perform the eigenvalue analysis and determine the natural frequencies and modal matrix for the system.
c) Study the charts/manuals that accompany the sensors and the charge amplifiers and note down the sensor sensitivities, sensor mass and factors to convert the measured electrical signal into mechanical units; this depends upon the amplifier settings used- see table 1.4.
d) Run the electric motor at a few frequencies and measure the amplitude of the base motion. These amplitudes are expected to be identical and also would remain unchanged as the speed of the motor is varied. Therefore, in the subsequent experimentation, the base motion itself need not be measured.

1.4.3 Studies on 3-storyed shear beam model

e) Arrange the experimental setup as shown in figures 1.1 and 1.5. Note that the accelerometer needs to be placed on slab in such a way that displacement along x-direction is picked up.
f) Set the frame into free vibration by applying an initial displacement. This can be achieved by gently pulling the frame at about the top slab and releasing it. Observe the free vibration decay on the oscilloscope and record the results as per the format given in table 1.5. Evaluate the logarithmic decrement and hence the damping ratio. One model for the damping can be obtained by assuming that the damping ration so determined would remain constant for all the modes.
g) Run the base motion test on the frame at different values of motor RPM making sure that readings at resonant frequencies are not missed. For a given motor RPM, allow the frame to oscillate for a few seconds so that the frame reaches its steady state. At this stage measure the amplitude of the frame response by using time history of displacement response acquired on the oscilloscope and record the amplitude data as in table 1.6. Note that the frequency of driving and the frequency of structural response can be assumed to be equal and this can be

measured from the trace of displacement response on the oscilloscope. It may be noted that the test could be conducted even if only two channel measurements are possible, in which case, the above steps need to be repeated suitably.

h) The frequencies at which the structure undergoes resonance can be identified by observing the variation of response amplitudes as motor RPM is varied. At resonant conditions, in addition to noting the amplitude of slab oscillations, also note if the slabs are vibrating in phase or not. Based on this information the modal vectors for the first three modes could be established. Compare these mode shapes with the analytical mode shapes obtained in step (b).

i) Plot X_1, X_2 and X_3 versus f.

j) From the plots in the previous step estimate the modal damping either by half-power bandwidth method or by relating the peak amplitude to the modal damping (see Paz, 1984, for details).

k) Using the modal damping ratios obtained in steps (f) or (j) determine the C matrix using the relation $C = \left[\Phi^t\right]^{-1}[\Xi]\left[\Phi\right]^{-1}$ where Ξ is a diagonal matrix with entry on the n^{th} row being $2\eta_n\omega_n$. It can be shown that $\left[\Phi^t\right]^{-1} = M\Phi$ and $\left[\Phi\right]^{-1} = \Phi^t M$, and, therefore, one gets $C = M\Phi\Xi\Phi^t M$ (see Appendix A). Using this C matrix and equation 1.3, solve the mathematical model to determine analytically the amplitude of floor responses as a function of the driving frequency. Compare these analytical predictions with the measured frequency response functions.

1.5 Report submission

1. Document the experimental observations and the deductions as per the format given in tables 1.2-1.8.
2. Develop the experimental model as per the simplifications suggested in figure 1.2.
3. Document the plots of floor response amplitudes as a function of the driving frequency obtained using analysis as well as experiment. Discuss the qualitative features of these plots. Explain the mutual agreement/disagreement between theoretical and experimental results.
4. Respond to the following questions:

   - Often, in analysis, we determine the normal modes by ignoring the effect of damping. What happens in an experimental situation?
   - Can the present set-up be used to simulate earthquake like ground motions?
   - Can you think of alternative ways of simulating response of building frames to earthquake ground motions without actually having to apply support motions, that is, without the help of a shake table?
   - What are the limitations of the testing a structure on a shake table? Consider for instance, issues related to soil structure interaction, spatial variability of ground motions and the need for geometric scaling of structures.

1.6 Reference

1. M Paz, 1984, Structural dynamics, CBS Publishers, New Delhi.

Figure 1.1 Experimental setup for three-story shear building frame

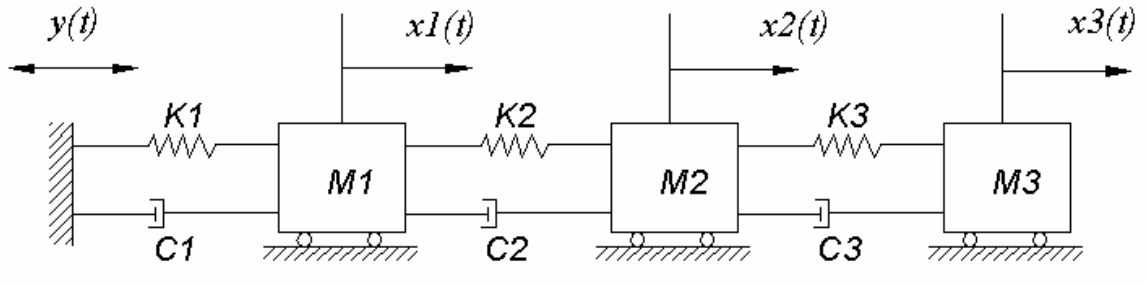

(a)

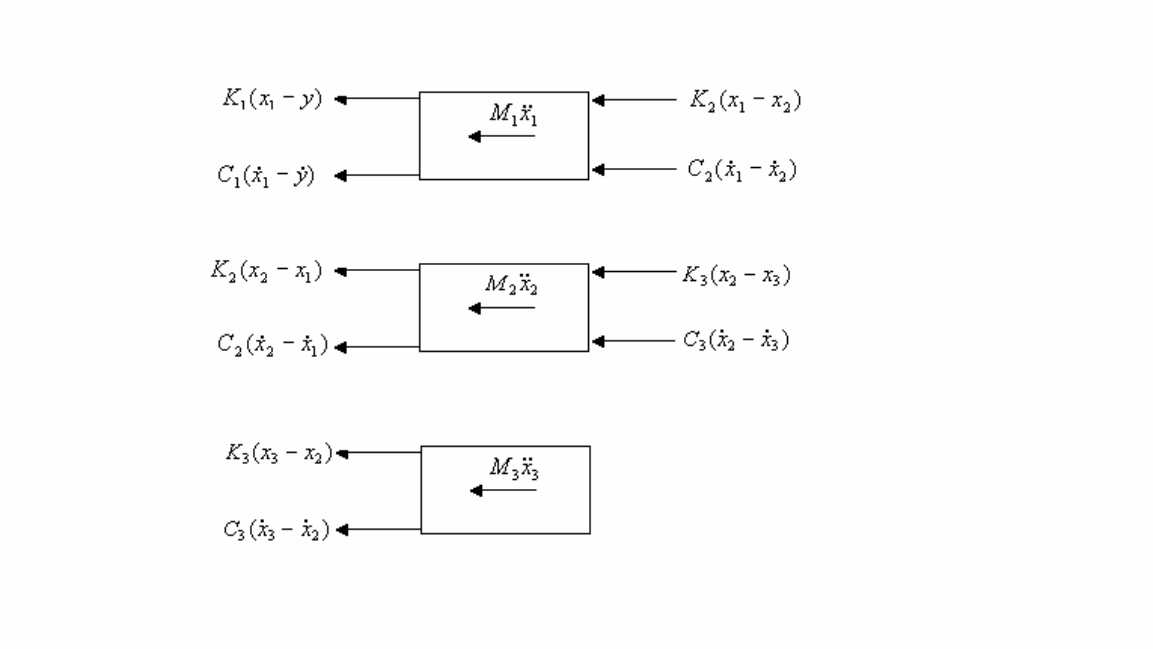

(b)

Figure 1.2 Multi mass-damper-spring model representation of a three-story shear building subjected to harmonic base motion, $y(t)=Ye^{i\omega t}$; (a) mathematical model (b) free body diagram

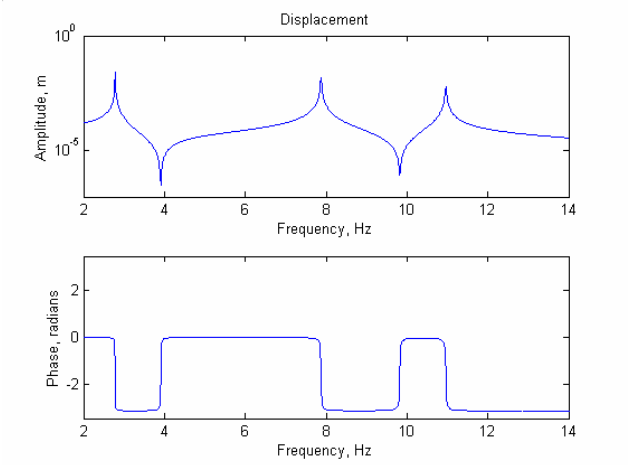

(a)

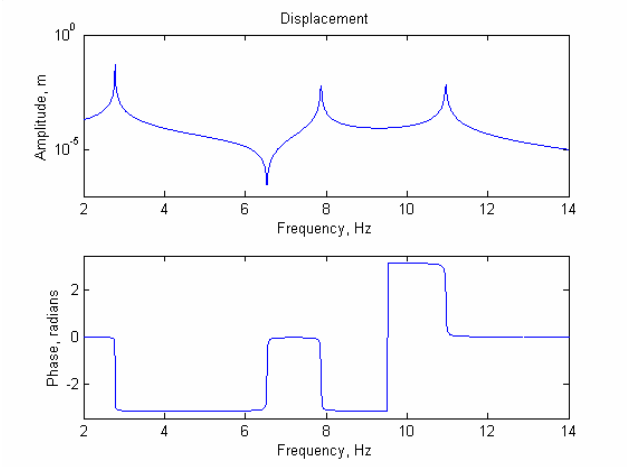

(b)

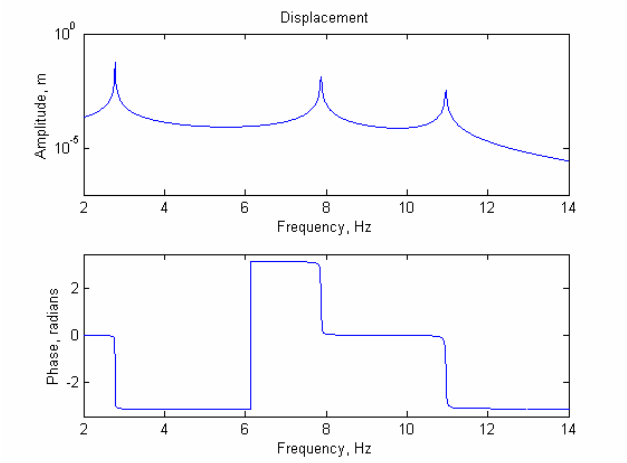

(c)

Figure 1.3 Amplitude and phase spectra of absolute responses of three-story building frame subjected to harmonic base motion; (a) response at I floor; (b) response at II floor; (c) response at III floor

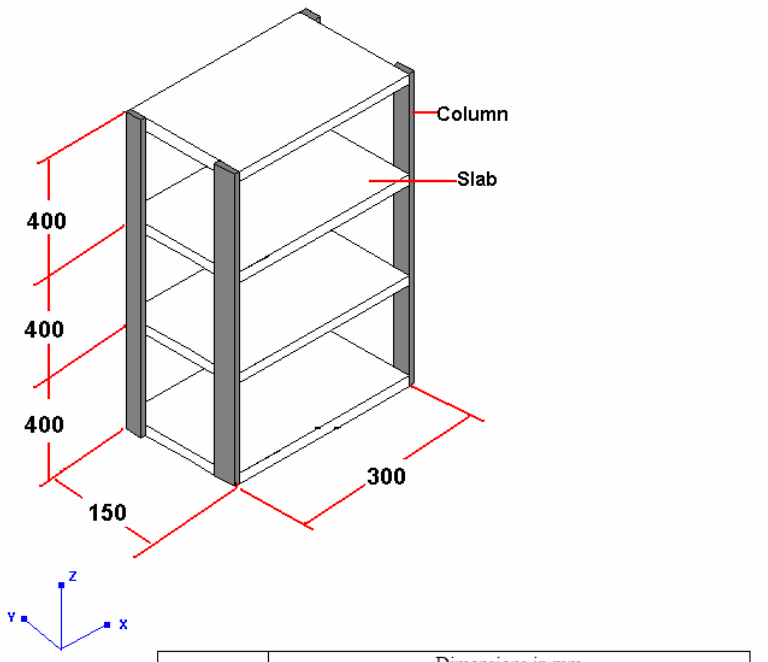

Part	Dimensions in mm		
	Depth (D)	Width (B)	Length (L)
Column	D_A =3.00	B_A =25.11	L_A = **400.00**
Slab	D_B =12.70	B_B =150.00	L_B =300.00

Figure1.4 Three-story shear building model used in experiment

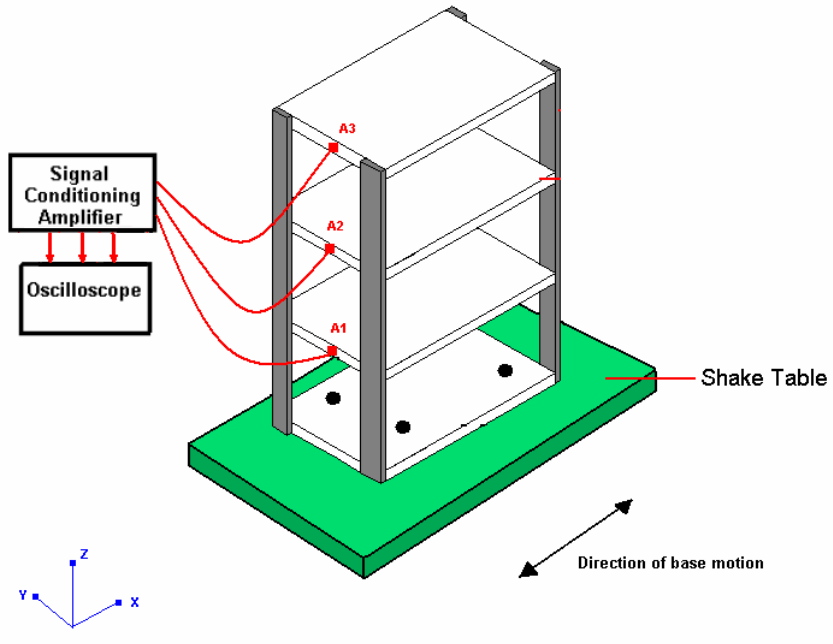

Figure 1.5. Setup for studies on three-story shear building frame

Table 1.1 Equipments used in free vibration and forced vibration test of three-story shear building frame

No.	Equipments	Quantity
1	Oscilloscope	1
2	Accelerometers	3
3	Transducers conditioning amplifiers	1
4	Shake table	1

Table 1.2 Physical properties of parts of the structure

No.	Part	Material	Mass kg	Material Properties	
				Young's Modulus (E) N/m^2	Mass density (ρ) kg/m^3
1	Column	Aluminum	M_c =		
2	Slab	Aluminum	$M_{s=}$		
3	Allen screw, M8	Steel	M_{sc}=	-	-

Table 1.3 Geometric data of the structure

No.	Part	Dimensions in mm		
		Depth (D)	Width (B)	Length (L)
1	Column	D_A =	B_A =	L_A =
2	Slab	D_B =	B_B =	L_B =

Table 1.4 Details of the sensors used; *CF*: conversion factor

No.	Sensor	Sensitivity, S		*CF*	Mass kg
		pC/ms^{-2}	pC/g		
1					
2					
3					

Table 1.5 Free vibration test data on three-story shear building frame

No.	Quantity	Notation	Observations
1	Amplitude of 0th peak	A_0	
2	Amplitude of nth peak	A_n	
3	Number of cycles	n	
4	Logarithmic decrement	δ	
5	Damping ratio	ζ	

Table 1.6.1 Base motion test data on three-story shear building frame

S.No.	Frequency, f (Hz)	Frequency $\omega=2\pi f$ (rad/s)	Amplitude σ_1 rms (V)	Amplitude σ_2 rms (V)	Amplitude σ_3 rms (V)	Displacement Amplitude $X_1 = \sqrt{2}\ (CF)\ \sigma_1$ (m)	Displacement Amplitude $X_2 = \sqrt{2}\ (CF)\ \sigma_2$ (m)	Displacement Amplitude $X_3 = \sqrt{2}\ (CF)\ \sigma_3$ (m)
1								
2								
3								
4								
5								
6								
7								
8								
9								
10								
11								
12								
13								
14								
15								
16								
17								
18								
19								
20								
21								
22								
23								
24								
25								

Table 1.6.2 Base motion test data on three-story shear building frame; measurement made at first floor

S.No.	Frequency, f (Hz)	Frequency $\omega=2\pi f$ (rad/s)	Amplitude σ_1 rms (mV)	Displacement Amplitude $X_1=\sqrt{2}\ (CF)\ \sigma_1$ (m)
1				
2				
3				
4				
5				
6				
7				
8				
9				
10				
11				
12				
13				
14				
15				
16				
17				
18				
19				
20				
21				
22				
23				
24				
25				

Table 1.6.3 Base motion test data on three-story shear building frame; measurement made at the second floor

S.No.	Frequency, f (Hz)	Frequency $\omega=2\pi f$ (rad/s)	Amplitude σ_2 rms (mV)	Displacement Amplitude $X_2=\sqrt{2}\ (CF)\ \sigma_2$ (m)
1				
2				
3				
4				
5				
6				
7				
8				
9				
10				
11				
12				
13				
14				
15				
16				
17				
18				
19				
20				
21				
22				
23				
24				
25				

Table 1.6.4 Base motion test data on three-story shear building frame; measurement made at the third floor

S.No.	Frequency, f (Hz)	Frequency $\omega=2\pi f$ (rad/s)	Amplitude σ_3 rms (mV)	Displacement Amplitude $X_3=\sqrt{2}\ (CF)\ \sigma_3$ (m)
1				
2				
3				
4				
5				
6				
7				
8				
9				
10				
11				
12				
13				
14				
15				
16				
17				
18				
19				
20				
21				
22				
23				
24				
25				

Note: The format in Table 1.6.1 can be used if all the three floor responses are measured simultaneously. If only one measurement at a time is possible (due to lack of availability of adequate number of sensors, signal conditioners or data acquisition channels), then the experiment need to be run repeatedly suitable number of times. In this case, the formats given in Tables 1.6.2 to 1.6.4 could be used for recording the observations. In case the tests are run repeatedly, it may not be possible to maintain identical steps in incrementing the driving frequency because of lack of perfect control on specifying driving frequency.

Table 1.7 Estimate of the natural frequencies of the three-story shear building frame

Mode No.	Natural frequencies in Hz	
	3-DOF Model	Experiment
1		
2		
3		

Table 1.8 Estimate of the mode shapes of the three-story shear building frame

Mode shapes					
3-DOF Model			Experiment		
I mode	II mode	III mode	I mode	II mode	III mode

Experiment 2

Dynamics of a one-storied building frame with planar asymmetry subjected to harmonic base motions.

2.1 Background

The earthquake response of building frames that are asymmetric in plan is characterized by coupling between translational and torsional degrees of freedom (dofs). Here the asymmetry could arise due to unsymmetrical distribution of mass, stiffness, damping and/or strength characteristics. Such structures, when subjected to horizontal support motions, display not only bending oscillations, but also, undergo torsional vibrations. The present experiment aims to demonstrate this phenomenon. The structure under study is a model for a single bay, single story-building frame (figures 2.1 and 2.2) that consists of a relatively rigid rectangular steel slab supported at the corners on three aluminum and one steel columns. Thus, in plan, the structure is asymmetric with the steel column possessing higher lateral stiffness than the other three aluminum columns. Apart from the distribution of stiffness, the mass and damping characteristics offered by the steel and aluminum columns would also contribute to the planar asymmetry of the structure. Since the slab is much stiffer than the columns, under the action of dynamic base motions, it is reasonable to assume that the slab would displace in its own plane. In the experimental setup the frame is mounted on a table that is driven by an electric motor (figure 2.1). This mount is designed in such a way that the angle of incidence of the base motion on to the frame can be varied over 0 to $\pi/2$. Thus, under the action of base motion, the slab displaces in x,y, and θ directions; see figure 2.3. This implies that the frame not only bends in x and y directions, but also, would twist about the z-axis. The objectives of the present experiment are:

(a) to understand the dynamics of the frame as the frequency of base motion is varied across the resonant frequencies of the frame, and
(b) to understand the influence of the angle of incidence of the base motion on the dynamic response of the frame.

2.2 Experimental setup

Figure 2.1 and 2.2 show the building frame mounted on the electric motor driven shake table. By varying the speed of the motor the frequency of the harmonic base motion could be varied. Also, the mounting device is capable of swiveling about the vertical axis, which would permit us to mount the frame at different angles relative to the axis of the table motion. Figure 2.4 shows a typical set up detailing the sensor placement for the purpose of conducting the experiment. The transducers A_1 and A_5 measure translation along x and y directions; A_1, A_2 and A_3 can be used to measure the angle θ; A_4 and A_6 measure the base motions in x and y directions respectively. Although this figure shows six displacements as being measured simultaneously, in the actual conduct of the experiment, however, this many measurement channels might not be needed. Depending

upon the availability of the number of transducers and signal conditioners, measurements on displacements in *x, y* and θ directions could be carried out is separate runs of the experiment. It may also be noted that the set up permits the measurement of the angle of incidence of the base motion onto the frame; also, the amplitude of the table motion could be held constant, while the frequency of excitation could be varied by changing the RPM of the electric motor. Thus it would not be absolutely essential to keep measuring the base motion during the entire process of experimentation. One can identify the amplitude of the base motion at the outset by measuring this quantity for a few selected RPMs. During the conduct of the experiment, when the base motion is not actually measured, the frequency of excitation could be inferred from the frequency of response of the slab. As is well know, the frequency of harmonic base motion and linear system response in the steady state are equal. Also, to measure the rotation of the slab about the *z*-axis, any two measurements among A_1, A_2 and A_3 could be used.

2.3 Mathematical model

To a first approximation, the building frame can be modeled as a three-dof system as shown in figure 2.5. The origin of reference is taken to coincide with the mass center of the frame. Figure 2.5 shows the idealized physical model in which the slab is assumed to be rigid and it is taken to displace in its own plane with two translations and one rotation. The four columns are replaced by a set of springs and dampers. Half of the mass of columns could be taken to participate in offering inertia. Figure 2.6 shows the free body diagram with all the forces acting on the slab explicitly displayed. The equation of motion can thus be deduced as

$$
\begin{aligned}
&m\ddot{x} + k_1(x - y_1\theta - x_g) + c_1(\dot{x} - y_1\dot{\theta} - \dot{x}_g) + k_4(x - y_1\theta - x_g) + c_4(\dot{x} - y_1\dot{\theta} - \dot{x}_g) + \\
&k_8(x + y_2\theta - x_g) + c_8(\dot{x} + y_2\dot{\theta} - \dot{x}_g) + k_5(x + y_2\theta - x_g) + c_5(\dot{x} + y_2\dot{\theta} - \dot{x}_g) = 0 \\
&m\ddot{y} + k_2(y + x_1\theta - y_g) + c_2(\dot{y} + x_1\dot{\theta} - \dot{y}_g) + k_7(y + x_1\theta - y_g) + c_7(\dot{y} + x_1\dot{\theta} - \dot{y}_g) + \\
&k_3(y - x_2\theta - y_g) + c_3(\dot{y} - x_2\dot{\theta} - \dot{y}_g) + k_6(y - x_2\theta - y_g) + c_6(\dot{y} - x_2\dot{\theta} - \dot{y}_g) = 0 \\
&I\ddot{\theta} + x_1\left[k_2(y + x_1\theta - y_g) + c_2(\dot{y} + x_1\dot{\theta} - \dot{y}_g) + k_7(y + x_1\theta - y_g) + c_7(\dot{y} + x_1\dot{\theta} - \dot{y}_g)\right] - \\
&x_2\left[k_3(y - x_2\theta - y_g) + c_3(\dot{y} - x_2\dot{\theta} - \dot{y}_g) + k_6(y - x_2\theta - y_g) + c_6(\dot{y} - x_2\dot{\theta} - \dot{y}_g)\right] + \\
&y_2\left[k_8(x + y_2\theta - x_g) + c_8(\dot{x} + y_2\dot{\theta} - \dot{x}_g) + k_5(x + y_2\theta - x_g) + c_5(\dot{x} + y_2\dot{\theta} - \dot{x}_g)\right] - \\
&y_1\left[k_1(x - y_1\theta - x_g) + c_1(\dot{x} - y_1\dot{\theta} - \dot{x}_g) + k_4(x - y_1\theta - x_g) + c_4(\dot{x} - y_1\dot{\theta} - \dot{x}_g)\right] = 0
\end{aligned}
\qquad \ldots(2.1)
$$

This equation can be recast in the matrix form as

$$M\ddot{u} + C\dot{u} + Ku = f(t) \qquad \ldots(2.2)$$

Here $u = \{x\, y\, \theta\}^t$ and the mass, damping and stiffness matrices are given, respectively, by

$$M = \begin{bmatrix} m & 0 & 0 \\ 0 & m & 0 \\ 0 & 0 & I \end{bmatrix}$$

$$K = \begin{bmatrix} k_1+k_4+k_8+k_5 & 0 & y_2(k_5+k_8)-y_1(k_1+k_4) \\ 0 & k_2+k_3+k_6+k_7 & x_1(k_2+k_7)-x_2(k_3+k_6) \\ y_2(k_5+k_8)-y_1(k_1+k_4) & x_1(k_2+k_7)-x_2(k_3+k_6) & x_1^2(k_2+k_7)+x_2^2(k_3+k_6)+y_1^2(k_1+k_4)+y_2^2(k_8+k_5) \end{bmatrix}$$

$$C = \begin{bmatrix} c_1+c_4+c_8+c_5 & 0 & y_2(c_5+c_8)-y_1(c_1+c_4) \\ 0 & c_2+c_3+c_6+c_7 & x_1(c_2+c_7)-x_2(c_3+c_6) \\ y_2(c_5+c_8)-y_1(c_1+c_4) & x_1(c_2+c_7)-x_2(c_3+c_6) & x_1^2(c_2+c_7)+x_2^2(c_3+c_6)+y_1^2(c_1+c_4)+y_2^2(c_8+c_5) \end{bmatrix}$$

...(2.3)

Furthermore, the forcing vector *f(t)* can be shown to be given by

$$f(t) = \begin{Bmatrix} x_g(k_1+k_4+k_5+k_8)+\dot{x}_g(c_1+c_4+c_5+c_8) \\ y_g(k_2+k_3+k_6+k_7)+\dot{y}_g(c_2+c_3+c_6+c_7) \\ x_g[(k_5+k_8)y_2-(k_1+k_4)y_1]+y_g[(k_2+k_7)x_1-(k_3+k_6)x_2]+\dot{x}_g[(c_5+c_8)y_2-(c_1+c_4)y_1]+\dot{y}_g[(c_2+c_7)x_1-(c_3+c_6)x_2] \end{Bmatrix} \quad ...(2.4)$$

The parameters appearing in the above model are evaluated as follows:

Location of mass center (see figure 2.7)

$$\bar{x} = \frac{m_S\frac{b_s}{2}+(m_1+m_4)\left(\frac{b_s-b_{s1}}{2}\right)+(m_2+m_3)\left(\frac{b_s+b_{s1}}{2}\right)}{\rho_s t b_s d_s+m_1+m_2+m_3+m_4}$$

$$\bar{y} = \frac{m_S\frac{d_s}{2}+(m_4+m_3)\left(\frac{d_s-d_{s1}}{2}\right)+(m_1+m_2)\left(\frac{d_s+d_{s1}}{2}\right)}{\rho_s t b_s d_s+m_1+m_2+m_3+m_4}$$

$$m_1 = m_2 = m_3 = A_a\rho_a(h/2)$$

$$m_4 = A_s\rho_s(h/2), \quad m_S = \rho_s t b_s d_s \qquad \ldots(2.5)$$

Here ρ_s=mass density of steel, ρ_a= mass density of aluminum, A_a, A_s=areas of cross section of aluminum and steel columns respectively, h=height of the columns; refer figure 2.7 for the meaning of other symbols appearing in the above equation.

Stiffness coefficients

$$k_1 = k_2 = k_3 = \frac{12E_aI_a}{h^3};\ k_4 = \frac{12E_sI_s}{h^3} \qquad \ldots(2.6)$$

It may be noted that we can add the following terms to the stiffness coefficient k_{33}

$$k^* = \frac{3G_{al}J_{al}}{h} + \frac{G_sJ_s}{h};\ J_{al} = \frac{\pi D_{al}^4}{32}\ J_s = \frac{\pi D_s^4}{32} \qquad \ldots(2.7)$$

These terms represent the contribution to the torsional stiffness of the frame by shear rigidity of the individual columns. Here *GJ*=shear modulus, *D*=diameter and the subscripts *al* and *s*, respectively, denote aluminum and steel.

Elements of mass matrix (see figure 2.8)

$$m = m_{slab} + m_{columns} = \rho_s t b_s d_s + 3\frac{\rho_a A_a h}{2} + \frac{\rho_s A_s h}{2}$$

$$I = \frac{\rho_s t b_s d_s}{12}\left(b_s^2 + d_s^2\right) + \rho_s t b_s d_s\left[\left(\bar{x} - \frac{b_s}{2}\right)^2 + \left(\bar{y} - \frac{d_s}{2}\right)^2\right] + \qquad \ldots(2.8)$$

$$\frac{\rho_a A_a h}{2}(x_1^2 + y_1^2 + x_2^2 + y_1^2 + x_1^2 + y_2^2) + \frac{\rho_s A_s h}{2}\left(x_2^2 + y_2^2\right) + 3\frac{\rho_a A_a h}{2}\left(\frac{r_{al}}{2}\right)^2 + \frac{\rho_s A_s h}{2}\left(\frac{r_s}{2}\right)^2$$

Here r_{al}, r_s= radii of the aluminum and steel columns respectively. It may be noted that the mass moment of inertia *I* is being computed with respect to the mass center of the system. The first term in the expression for I above denotes the mass moment of inertia of the steel slab with respect to its own center computed using the expression

$$4\int_0^{b_s/s}\int_0^{d_s/2} \rho_s t(\alpha^2 + \beta^2)\,d\alpha d\beta = \frac{\rho_s t b_s d_s}{12}\left(b_s^2 + d_s^2\right) \qquad \ldots(2.9)$$

As has been mentioned already, the experimental setup permits the mounting of the building frame at different angles. Thus if α is the angle of incidence of the base motion with respect to the horizontal reference axis of the building frame model (see figure 2.3), and, if $\Delta(t)$ is the applied base motion along the axis of the table motion, we get

$$x_g(t) = \Delta(t)\cos\alpha \quad y_g(t) = \Delta(t)\sin\alpha \qquad \ldots(2.10)$$

The elements of damping matrix can be computed, if need be, based on the measurement of modal damping ratios.

Once the elements of the structural matrices are computed, the governing equation of motion can be solved either by using the modal expansion technique or by inverting the dynamic stiffness matrix (see Appendix A). Since the base excitations are harmonic, the method based on inversion of dynamic stiffness matrix leads to steady state response given by

$$u(t) = U(\omega)\exp(i\omega t)$$
$$U(\omega) = \left[-\omega^2 M + i\omega C + K\right]^{-1} F(\omega) \qquad \ldots(2.11)$$

Figure 2.9 shows plots of typical amplitude and phase spectra of floor displacements for the problem on hand.

2.4.0 Experimental procedure

2.4.1 Instruments and sensors

Table 2.1 provides the details of instruments to be used in the experimental study.

2.4.2 Preliminary measurements

1. Collect the data pertaining to geometric and material properties of the vibrating system (tables 2.2 and 2.3). Parts of data in table 2.2 have to be obtained from instructor/handbooks.
2. Locate the mass center.
3. Using the three-degrees of freedom model, form the mass and stiffness matrices of the structure. Perform the eigenvalue analysis and determine the natural frequencies and modal matrix for the system.
4. Study the charts/manuals that accompany the sensors and the charge amplifiers and note the sensor sensitivities, sensor mass and factors to convert the measured electrical signal into mechanical units; this, in turn, depends upon the amplifier settings used; see table 2.4.
5. Run the electric motor at a few frequencies and measure the amplitude of the base motion. These amplitudes are expected to be identical and also would remain unchanged as the speed of the motor is varied. Therefore, in the subsequent experimentation, the base motion itself need not be measured.

2.4.3 Studies with fixed angle of incidence of base motion ($\alpha=0$)

1. Arrange the experimental setup as shown in figure 2.4. Note that the accelerometer needs to be placed on slab in such a way that displacement along *x*-direction is picked up. It is advantageous to mount the sensor along axes passing through the mass center; this however is not essential.
2. Run the base motion test on the frame at different values of motor RPM making sure that readings at resonant frequencies are not missed. For a given motor RPM, allow the frame to oscillate for a few seconds so that the frame

reaches its steady state. At this stage measure the amplitude of the frame response by using time history of displacement response acquired on the oscilloscope and record the amplitude data as in table 2.5. Note that the frequency of driving and the frequency of structural response can be assumed to be equal and this can be measured from the trace of displacement response on the oscilloscope. It may be noted that the test could be conducted even if only two channel measurements are possible; in which case, the above steps need to be repeated suitably.

3. The frequencies at which the structure undergoes resonance can be identified by observing the variation of response amplitudes as motor RPM is varied. At resonant conditions, note the amplitude of slab oscillations. Record the natural frequencies obtained from the theory and experiments as in Table 2.6.
4. Plot the response amplitudes along *x*-axis and the rotation as a function of the driving frequency.
5. From the plots in the previous step estimate the modal damping either by half-power bandwidth method or by relating the peak amplitude to the modal damping (see the book M Paz, 1984, Structural dynamics, CBS Publisher, New Delhi, for details).
6. Using the modal damping ratios obtained in the previous step determine the C matrix using the relation $C = \left[\Phi^t\right]^{-1}[\Xi]\left[\Phi\right]^{-1}$ where Ξ is a diagonal matrix with entry on the nth row being $2\eta_n\omega_n$. It can be shown that $\left[\Phi^t\right]^{-1} = M\Phi$ and $\left[\Phi\right]^{-1} = \Phi^t M$, and, therefore, one gets $C = M\Phi\Xi\Phi^t M$ (see Appendix A). Using this C matrix and equation 2.2, solve the mathematical model to determine analytically the amplitude of floor responses as a function of the driving frequency. Compare these analytical predictions with the measured frequency response functions.

2.4.4 Studies with varying angle of incidence of base motion

Here we hold the motor RPM fixed and vary the angle of incidence of the base motion by mounting the frame on the table at a desired angle in the range of 0 to π/2. Table 2.7 provides the format for recording the data. Theoretical predictions for this situation could also be obtained by solving equation 2.2 with $x_g(t) = \Delta(t)\cos\alpha$ & $y_g(t) = \Delta(t)\sin\alpha$.

2.5 Report submission

1. Document the experimental observations as per format given in tables 2.2-2.7.
2. Develop the experimental model as per the simplifications suggested in figures 2.4 and 2.5.
3. For $\alpha=0$, document the plots of floor response amplitudes as a function of the driving frequency obtained using analysis as well as experiment. Discuss the qualitative features of these plots. Explain the mutual agreement/disagreement between theoretical and experimental results.

4. For a few fixed values of driving frequency vary α and plot the system response as function of α. Obtain the corresponding results from the analysis of the mathematical model. Compare the theoretical and experimental predictions on system behavior and discuss the reasons for mutual agreement/disagreement.
5. Respond to the following questions:

    - Discuss the structure of equation of motion *vis-à-vis* the choice of the coordinate system chosen for setting up the equation of motion. Just as we have located the mass center we can also locate the elastic center and the damping center. Carry out this exercise. What would happen if we were to choose coordinate system with these alternative points as origins? Would the natural frequencies, mode shapes and modal damping ratios change if we change the coordinate system?
    - Derive terms in equations 2.6,2.7 and 2.8.
    - If we replace the steel column by a aluminum column, identical to the other three columns, what changes would you expect in the dynamic behavior of the frame?
    - Because of the torsional oscillation of the frame, what type of stresses do you expect in the columns?
    - Provide five examples of structures in practice that possess asymmetric plan.

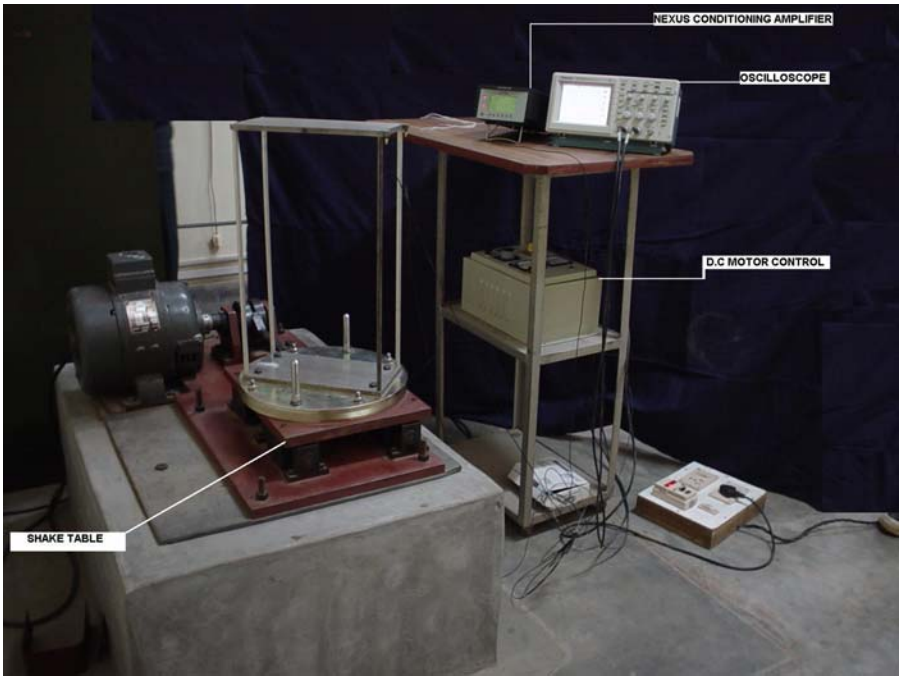

Figure 2.1 Experimental setup for one-story building frame. Notice that the building frame can be mounted on the base plate at any desired angle relative to the axis of the table motion.

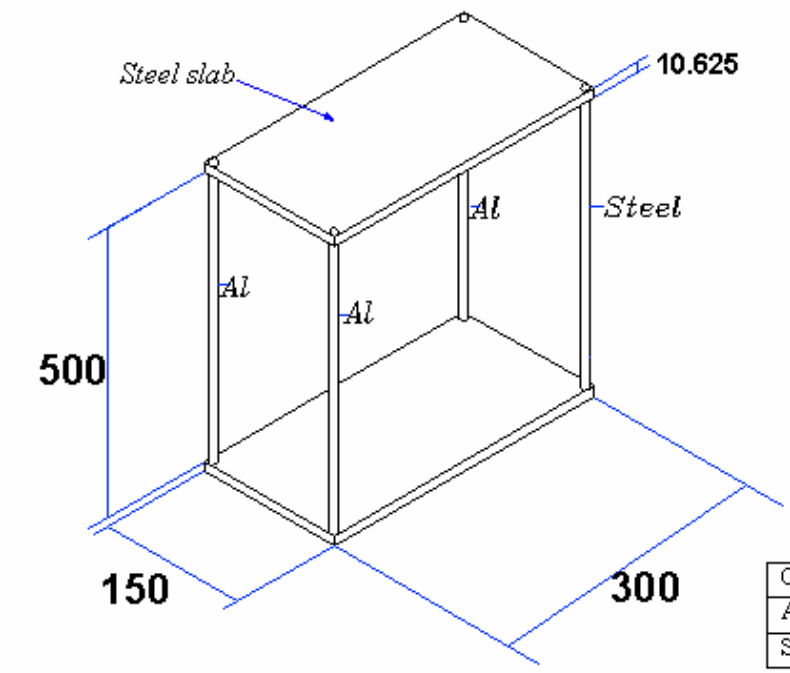

Columns	Diameter (mm)
Aluminum	10.13
Steel	9.958

All dimensions in mm

Figure 2.2 Details of the frame made up of a steel slab supported on one steel column and three aluminum columns.

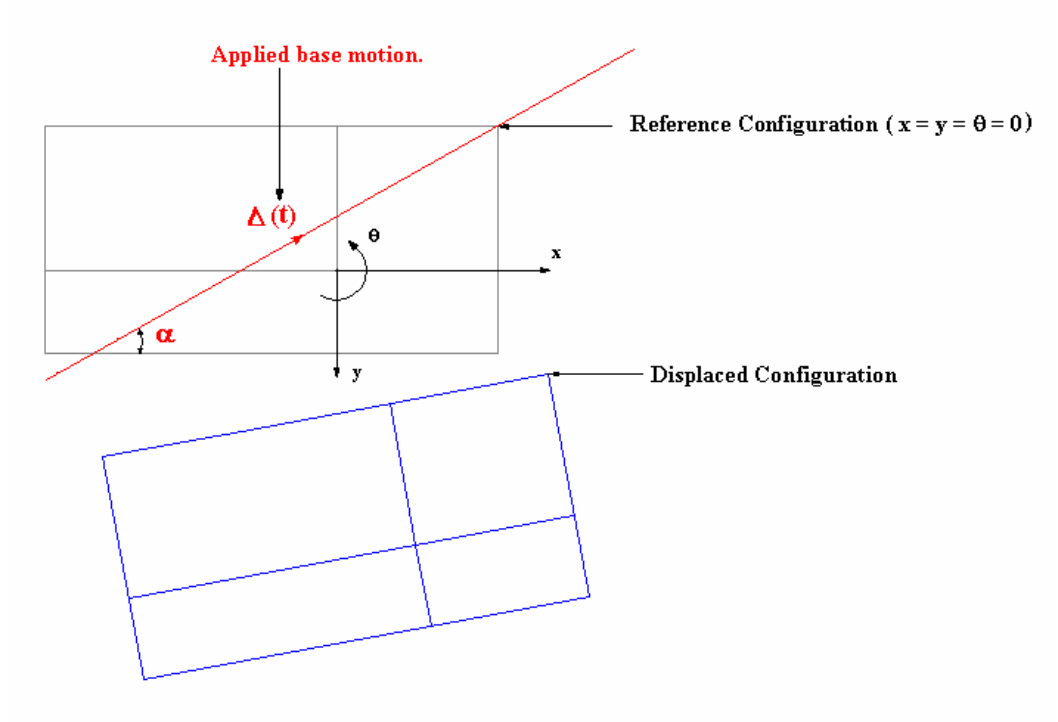

Figure 2.3 Displacement of the steel slab in its own plane. The origin here is taken to coincide with the mass center of the structure.

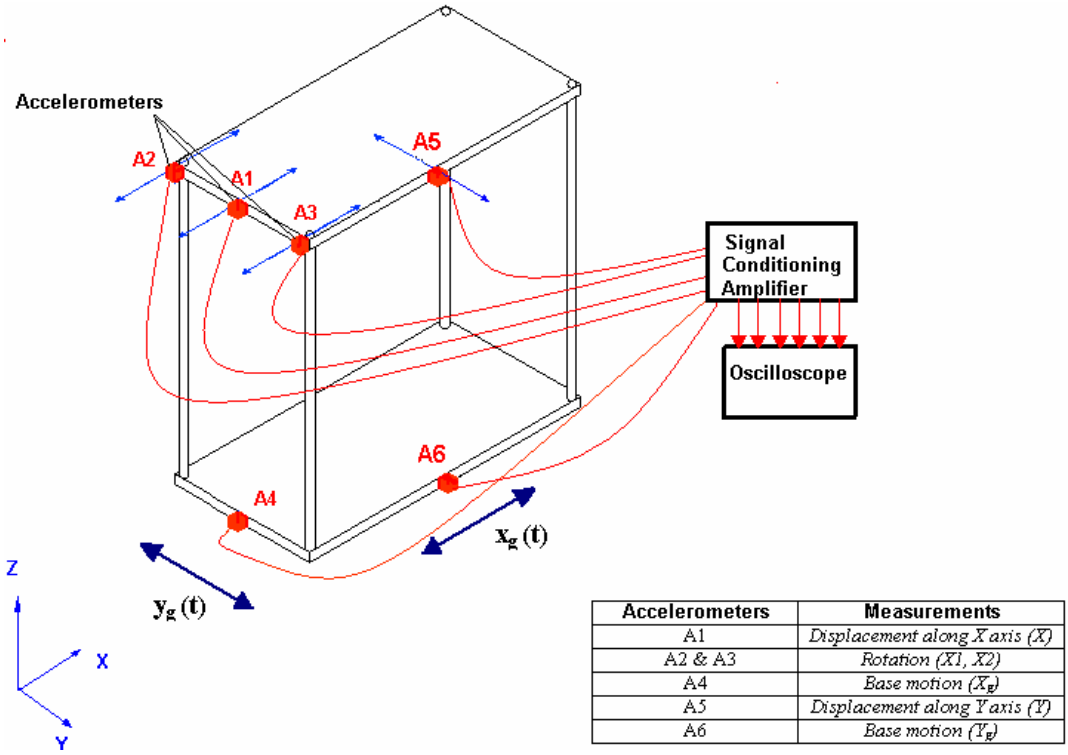

Accelerometers	Measurements
A1	*Displacement along X axis (X)*
A2 & A3	*Rotation (X1, X2)*
A4	*Base motion (X_g)*
A5	*Displacement along Y axis (Y)*
A6	*Base motion (Y_g)*

Figure 2.4 Setup for studies on one-story building frame

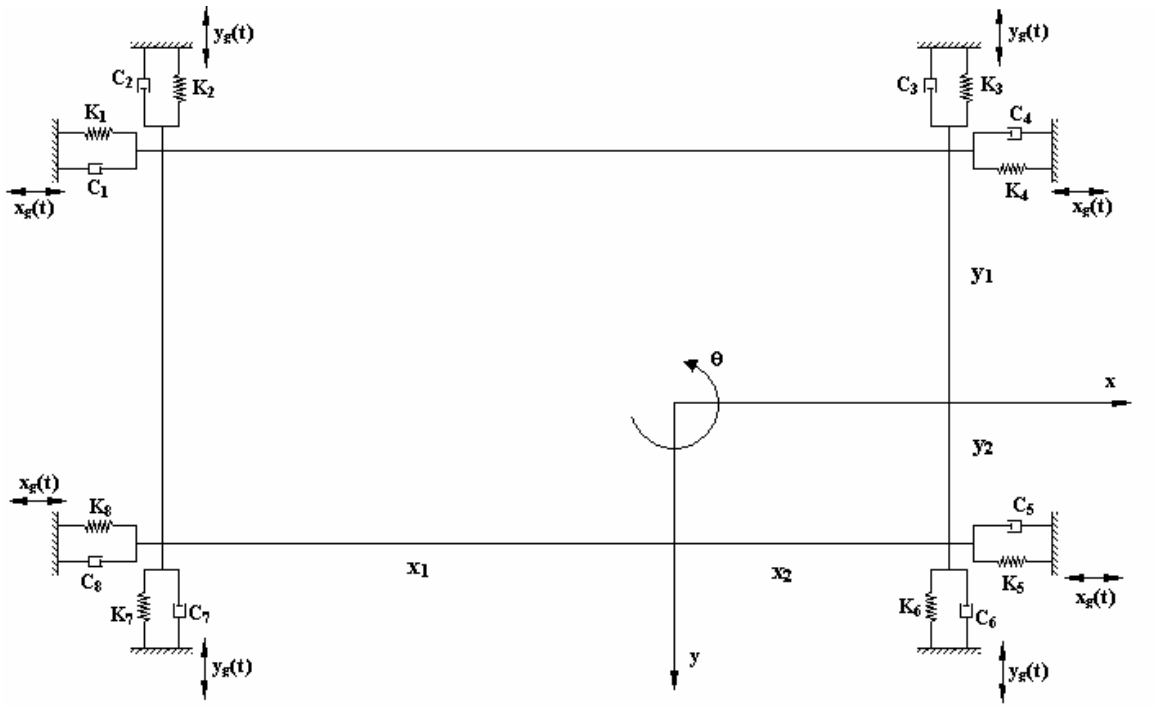

Figure 2.5 Rigid mass-damper-spring model representation of the frame subjected to harmonic base motions $x_g(t)$ and $y_g(t)$.

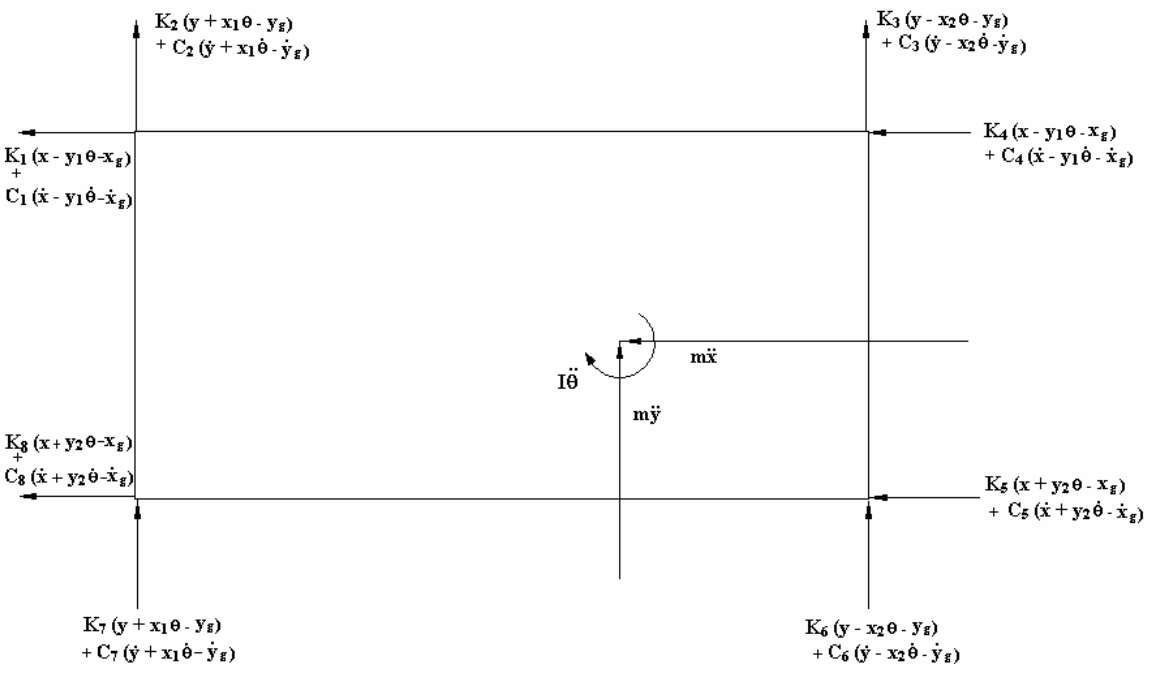

Figure 2.6 Free body diagram showing the forces acting on the frame.

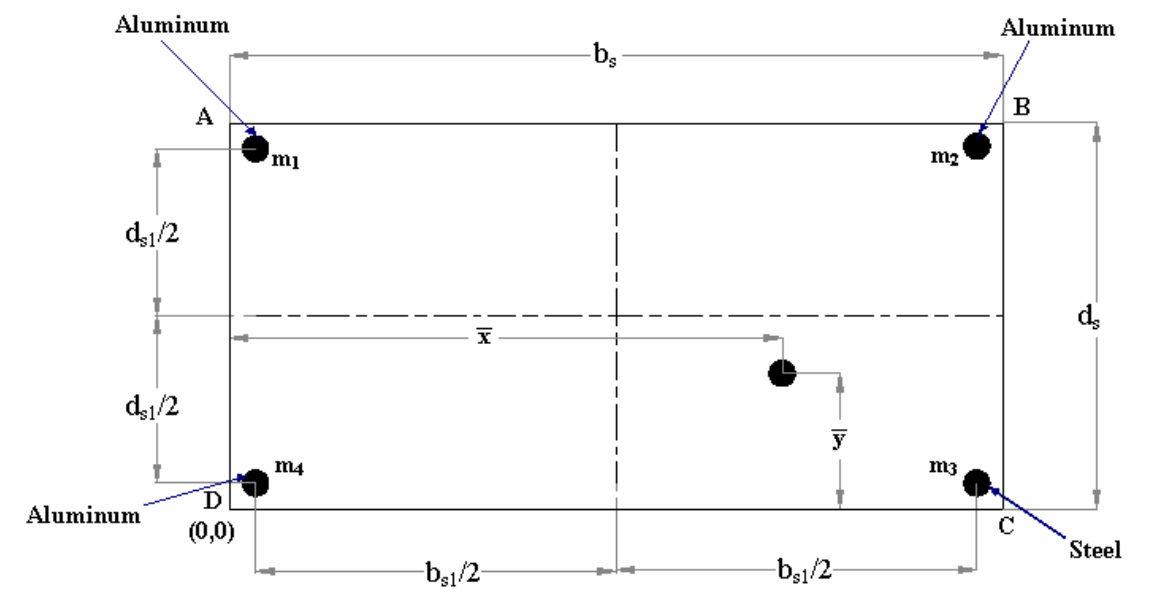

Figure 2.7 Location of the mass center.

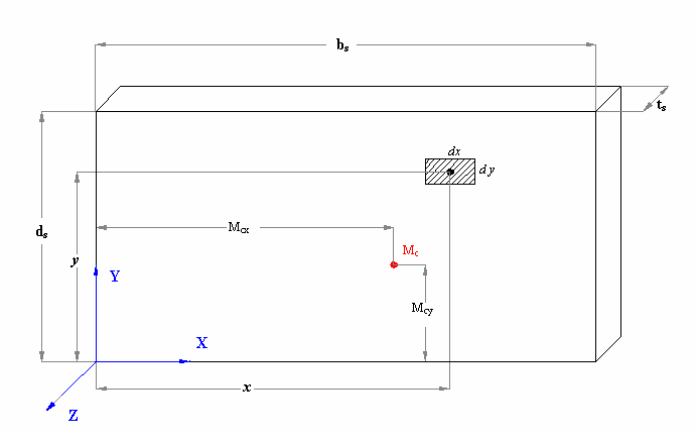

(a)

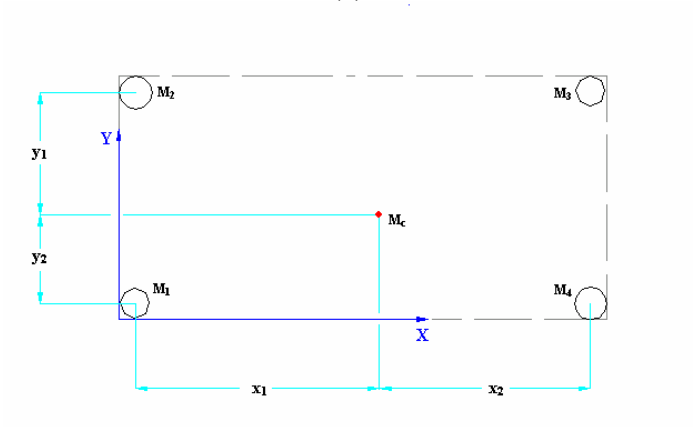

(b)

Figure 2.8 Illustrative sketch for the computation of mass moment of inertia I. (a) contribution from the slab; (b) contributions from the four columns.

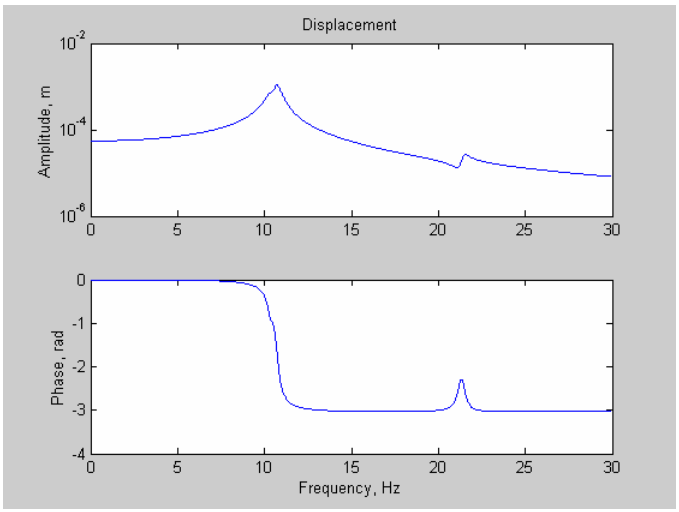

(a)

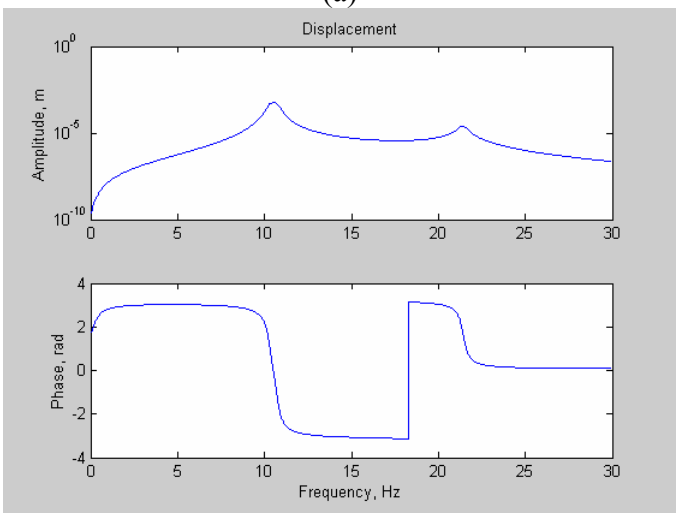

(b)

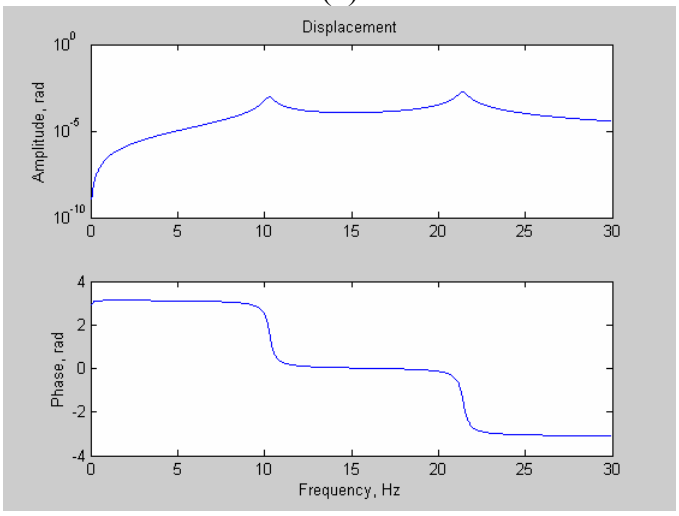

(c)

Figure 2.9 Amplitude and phase spectra of absolute responses of one-story building frame subjected to harmonic base motion; $\alpha=0;$ responses along (a) x (b) y and (c) θ directions

Table 2.1 Equipment used in free vibration and forced vibration test of one-story building frame

S.No.	Equipment	Quantity
1	Oscilloscope	1
2	Accelerometers	2
3	Conditioning amplifiers	2 channels
4	Shake table	1

Table 2.2Physical properties of parts of the structure

Sl. No.	Part	Material	Mass kg	Material Properties		
				Mass Density (ρ)	Modulus of elasticity (E)	Poisson's ratio (μ)
1	Columns (3 nos.)	Aluminum	$(m_1+m_2+m_3)$ =			
2	Column (1 no.)	Steel	m_4=			
3	Slab (1 no.)	Steel	$M_{s=}$			

Table 2.3 Geometric data of the structure

Sl. No.	Part	Dimensions in mm	
1	Slab	Depth (t)	
		Length (b_s)	
		Width (d_s)	
2	Aluminum Column	Diameter (D_{al})	
		Length (L)	
3	Steel Column	Diameter (D_s)	
		Length (L)	

Table 2.4 Details of the sensors used

Sl. No.	Sensor	Sensitivity, S		Mass kg
		mV/ms^{-2}	mV/g	
1				
2				
3				

*Table 2.5 Base motion test data on one-story building frame; Amplitude of base motion, Δ = mm

Sl. No.	Frequency, f (Hz)	Frequency $\omega=2\pi f$ (rad/s)	Amplitude σ_1 rms (V)	Amplitude σ_2 rms (V)	Amplitude σ_3 rms (V)	Conversion Factor CF_1 (V/m)	Displacement Amplitude $X = \sqrt{2}\ (CF_1)\ \sigma_x$ (m)	Conversion Factor CF_2 (V/m)	Displacement Amplitude $X_1 = \sqrt{2}\ (CF_2)\ \sigma_{x1}$ (m)	Conversion Factor CF_3 (V/m)	Displacement Amplitude $X_2 = \sqrt{2}\ (CF_3)\ \sigma_{x2}$ (m)	Torsion** θ_z (rad)
1												
2												
3												
4												
5												
6												
7												
8												
9												
10												
11												
12												
13												
14												
15												
16												
17												
18												
19												
20												

*This table can be used if all responses are measured simultaneously **The formula used to find rotation is $\theta = \tan^{-1}\left[\frac{(x_1 - x_2)}{d_{S1}}\right]$

Table 2.5.1 Base motion test data on one-story building frame; Measurement made at first floor along X direction; Amplitude of base motion, Δ = mm

S.No.	Frequency, f (Hz)	Frequency $\omega=2\pi f$ (rad/s)	Amplitude σ_x rms (mV)	Conversion Factor CF (V/m)	Displacement Amplitude $X=\sqrt{2}\ (CF)\ \sigma_x$ (m)
1					
2					
3					
4					
5					
6					
7					
8					
9					
10					
11					
12					
13					
14					
15					
16					
17					
18					
19					
20					

Table 2.5.2 Base motion test data on one-story building frame; measurement made at first floor along X direction; Amplitude of base motion, Δ = mm

Sl. No	Frequency f (Hz)	Frequency $\omega=2\pi f$ (rad/s)	Amplitude σ_{x1} rms (mV)	Amplitude σ_{x2} rms (mV)	Conversion Factor CF (V/m)	Displacement Amplitude $X_1 = \sqrt{2}\ (CF)\ \sigma_{x1}$ (m)	Displacement Amplitude $X_2 = \sqrt{2}\ (CF)\ \sigma_{x2}$ (m)	Rotation** θ_z (rad)
1								
2								
3								
4								
5								
6								
7								
8								
9								
10								
11								
12								
13								
14								
15								
16								
17								
18								
19								
20								

**The formula used to find rotation is $\theta = \tan^{-1}\left[\frac{(x_1 - x_2)}{d_{S1}}\right]$.

Table 2.6 Estimate of the natural frequencies of the one-story building frame

Mode No.	Natural frequencies in Hz	
	3-DOF Model	Experiment
1		
2		
3		

Table 2.7 Base motion test data on one-story building frame; Frequency of excitation = Hz; Amplitude of base motion = mm

Sl. No.	Angle of Incidence (degrees)	Amplitude σ_x rms (mV)	Amplitude σ_y rms (mV)	Conversion Factor CF (V/m)	Displacement Amplitude $X = \sqrt{2}\ (CF)\ \sigma_x$ (mm)	Displacement Amplitude $Y = \sqrt{2}\ (CF)\ \sigma_y$ (mm)
1	0					
2	5					
3	10					
4	15					
5	20					
6	25					
7	30					
8	35					
9	40					
10	45					
11	50					
12	55					
13	60					
14	65					
15	70					
16	75					
17	80					
18	85					
19	90					

Experiment 3

Dynamics of a three storied building frame subjected to periodic (non-harmonic) base motion.

3.1. Background

In Experiment 1 we have studied the dynamic behavior of a three-storied building frame model subjected to harmonic base motions. We learnt that the dynamic response of the system could be construed as being the sum of contributions from a set of uncoupled modes of the system. The present experiment is a follow-up on this previous experiment. Herein we study the dynamic behavior of the same frame when subjected to non-harmonic but periodic base motions. These base motions will be provided by a cam-follower arrangement on the shake table as shown in figures 3.1 and 3.2. The table is driven by an electric motor whose speed can be varied. By doing so, we would be in a position to generate periodic base motions of differing periods. Figure 3.3 shows the plot of a typical base motion measured on the table. Just as a vibrating system can be mathematically built-up in terms of uncoupled single degree of freedom oscillators, we can build periodic motions in terms of sine and cosine functions. The theory of Fourier series representations provides the necessary mathematical tools to achieve this. Thus, it turns out that the dynamic response of a single degree of freedom system to a single harmonic excitation holds the key to the understanding of dynamical behavior of built-up structures under general periodic excitations.

3.2 Fourier series representation of periodic functions

Let *y(t)* be a periodic function with period *T* so that *y(t+nT)=y(t)* for *n*=1,2,… According to the theory of Fourier series, *y(t)* can be expressed in terms of a series given by

$$y(t) = \frac{a_0}{2} + \sum_{n=1}^{\infty} a_n \cos n\omega t + b_n \sin n\omega t \qquad \ldots(3.1)$$

Here $\omega = 2\pi / T$. This representation is permissible when *y(t)* satisfies a set of general requirements and the series converges to *y(t)* at all points excepting the points at which the function *y(t)* has discontinuities: see the book by Kreysizig (1990) for the relevant background. The quantities a_0 and $\{a_n, b_n\}_{n=1}^{\infty}$ are known as the Fourier coefficients of *y(t)*. These coefficients can be evaluated using the equations

$$a_0 = \frac{2}{T}\int_0^T y(t)dt$$

$$a_n = \frac{2}{T}\int_0^T y(t)\cos n\omega t dt; \quad n = 0,1,2,\cdots \qquad \ldots(3.2)$$

$$b_n = \frac{2}{T}\int_0^T y(t)\sin n\omega t dt; \quad n = 1,2,\cdots$$

Furthermore, if *y(t)* is differentiable, we can write

$$\dot{y}(t) = \sum_{n=1}^{\infty} -a_n n\omega \sin n\omega t + b_n n\omega s \cos n\omega t \qquad \ldots(3.3)$$

where, the dot over *y(t)* represents the derivative with respect to time *t*. Figure 3.4 shows the Fourier coefficients for the periodic function shown in figure 3.3. It may noted that figure 3.3 shows not only the measured base motion but also the base motion re-constructed using the Fourier series.

3.3 Mathematical model

The frame shown in figure 3.1 is idealized as a three-dof system as shown in figure 3.5. The equation of motion for this system can be derived as follows:

$$\begin{bmatrix} M_1 & 0 & 0 \\ 0 & M_2 & 0 \\ 0 & 0 & M_3 \end{bmatrix} \begin{Bmatrix} \ddot{x}_1 \\ \ddot{x}_2 \\ \ddot{x}_3 \end{Bmatrix} + \begin{bmatrix} C_1 + C_2 & -C_2 & 0 \\ -C_2 & C_2 + C_3 & -C_3 \\ 0 & -C_3 & C_3 \end{bmatrix} \begin{Bmatrix} \dot{x}_1 \\ \dot{x}_2 \\ \dot{x}_3 \end{Bmatrix} + \begin{bmatrix} K_1 + K_2 & -K_2 & 0 \\ -K_2 & K_2 + K_3 & -K_3 \\ 0 & -K_3 & K_3 \end{bmatrix} \begin{Bmatrix} x_1 \\ x_2 \\ x_3 \end{Bmatrix} = \begin{Bmatrix} K_1 y + C_1 \dot{y} \\ 0 \\ 0 \end{Bmatrix} \qquad \ldots(3.4)$$

Using the Fourier series representation for the base motion *y(t),* and its derivative, as in equations 3.1 & 3.3, one gets

$$K_1 y + C_1 \dot{y} = \frac{K_1 a_0}{2} + K_1 \left\{ \sum_{n=1}^{\infty} a_n \cos n\omega t + b_n \sin n\omega t \right\} + C_1 \left\{ \sum_{n=1}^{\infty} -a_n n\omega \sin n\omega t + b_n n\omega \cos n\omega t \right\}$$

$$= \frac{K_1 a_0}{2} + \sum_{n=1}^{\infty} A_n \cos n\omega t + B_n \sin n\omega t$$

$$A_n = K_1 a_n + C_1 b_n n\omega; \quad B_n = K_1 b_n - C_1 a_n n\omega \qquad \ldots(3.5)$$

The solution of equation 4 can be obtained by using the method of normal mode expansion; see Annexure A for the details of this method. Thus, we begin by solving the eigenvalue problem $K\phi = \omega^2 M\phi$, which leads to the natural frequencies $\{\omega_n\}$ and modal matrix Φ that has the following orthogonality properties:

$$\Phi^t M \Phi = I \;\&\; \Phi^t K \Phi = diag[\omega_n^2] \qquad \ldots(3.6)$$

Here the superscript t denotes the matrix transposition. It may be noted that the modal matrix here has been normalized with respect to the mass matrix. Furthermore, assuming that the damping matrix is such that the matrix $\Phi^t C \Phi$ is also diagonal, one can uncouple the equations of motion given by equation 3.4. Thus, using the transformation $x = \Phi z$, it can be shown that the equation governing the n^{th} generalized coordinate is given by

$$\ddot{z}_n + 2\eta_n \omega_n \dot{z}_n + \omega_n^2 z_n = \frac{\Phi_{1n} K_1 a_0}{2} + \Phi_{1n} \left\{ \sum_{k=1}^{\infty} A_k \cos k\pi t + B_k \sin k\pi t \right\}; n = 1,2,\cdots,N. \qquad \ldots(3.7)$$

In the experimental study, it is reasonable to assume that the system is initially at rest, and, therefore, the initial conditions associated with the above equation becomes $z_n(0) = 0 \;\&\; \dot{z}_n = 0$. The solution of the above equation can be shown to be given by

$$z_n(t) = \frac{\Phi_{1n} K_1 a_0}{2}\left\{\exp(-\eta_n\omega_n t)\left[G_0\cos\omega_{dn}t + H_0\sin\omega_{dn}t\right] + \frac{1}{\omega_n^2}\right\} +$$

$$\sum_{k=1}^{\infty}\left\{\exp(-\eta_n\omega_n t)\left[G_k\cos\omega_{dn}t + H_k\sin\omega_{dn}t\right] + \Delta_k\cos k\omega t + \Gamma_k\sin k\omega t\right\}$$

$$G_0 = -\frac{1}{\omega_n^2}; H_0 = \frac{\eta_n\omega_n G_0}{\omega_{dn}} \qquad \ldots(3.8)$$

$$\begin{Bmatrix}\Delta_k \\ \Gamma_k\end{Bmatrix} = \begin{bmatrix}-k^2\omega^2 + \omega_n^2 & 2\eta_n\omega_n k\omega \\ -2\eta_n\omega_n k\omega & -k^2\omega^2 + \omega_n^2\end{bmatrix}^{-1}\begin{Bmatrix}\Phi_{1n}A_k \\ \Phi_{1n}B_k\end{Bmatrix}$$

$$G_k = -\Delta_k; H_k = \frac{-\Gamma_k k\omega + \eta_n\omega G_k}{\omega_{dn}}$$

$$\omega_{dn} = \omega_n\sqrt{1-\eta_n^2}$$

In constructing this solution it has been noted that the right hand side of equation 7 consists of a constant term and a summation of harmonic terms, and, also, that the system starts from rest. The solution, therefore, can be constructed by suitably combining the indicial response and harmonic response of a sdof system. Once the solution for the generalized coordinates are obtained, the displacement of the floors can be evaluated by using the transformation given by

$$x = \Phi z \qquad \ldots(3.9)$$

It is crucial to note in the conduct of this experiment that the transducers placed on the floors would measure the total displacement about an equilibrium position, while, the solution derived above, in the steady state, contains a zero frequency component, which needs to be removed before the theoretical results can be compared with the experimental observations on floor displacements.

The necessary information needed to identify the parameters of the model in equation 3.4 for the system shown in figure 3.1 has already provided in the description of the Experiment 1 and it will not be repeated here.

3.4 Experimental procedure

As has been noted already, the present experiment is a follow up of experiment 1, and therefore, the steps related to determination of mass, stiffness and damping matrices would not be repeated here. Table 3.1 provides the details of instruments to be used in the present study; the physical properties and details of the structure can be recorded in the format given in Tables 3.2 and 3.3 respectively.

3.4.1 Preliminary measurements

1. Study the charts/manuals that accompany the sensors and the charge amplifiers and note down the sensor sensitivities, sensor mass and factors to convert the measured electrical signal into mechanical units; this depends upon the amplifier settings used- see Table 3.4.
2. Derive the details of the structure mass, stiffness and damping matrices as per the details given in Experiment 1.

3.4.2 Studies on 3-storyed shear beam model

1. Arrange the experimental setup as shown in figures 3.1 & 3.6. Note that the accelerometer needs to be placed on slab in such a way that displacement along *x*-direction is picked up.
2. Drive the motor at a fixed RPM. The RPM could be selected in the neighborhood of the first natural frequency of the system. In the studies conducted at IISc it was found desirable to avoid the resonant frequencies.
3. Acquire the data on base motion and also the displacement of the three floors.
4. Identify one repetitive cycle of the base motion and, using equation 3.2, derive the Fourier coefficients for the base motion. For this purpose one can suitably approximate the variation of the base motion over one cycle by a set of straight lines and derive the Fourier coefficients in closed form. Alternatively, one can directly use numerical integration tools to carry out the integrations appearing in equation 3.2. The latter option would necessitate the use of a suitable computer program.
5. Once the Fourier coefficients are determined, determine the solution for the generalized coordinates using equation 3.8 and subsequently the floor displacements using the transformation $x = \Phi z$.
6. Isolate a segment containing about 10 cycles of oscillation from the solution derived above, and determine the time average of the displacement. The oscillatory motion about this average position can be determined by deducting this average from *x(t)*. Compare the time histories of these oscillatory motions with the experimentally observed floor displacements.

3.4 Report submission

1. Derive equations 3.4-3.8.
2. Document the experimentally observed time histories of base motion and floor displacements.
3. Plot the spectrum of Fourier coefficients, that is, $\{a_n\}_{n=0}^{L}$ & $\{b_n\}_{n=1}^{L}$ versus n.
4. Reconstruct the support displacement using the Fourier series representation and compare it with the observed base motion. This comparison must provide a clue as to how many terms need to be retained in the Fourier expansion.
5. Compute the floor displacement by using equations 3.8 & 3.9 and compare them with the corresponding experimental observations. Explain the differences (if any).

6. Respond to the following questions:
    (a) Are resonant type oscillations possible for structures under non-harmonic periodic motions?
    (b) Can you device an excitation that would send the first three modes of the structure into resonance?
    (c) Can the Fourier series representation be generalized to include aperiodic functions? If so, what type of aperiodic functions admits this generalization? Consider if the summation in the Fourier series tends to an integral if the function becomes aperiodic.
    (d) Figure 3.7 shows the distribution of average power in loads caused due to wind, waves and earthquakes. Also shown in this figure are the typical ranges of natural frequencies of typical engineering structures. Study this figure and list five important conclusions that you can draw from this.

3.5 Reference:

1. E Kreyszig, Advanced Engineering Mathematics, Wiley Eastern Limited, 1990

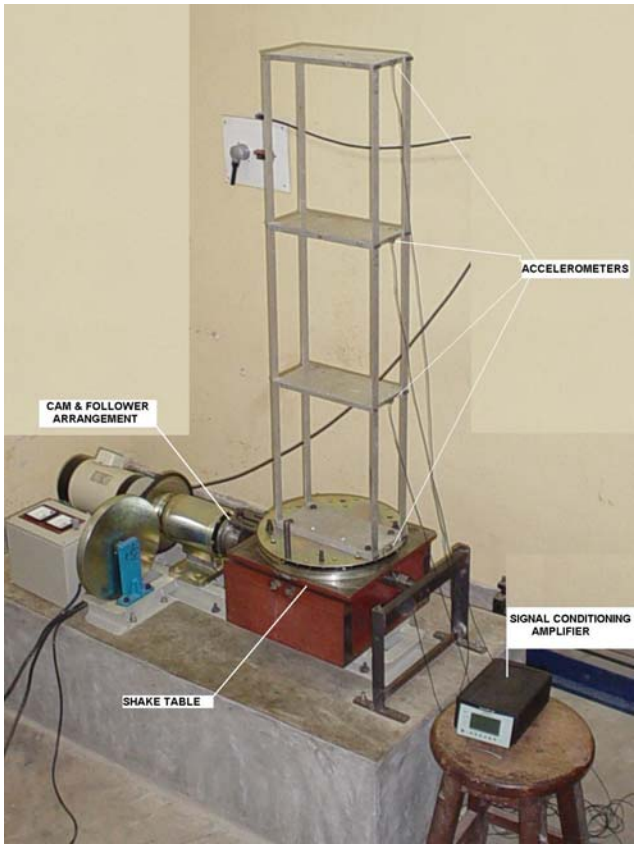

Figure 3.1 Electric motor driven shake table showing the cam and follower arrangement for generating non-harmonic periodic base motions with the three storied building frame model mounted on it

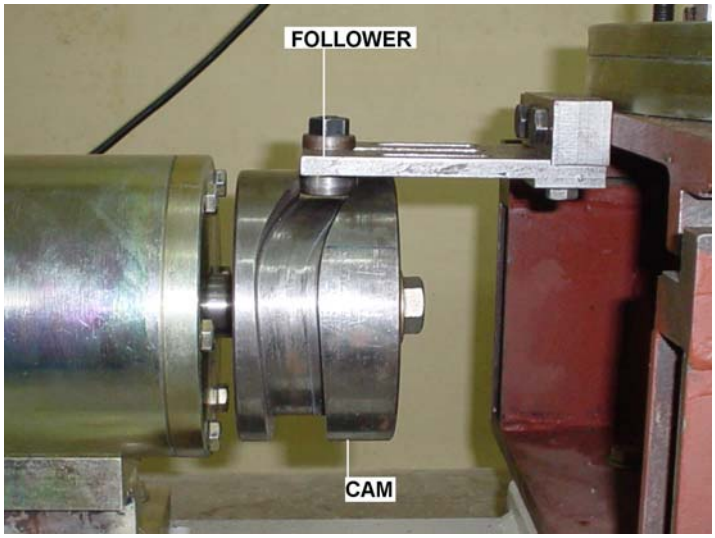

Figure 3.2 Close-up view of the follower-cam arrangement

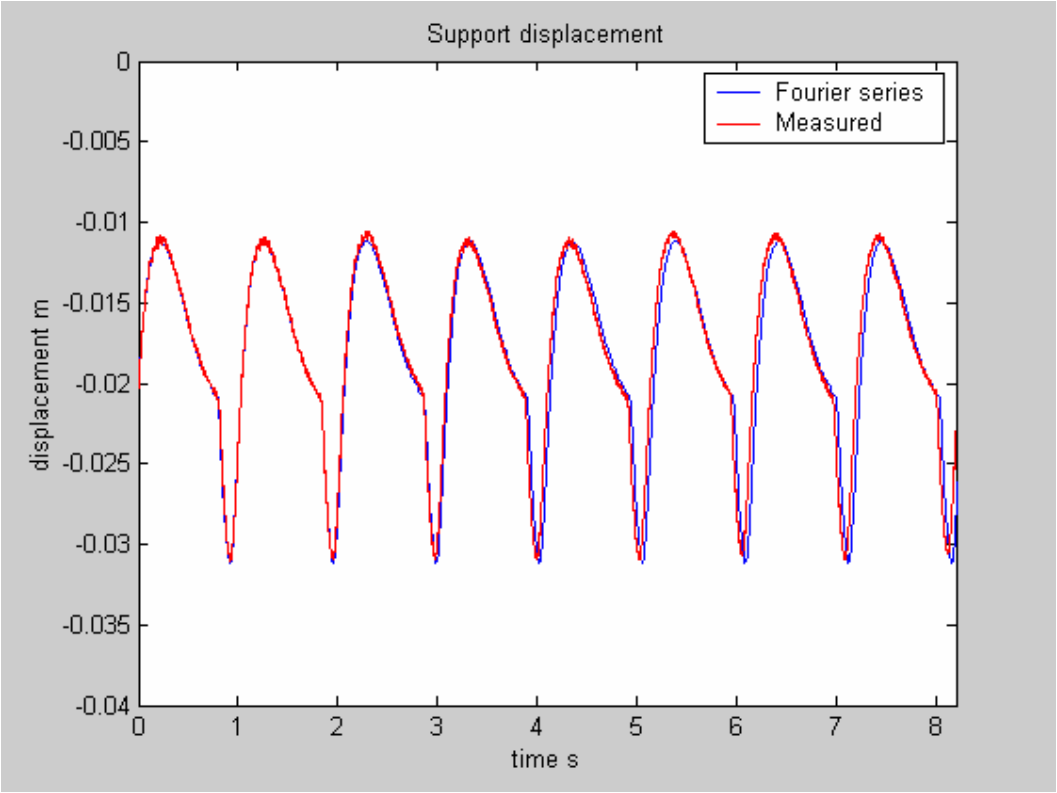

Figure 3.3 Periodic base motion s with period =1.0328 s measured on the table.

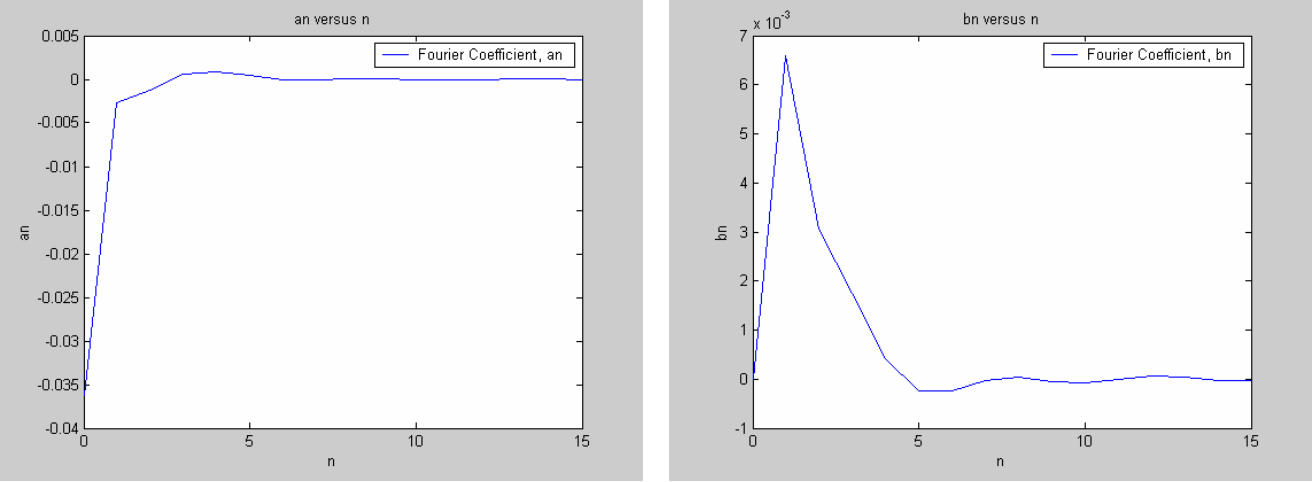

Figure 3.4 Plot of Fourier coefficients a_n & b_n versus number of terms n (period=1.0328 s).

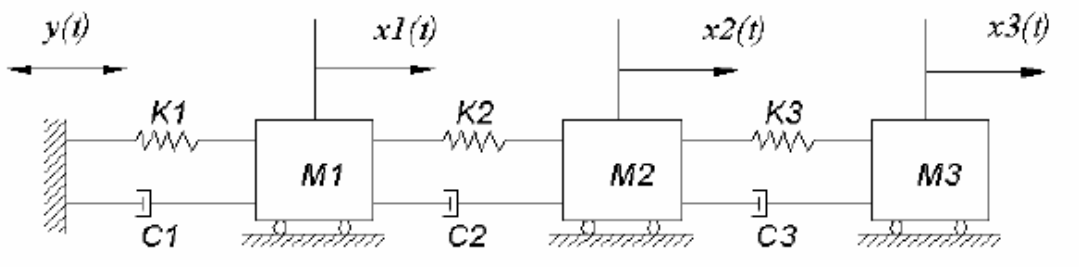

(a)

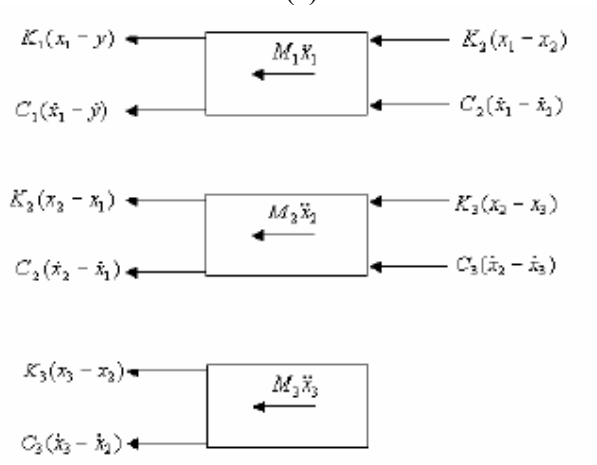

(b)

Figure 3.5 Multi mass-damper-spring model representation of a three-story shear building subjected to periodic base motion, *y(t)*; (a) mathematical model (b) free body diagram.

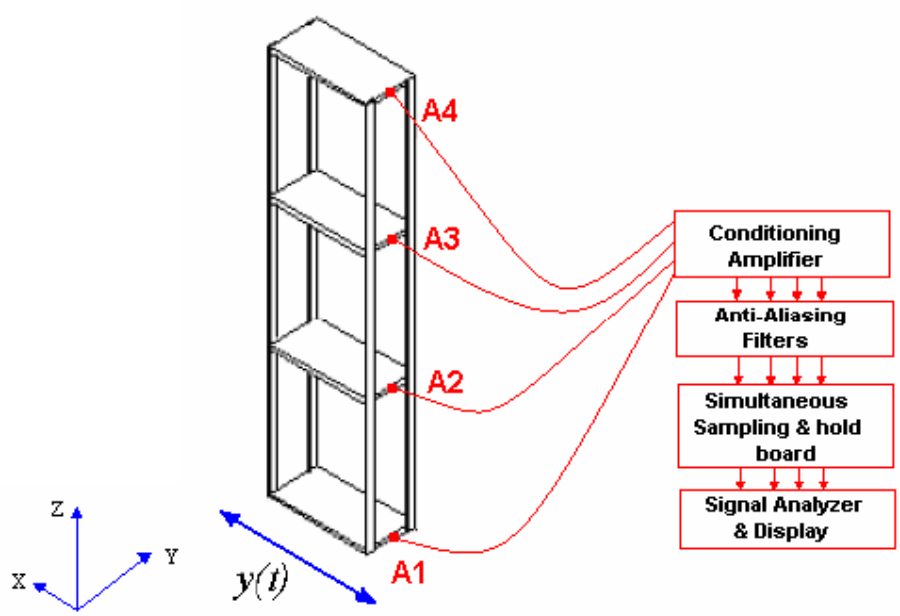

Figure 3.6 Set-up for studies on three-story shear building model; A1-A4 Accelerometers

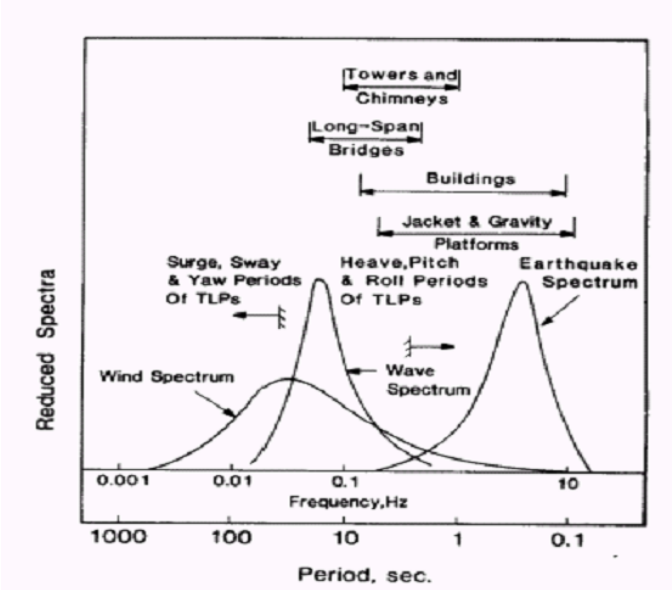

Figure 3.7 Spectral representation of wind, waves and earthquake loads on engineering

Table 3.1 Equipments used in free vibration and forced vibration test of three-story shear building frame

S.No.	Equipments	Quantity
1	Oscilloscope	1
2	Accelerometers	4
3	Transducers conditioning amplifiers	1
4	Shake table	1

Table 3.2 Physical properties of parts of the structure

Sl. No.	Part	Material	Mass kg	Material Properties	
				Young's Modulus (E) N/m^2	Mass density (ρ) kg/m^3
1	Column	Aluminum	M_c =		
2	Slab	Aluminum	M_s=		
3	Allen screw, M8	Steel	M_{sc}=	-	-

Table 3.3 Geometric data of the structure

Sl. No.	Part	Dimensions in mm		
		Depth (D)	Width (B)	Length (L)
1	Column	D_A =	B_A =	L_A =
2	Slab	D_B =	B_B =	L_B =

Table 3.4 Details of the sensors used; *CF*: conversion factor

Sl. No.	Sensor	Sensitivity, S		*CF*	Mass kg
		pC/ms^{-2}	pC/g		
1					
2					
3					

Experiment 4

Vibration isolation of a secondary system

4.1 Background

Vibration isolation is a means of controlling vibration by modifying the transmission path between source of excitation and the vibrating structure by introducing specifically designed structural elements. The design of these elements depends upon not only the dynamic properties of the structure being isolated but also on the nature of excitations. In this experiment we consider the three storied building frame model as shown in figures 4.1a and b. This frame houses an "equipment", marked as A, which is designed to be much rigid in relation to the lateral stiffness of the frame. If this frame were to be subjected to dynamic base motions, the vibration response of the equipment would be very close to that of the slab on which it rests. We wish to reduce the vibration by mounting the equipment on an "isolator", which is made up of a thin steel strip, as shown in figure 4.1c and d. The objective of this experiment is to understand how the dynamic behavior of the equipment changes due to the insertion of the isolator.

4.2 Displacement Transmissibility Ratio

Consider the mass m supported on the isolator spring k and damper c as shown in figure 4.2. Let the support be subjected to dynamic support displacement given by $\Delta(t) = \delta \exp(i\omega t)$. In the absence of the isolator, that is, with k=0 and c=0, the displacement of the mass m would be equal to $\Delta(t) = \delta \exp(i\omega t)$. This situation is considered undesirable and we wish to remedy this by selecting k and c so that the displacement of m gets reduced. To understand how this can be done, we begin by writing the equation of motion

$$m\ddot{x} + c\dot{x} + kx = (k + i\omega c)\delta \exp(i\omega t) \qquad \ldots(4.1)$$

Here a dot represents derivative with respect to time. As $t \to \infty$, we seek the solution in the form, $x(t) = X_0 \exp(i\omega t))$, which leads to

$$(-m\omega^2 + i\omega c + k)X_0 = (k + i\omega c)\delta \qquad \ldots(4.2)$$

Noting that the undamped natural frequency $\omega_n = \sqrt{(k/m)}$, bandwidth $2\eta\omega_n = c/m$, and frequency ratio $r = \omega/\omega_n$, the above equation can be re-written as

$$\frac{X_0}{\delta} = \frac{k + i\omega c}{-m\omega^2 + i\omega c + k} = \frac{\omega_n^2 + i2\eta\omega\omega_n}{\omega_n^2 - \omega^2 + i2\eta\omega\omega_n} = \frac{1 + i2\eta r}{1 - r^2 + i2\eta r} \qquad \ldots(4.3)$$

This equation represents the ratio of the amplitude of displacements of mass m with and without the presence of the isolator. The amplitude of this ratio, given by

$$\left|\frac{X_0}{\delta}\right| = \sqrt{\frac{1 + 4\eta^2 r^2}{(1 - r^2)^2 + (2\eta r)^2}} \qquad \ldots(4.4)$$

is known as the displacement transmissibility ratio (DTR). Clearly, for the isolation to be effective, DTR<1. Figure 4.3 shows the plot of DTR versus *r*. It may be noticed that for $r > \sqrt{2}$, DTR<1 for all *r*. Thus $r > \sqrt{2}$ represents the region in which the isolation would be effective.

4.3 Mathematical model

Let us now consider the dynamics of structure shown in figure 4.1c and 4.1d. A preliminary single degree of freedom (sdof) model for the mass A and the isolator can be made by assuming that the dynamics of the isolated mass and the three-storied frame are dynamically uncoupled. This sdof system would have mass = mass of the isolated mass + mass of isolator spring participating in the vibration + mass of the accelerometer mounted on the mass to be isolated + mass of screws *(used to assemble isolated mass and spring)*. The spring stiffness can be evaluated by using the formula $k = \frac{3EI}{L^3}$ where *E, I,* and *L,* respectively, denote the Young's modulus, moment of inertia and length of the isolator beam strip. A more detailed model can be made by assuming that the frame, along with the isolated mass, constitute a four degree of freedom system as shown in figure 4.4a. With the help of the free body diagram shown in figure 4.4b, the equation of motion for this system can be written as

$$
\begin{aligned}
&m_1\ddot{x}_1 + c_1(\dot{x}_1 - \dot{\Delta}) + c_2(\dot{x}_1 - \dot{x}_2) + k_1(x_1 - \Delta) + k_2(x_1 - x_2) = 0\\
&m_2\ddot{x}_2 + c_2(\dot{x}_2 - \dot{x}_1) + c_3(\dot{x}_2 - \dot{x}_3) + c_4(\dot{x}_2 - \dot{x}_4) + k_2(x_2 - x_1) + k_3(x_2 - x_3) + k_4(x_2 - x_4) = 0\\
&m_3\ddot{x}_3 + c_3(\dot{x}_3 - \dot{x}_2) + k_3(x_3 - x_2) = 0\\
&m_4\ddot{x}_4 + c_4(\dot{x}_4 - \dot{x}_2) + k_4(x_4 - x_2) = 0
\end{aligned}
\qquad \ldots(4.5)
$$

This can be re-written using matrix notations as

$$
\begin{bmatrix} m_1 & 0 & 0 & 0 \\ 0 & m_2 & 0 & 0 \\ 0 & 0 & m_3 & 0 \\ 0 & 0 & 0 & m_4 \end{bmatrix} \begin{Bmatrix} \ddot{x}_1 \\ \ddot{x}_2 \\ \ddot{x}_3 \\ \ddot{x}_4 \end{Bmatrix} + \begin{bmatrix} c_1 + c_2 & -c_2 & 0 & 0 \\ -c_2 & c_2 + c_3 + c_4 & -c_3 & -c_4 \\ 0 & -c_3 & c_3 & 0 \\ 0 & -c_4 & 0 & c_4 \end{bmatrix} \begin{Bmatrix} \dot{x}_1 \\ \dot{x}_2 \\ \dot{x}_3 \\ \dot{x}_4 \end{Bmatrix} + \begin{bmatrix} k_1 + k_2 & -k_2 & 0 & 0 \\ -k_2 & k_2 + k_3 + k_4 & -k_3 & -k_4 \\ 0 & -k_3 & k_3 & 0 \\ 0 & -k_4 & 0 & k_4 \end{bmatrix} \begin{Bmatrix} x_1 \\ x_2 \\ x_3 \\ x_4 \end{Bmatrix} = \begin{Bmatrix} c_1\dot{\Delta} + k_1\Delta \\ 0 \\ 0 \\ 0 \end{Bmatrix}
$$

$\ldots(4.6)$

The parameters of this model are established as follows:

$$
\begin{aligned}
&K_c = \frac{12EI}{L_C^3} \;;\; I = \frac{B_C D_C^3}{12}\\
&k_1 = k_2 = k_3 = 4K_c;\\
&k_4 = \frac{3E_2I_2}{L_{E2}^3} \;;\; I_2 = \frac{bd^3}{12}\\
&m_1 = M_s + 4M_c + M_{sc1}\\
&m_2 = M_s + 4M_c + M_{sc1} + M_{bb} + 0.5 * M_{sp} + M_{acc}\\
&m_3 = M_s + 4 * 0.5 * M_c + M_{sc1}\\
&m_4 = M_{iso} + 0.5 * M_{sp} + M_{acc} + M_{sc2}
\end{aligned}
\qquad \ldots(4.7)
$$

Here M_c= mass of a column, $M_{sc1\ (to\ clamp\ slab\ and\ column)}$ = mass of screw1, M_{bb}= mass of the base block, M_{sp}= mass of isolator beam strip, M_{iso}= mass to be isolated, M_{acc}= mass of the accelerometer, $M_{sc2\ (to\ clamp\ M_{iso}\ and\ isolator\ beam\ strip)}$ = mass of screw2, L_C=length of the frame column, L_{E2}= effective length of the isolator beam strip, B_C, D_C= respectively the breadth and depth of the frame column, and b, d= respectively the breadth and depth of the isolator beam strip. Equation 4.6 can be solved using either the normal mode expansion method or by inverting the dynamic stiffness matrix; see Appendix A for the relevant background. Figure 4.5a and 4.5b shows typical plots of the response of second floor and the isolator mass when the base is subjected to harmonic base motion. Figure 4.5c displays the DTR for the isolator.

4.4 Experimental procedure

4.4.1 Instruments and sensors

Table 4.1 provides the details of instruments and sensors to be used in the experimental study.

4.4.2 Preliminary measurements

a) Collect the data pertaining to geometric and material properties of the vibrating system (tables 4.2 and 4.3). Parts of data in table 4.2 have to be obtained from instructor/handbooks.
b) Using the four-degrees of freedom model, form the mass and stiffness matrices of the structure. Perform the eigen value analysis and determine the natural frequencies and modal matrix for the system. Alternatively, a simpler sdof model, which takes into account only the mass-isolator system, could also be made.
c) Study the charts/manuals that accompany the sensors and the charge amplifiers and note down the sensor sensitivities, sensor mass and factors to convert the measured electrical signal into mechanical units; this depends upon the amplifier settings used: see table 4.4.
d) The amplitude of the base motion is expected to be constant for all motor RPMs. This can be verified at the outset by running the motor at different speeds and measuring the base motion. Once you are satisfied with this, you need not have to measure the displacement of the base in subsequent experimentation.

4.4.3 Frame under harmonic base motions

e) Arrange the experimental setup as shown in figures 4.7; also see figures 4.1c,d and 4.6. Note that the three accelerometers, one on base, one on II floor slab and one on the mass to be isolated, are mounted in such a way that displacement along x-direction is picked up.
f) Set the frame into free vibration by applying an initial displacement. This can be achieved by gently pulling the frame at about the top slab and releasing it. Observe the free vibration decay on the oscilloscope and record the results as per the format given in table 4.5. Evaluate the logarithmic decrement and hence the damping ratio. One model for the damping can be obtained by

assuming that the damping ratio so determined would remain constant for all the modes.

g) Run the base motion test on the frame at different values of motor RPM making sure that readings at resonant frequencies are not missed. For a given motor RPM, allow the frame to oscillate for a few seconds so that the frame reaches its steady state. At this stage measure the amplitude of the frame response by using time history of displacement response acquired on the oscilloscope and record the amplitude data as in table 4.6. Note that the frequency of driving and the frequency of structural response can be assumed to be equal and this can be measured from the trace of displacement response on the oscilloscope. It may be noted that the test could be conducted even if only two channel measurements are possible, in which case, the above steps need to be repeated suitably.

h) The frequencies at which the structure undergoes resonance can be identified by observing the variation of response amplitudes as motor RPM is varied. At resonant conditions, in addition to noting the amplitude of slab oscillations, also note if the slabs are vibrating in phase or not. Based on this information the modal vectors for the first three modes could be established. Compare these mode shapes with the analytical mode shapes obtained in step (b).

i) Plot the variation of δ, X_2, and X_4 as the frequency of base motion, ω, is varied. Also plot X_4/X_2 versus ω/ω_n. Here ω_n is the modal frequency of the system in the mode in which the mode shape is dominated by the displacement of the isolator mass. If a sdof approximation is used, ω_n can be taken to be the natural frequency of the mass-isolator system.

j) From the plots in the previous step estimate the modal damping either by half-power bandwidth method or by relating the peak amplitude to the modal damping (see the book M Paz, 1984, Structural dynamics, CBS Publisher, New Delhi, for details).

k) Using the modal damping ratios obtained in steps (f) or (j) determine the C matrix using the relation $C = \left[\Phi^t\right]^{-1}[\Xi]\left[\Phi\right]^{-1}$ where Ξ is a diagonal matrix with entry on the nth row being $2\eta_n\omega_n$. It can be shown that $\left[\Phi^t\right]^{-1} = M\Phi$ and $\left[\Phi\right]^{-1} = \Phi^t M$, and, therefore, one gets $C = M\Phi\Xi\Phi^t M$ (see Appendix A). Using this C matrix and equation 4.6, solve the mathematical model to determine analytically the amplitude of floor responses as a function of the driving frequency.

4.5 Report submission

1. Document the experimental observations as per format given in tables 4.2-4.8.
2. Develop the mathematical model as per the simplifications suggested in figures 4.2 and 4.4.
3. Compare the experimentally observed plots of X_2 *versus f*, X_4 *versus f* and X_4/X_2 versus ω/ω_n with corresponding predictions from the mathematical model. Discuss the qualitative features of these plots and explain the mutual agreement /disagreement between theoretical and experimental results.
4. Respond to the following questions:

1. If the mass to be isolated were to be mounted on a rubber pad, instead through a metal strip, as has been done in the present set up, what changes would you expect in the dynamic behavior of the mass?
2. In the present set up, what role does the damping characteristic of the isolator beam strip play? Does it have a favorable influence in the process of isolation? What would happen if this damping were to be zero?
3. Is the concept of vibration isolation useful in controlling vibrations induced by earthquakes on buildings? Frame your response keeping in mind the following facts: earthquake loads are transient in nature, these loads contain several frequency components, several modes of vibration could participate in structural vibration and the structure could behave nonlinearly in the event of a strong earthquake.
4. Does base isolation of building frames produce any undesirable effects on the overall performance of the building in terms of its ability to carry other loads such as dead, live and wind loads?
5. Items such as TV monitors, computer central processing units and such other electronic items, need to be carefully packaged while they are transported. What considerations are relevant in the design of these packages?

(a)

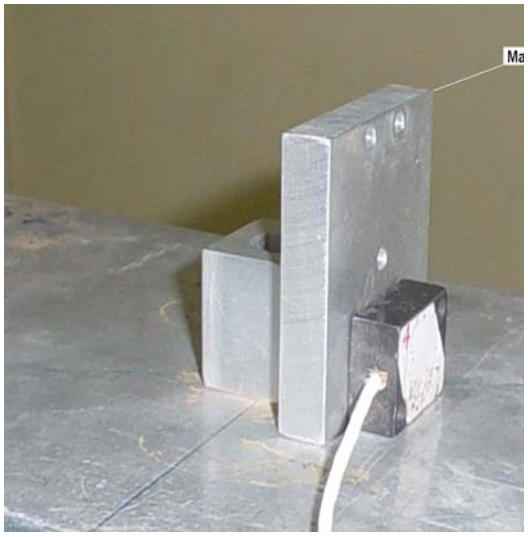

(b)

(c)

(d)

Figure 4.1 (a) Frame carrying mass A; (b) Direct mounting of the mass A on the slab; (c) Frame carrying mass A mounted on the isolator; (d) close view of the isolator.

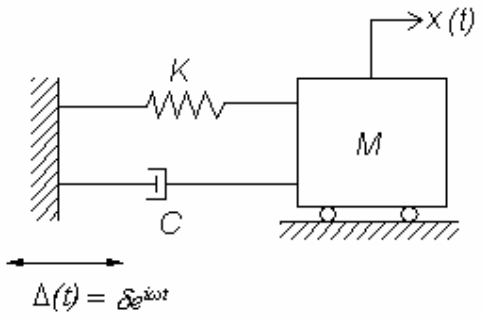

Figure 4.2 Mass M being isolated from the base motion $\Delta(t)$ by spring K and damper C.

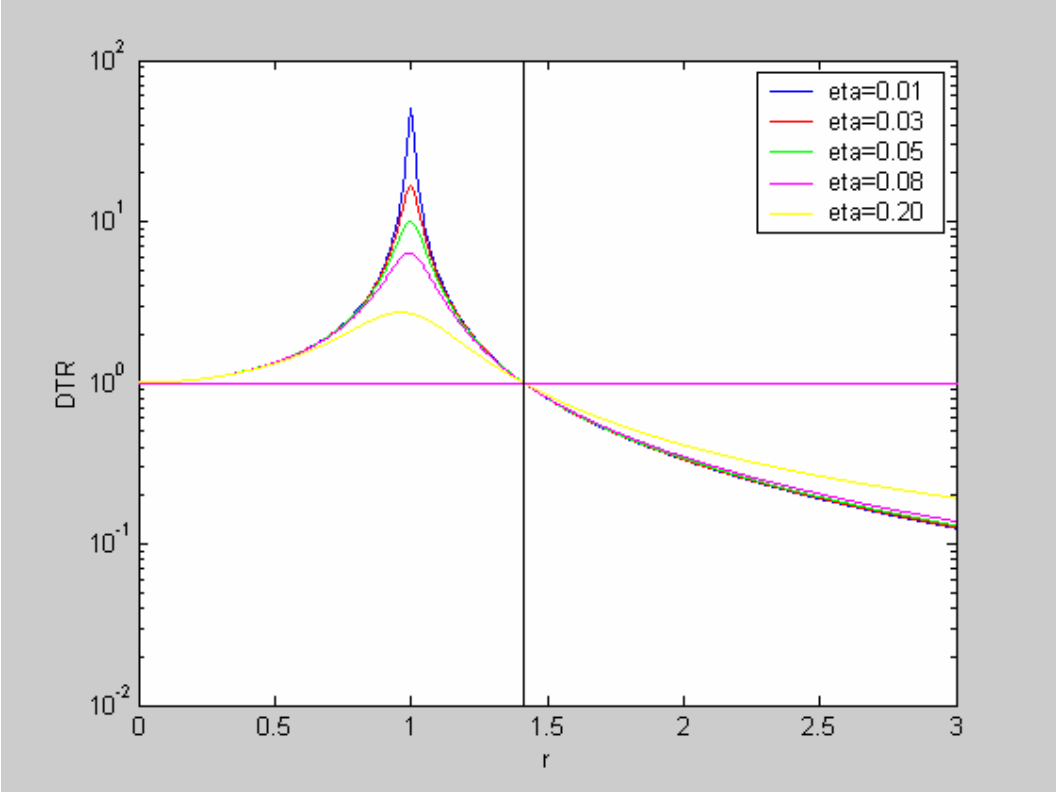

Figure 4.3 Displacement transmissibility ratio (DTR); region of successful isolation (DTR<1) lies to the right of $r = \sqrt{2}$; also, note that for $r = \sqrt{2}$, DTR=1 for all values of damping ratio η; for $r > \sqrt{2}, \eta_1 > \eta_2 \Rightarrow DTR(\eta_1) > DTR(\eta_2)$; and $r < \sqrt{2}, \eta_1 > \eta_2 \Rightarrow DTR(\eta_1) < DTR(\eta_2)$.

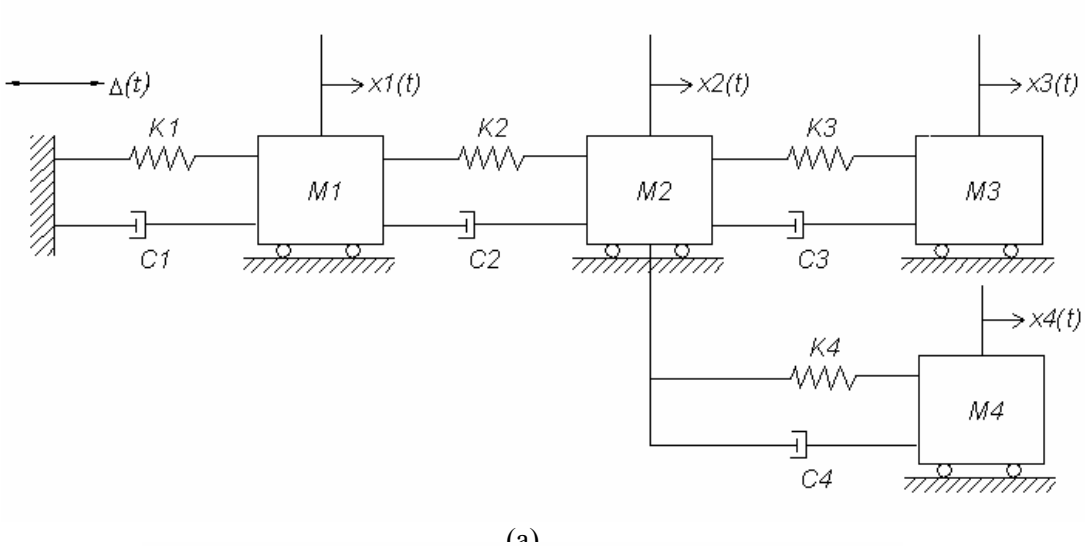

(a)

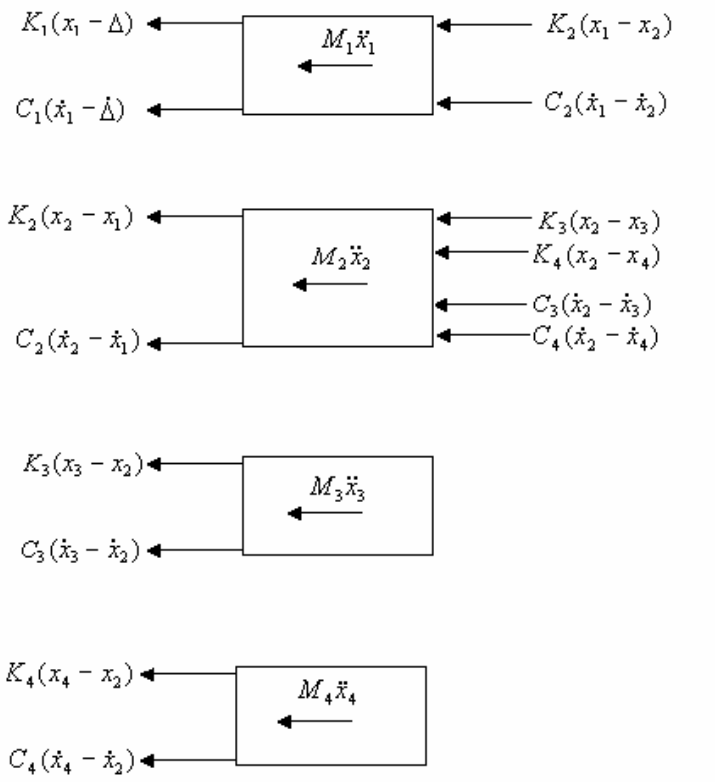

(b)

Figure 4.4 (a) A 4-dof model for the frame in figures 4.1c and d; (b) Free body diagram of the four masses.

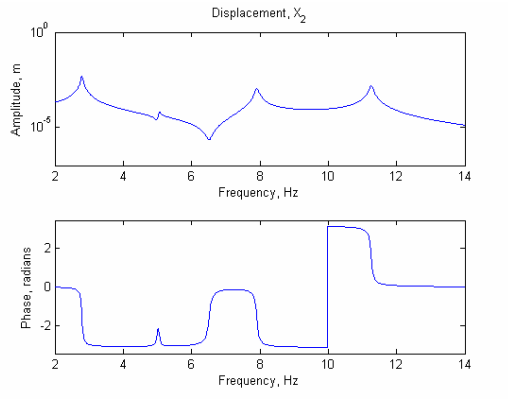

(a)

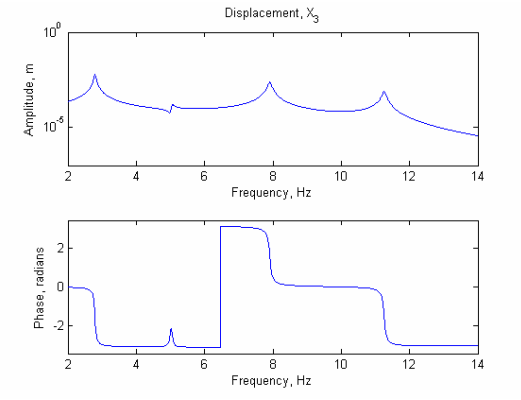

(b)

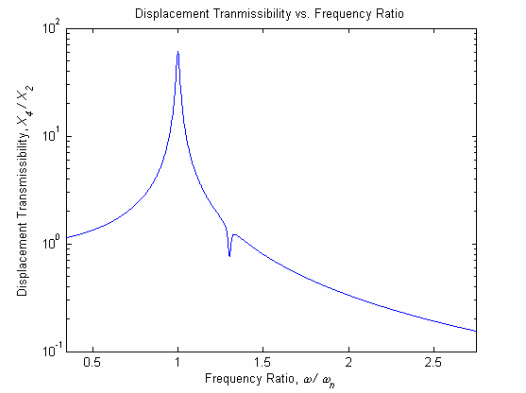

(c)

Figure 4.5 Amplitude and phase spectra of absolute responses of the frame in figures 4.1c and d (a) response of II floor; (b) response of mass to be isolated; (c) Displacement transmissibility ratio.

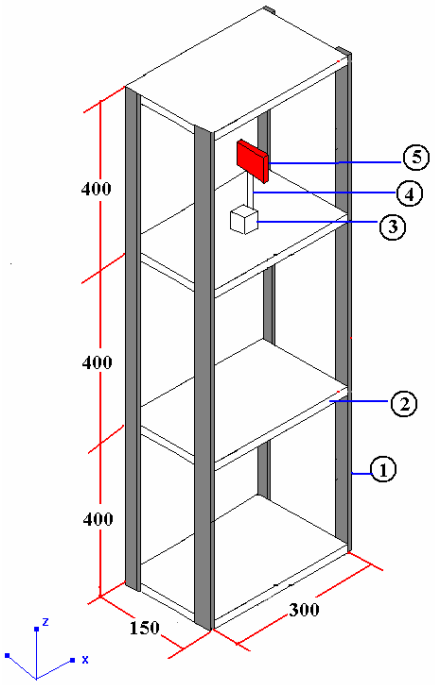

Figure 4.6 Three-story shear building model with a mass, on second floor, to be isolated used in experiment; 1 column; 2 slabs; 3 base block; 4 spring (aluminum beam); 5 mass to be isolated

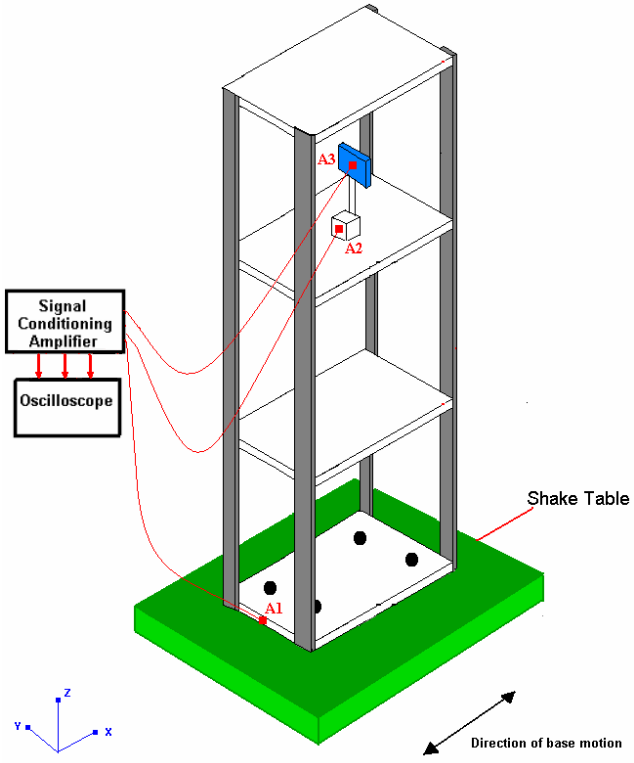

Figure 4.7. Setup for studies on three-story shear building frame with a mass, on second floor, to be isolated

Table 4.1 Equipment used in free vibration and forced vibration test of frame in figures 4.1c and d

No.	Equipments	Quantity
1	Oscilloscope/Data acquisition system	1
2	Accelerometer	3
3	Charge amplifier/Transducers conditioner	3
4	Shake table	1

Table 4.2 Physical properties of parts of the structure

No.	Part	Material	Mass kg	Material Properties	
				Young's Modulus (E) N/m^2	Mass density (ρ) kg/m^3
1	Column	Aluminum	M_c =		
2	Slab	Aluminum	M_s=		
3	Allen screw, M8	Steel	M_{sc1}=		
4	Allen screw, M3	Steel	M_{sc2}=		
5	Base block	Aluminum	M_{bb}=		
6	Spring (Al strip)	Aluminum	M_{sp}^*=		
7	Mass to be isolated	Aluminum	M_{iso}=		
8	Mass of accelerometer	-	M_{acc}=		

* $M_{sp} = \rho * d * b * L_2$

Table 4.3 Geometric data of the structure

No.	Part	Dimensions in mm			
		Depth (D)	Width (B)	Length (L)	Effective length
1	Column	D_C =	B_C =	L_C =	-
2	Slab	D_S =	B_S =	L_S =	-
3	Base block	D_{bb} =	B_{bb} =	L_{bb} =	-
4	Spring (Al strip)	d =	b =	L_2 =	L_{E2} =
5	Mass to be isolated	D_{iso} =	B_{iso} =	L_{iso} =	-

Table 4.4 Details of the sensors used; *CF*: conversion factor

No.	Sensor	Sensitivity, S		*CF*	Mass kg
		pC/ms^{-2}	pC/g		
1					
2					
3					

Table 4.5 Free vibration test data on three-story shear building frame with a mass, on second floor, to be isolated

No.	Quantity	Notation	Observations
1	Amplitude of 0^{th} peak	A_0	
2	Amplitude of n^{th} peak	A_n	
3	Number of cycles	n	
4	Logarithmic decrement	δ	
5	Damping ratio	ζ	

Table 4.6 Base motion test data on frame in figures 4.1c and d

(This table can be used if all responses are measured simultaneously)

No.	Frequency, f (Hz)	Frequency $\omega=2\pi f$ (rad/s)	Amplitude σ_1 rms (mm)	Amplitude σ_2 rms (mm)	Amplitude σ_3 rms (mm)	Displacement Amplitude $Y = \sqrt{2}$ (CF) σ_1 (mm)	Displacement Amplitude $X_2 = \sqrt{2}$ (CF) σ_2 (mm)	Displacement Amplitude $X_4 = \sqrt{2}$ (CF) σ_3 (mm)
1								
2								
3								
4								
5								
6								
7								
8								
9								
10								
11								
12								
13								
14								
15								
16								
17								
18								
19								
20								

Table 4.6.1 Base motion test data on frame in figures 4.1c and d

(measurement made on ground floor)

S.No.	Frequency, f (Hz)	Frequency $\omega=2\pi f$ (rad/s)	Amplitude σ_1 rms (mV)	Displacement Amplitude $Y=\sqrt{2}$ (CF) σ_1 (m)
1				
2				
3				
4				
5				
6				

7				
8				
9				
10				
11				
12				
13				
14				
15				
16				
17				
18				
19				
20				
21				
22				
23				
24				
25				

Table 4.6.2 Base motion test data on frame in figures 4.1c and d

(measurement made on second floor)

S.No.	Frequency, f (Hz)	Frequency $\omega=2\pi f$ (rad/s)	Amplitude σ_2 rms (mV)	Displacement Amplitude $X_2=\sqrt{2}\ (CF)\ \sigma_2$ (m)
1				
2				
3				
4				
5				
6				
7				
8				
9				
10				
11				
12				
13				
14				
15				
16				
17				
18				
19				
20				
21				

22				
23				
24				
25				

Table 4.6.3 Base motion test data on frame in figures 4.1c and d

(measurement made on the mass to be isolated)

S.No.	Frequency, f (Hz)	Frequency $\omega=2\pi f$ (rad/s)	Amplitude σ_3 rms (mV)	Displacement Amplitude $X_4=\sqrt{2}\ (CF)\ \sigma_3$ (m)
1				
2				
3				
4				
5				
6				
7				
8				
9				
10				
11				
12				
13				
14				
15				
16				
17				
18				
19				
20				
21				
22				
23				
24				
25				

*Tables 4.6.1 to 4.6.3 can be used if there is only one accelerometer and each response is measured individually

Table 4.7 Frequency ratio and the displacement transmissibility

No.	Frequency ratio f / f_n	Amplitude ratio X_4 / X_2
1		
2		
3		
4		
5		
6		
7		
8		
9		
10		
11		
12		
13		
14		
15		
16		
17		
18		
19		
20		
21		
22		
23		
24		
25		

Table 4.8 Estimate of the natural frequencies of the frame in figures 4.1c and d

Mode No.	Natural frequencies in Hz	
	4-DOF Model	Experiment
1		
2		
3		
4		

Experiment 5

Dynamics of a vibration absorber

5.0 Background

Dynamic vibration absorber (DVA), also known as the mass tuned damper, is an auxiliary vibrating element attached to a primary vibrating system with a view to reduce the vibrations of the primary system. The Stockbridge dampers attached to transmission cable lines (figure 5.1) are classical examples for a DVA. These dampers are used to reduce the wind-induced oscillations of cables and thereby extending the fatigue life of the cables. The principle of DVA is widely discussed in many books: see for instance, the book by J P Den Hartog (Mechanical Vibrations, 1986, Dover Publications, NY, pp. 87-106).

To illustrate the working of the DVA, let us begin by considering a harmonically driven single degree of freedom (sdof) system (figure 5.2). Let us call this system as the primary system. Let us assume that the harmonic driving of the system is near the system natural frequency so that $\omega \approx \omega_n = \sqrt{(K/M)}$, and resonant conditions prevail. In case the amplitude of response of mass M is considered unacceptably high, what can we do to control the vibration? A straightforward answer to this question would be to alter K, M and/or C so that either we avoid resonant conditions or we limit the resonant amplitude to acceptable limits. This would essentially mean that we are re-designing the system. This, of course, is not possible if we have already produced the vibrating system. In such a situation, we would rather like to modify the existing system to achieve the desired vibration control. To see how this can be done, let us add an auxiliary spring-mass system to the primary system (figure 5.3). This modification would clearly alter the dynamics of the system: thus, for instance, the system would now have two natural frequencies. Consequently, the dynamic response of mass M would now be altered. Can this alteration be to the advantage of mass M? Or, in other words, can we select k and m so that the undesirably high response of mass M, that prevailed before addition of k and m, can now be reduced to acceptable levels? This indeed is possible, and, to see this, we write the equation of motion governing the systems shown in figures 5.2 and 5.3 respectively as

$$M\ddot{x} + C\dot{x} + Kx = Fe^{i\omega t} \qquad \ldots (5.1)$$

and

$$\begin{aligned} &M\ddot{y} + C\dot{y} + Ky + k(y - z) = Fe^{i\omega t} \\ &m\ddot{z} + k(z - y) = 0 \end{aligned} \qquad \ldots(5.2)$$

The steady state amplitude of response of these systems are obtained respectively as

$$X(\omega) = \frac{F}{(-\omega^2 M + i\omega C + K)} \qquad \ldots(5.3)$$

and

$$Y(\omega) = \frac{F(-\omega^2 m + k)}{[(-\omega^2 M + i\omega C + K + k)(-\omega^2 m + k)] - k^2}$$

$$Z(\omega) = \frac{Fk}{[(-\omega^2 M + i\omega C + K + k)(-\omega^2 m + k)] - k^2} \quad \ldots(5.4)$$

Figure 5.4 shows typical plots of amplitude and phase of *X (ω), Y (ω)* and *Z (ω)*. It can be observed from equation (5.4) that, when the condition $k\text{-}m\omega^2=0$ is satisfied, the response amplitude of mass *M, Y (ω),* becomes zero. Indeed the plots shown in figure 5.4b reveal that at $\omega \approx \omega_n = \sqrt{(K/M)}$, the response of mass *M* becomes zero. This means that if we can "tune" the "absorber" mass and stiffness such that the condition $k\text{-}m\omega^2=0$ is satisfied, we could succeed in dramatically reducing the vibration levels of the primary system. This, in essence, is the principle of working of DVA.

5.1 Experimental setup

Figures 5.5a and 5.5b show the experimental setup. This consists of a steel clamped beam A (primary system) that is driven harmonically by an electric motor (B) with two flywheels (C) that carry eccentric masses (D). The absorber system consists of an aluminum beam (G) with two symmetrically placed discrete masses (H), which is connected to the primary system through the rod F. The system is configured such that the rod F and the absorber beam G can be detached from the primary beam. The motor with imbalance provides harmonic excitations to the primary beam. By varying the speed of the motor, one can vary the frequency of this excitation. Similarly by changing the eccentricity and/or the eccentric mass on the flywheels, one can also vary the amplitude of the excitation.

5.2 Mathematical model

The structure shown in figure 5.5 can be idealized as shown in figure 5.6a. The model consists of two beams; the primary beam has a flexural rigidity E_1I_1 and mass per unit length m_1. The motor assembly is modeled as a point mass M_t and is placed at the mid-span of the primary beam. The detachable rod F is taken to be rigid and the absorber system is modeled as a double cantilever beam with flexural rigidity E_2I_2 and mass per unit length m_2. The discrete masses H are modeled as point masses. Furthermore the system shown in figure 5.6a is approximately modeled as a 2-dof system as shown in figure 5.6b. The parameters of this model are established as follows.

$$K = \frac{192E_1I_1}{L_{e1}^3};\ k = 2\frac{3E_2I_2}{L_{e2}^3}$$

$$M = M_{Aeff} + M_t + M_F + m_{ac1}$$

$$M_t = M_B + M_C + 2M_D + M_E$$

$$m = M_{Geff} + 2M_H + m_{ac2} \quad \ldots(5.5)$$

Here masses M_{Aeff} and M_{Geff} are the equivalent masses of beams A and G respectively; M_t is the total mass of the motor assembly consisting of mass of the motor body (M_B), flywheels (M_C), connecting plate (M_E) and discrete masses (M_D); m_{ac1} and m_{ac2} are the accelerometer masses. To compute M_{Aeff} and M_{Geff} one need to consider the effective

mass participating in vibration. To approximate this, we note that the deflection of a fixed-fixed beam due to a concentrated load at mid-span is given by

$$y(x) = y_{\max}\left[12\left(\frac{x}{L_{e1}}\right)^2 - 16\left(\frac{x}{L_{e1}}\right)^3\right] \quad \ldots(5.6)$$

The maximum kinetic energy of the beam itself is then

$$T_{\max} = \frac{1}{2}\int_0^{L_{e1}/2} 2m_1\left\{\dot{y}_{\max}\left[12\left(\frac{x}{L_{e1}}\right)^2 - 16\left(\frac{x}{L_{e1}}\right)^3\right]\right\}^2 dx = \frac{1}{2}(0.3714 m_1 L_{e1})\dot{y}_{\max}^2 \quad \ldots(5.7)$$

The effective mass for the beam at mid-span is then equal to

$$M_{Aeff} = 0.3714 m_1 L_{e1} \quad \ldots(5.8)$$

Similarly, by using the deflection profile of the form

$$y(x) = y_{\max}\left\{\frac{3}{2}\left[\frac{x}{(L_2)}\right]^2 - \frac{1}{2}\left[\frac{x}{(L_2)}\right]^3\right\} \quad \ldots(5.9)$$

an approximation to the equivalent mass for the cantilever beam in the absorber portion is obtained as

$$M_{Geff} = 0.2357 m_2 (L_2) \quad \ldots(5.10)$$

The equivalent stiffness of the clamped beam is obtained by noting that the mid-span deflection under a central unit concentrated load is $L^3/(192EI)$. Similarly, the equivalent stiffness for the cantilever beam is obtained by noting that the tip deflection under a unit concentrated load at tip is $L^3/(3EI)$. Finally, it may be noted that when the primary system alone is to be analyzed, the model shown in figure 5.7 can be employed.

5.3 Experimental procedure

5.3.1 Instruments and sensors

Table 5.1 provides the details of instruments to be used in the experimental study.

5.3.2 Preliminary measurements

- Collect the data pertaining to geometric and material properties of the vibrating system (tables 5.2 and 5.3). Parts of data in table 5.2 have to be obtained from instructor/handbooks.
- Study the charts/manuals that accompany the sensors and the charge amplifiers and note down the sensor sensitivities, sensor mass and factors to convert the

measured electrical signal into mechanical units; this depends upon the amplifier settings used- see table 5.4.

5.3.3 Studies on primary beam without absorber

- Arrange the experimental setup as shown in figure 5.8. Note that the accelerometer needs to be placed as close as possible at mid-span of the primary beam.
- Set the beam into free vibration by applying an initial displacement. This can be achieved by gently pulling down the beam at about the mid-span and releasing it. Observe the free vibration decay on the oscilloscope and record the results as per the format given in table 5.5. Evaluate the logarithmic decrement and hence the damping ratio.
- Run the forced vibration test on the beam at different values of motor RPM.
- For a given motor RPM, allow the beam to oscillate for a few seconds so that the beam reaches its steady state. At this stage measure the amplitude of the beam response by using time history of displacement response acquired on the oscilloscope and record the amplitude data as in table 5.6. Note that the frequency of driving and the frequency of structural response can be assumed to be equal and this can be measured from the trace of displacement response on the oscilloscope.
- Plot the *X/F* versus *f* and compare this plot with the results from mathematical model of the structure shown in figure 5.8 (see equations 5.1 and 5.3).

5.3.4 Studies on combined system of primary beam and DVA

- Arrange the experimental setup as shown in figure 5.9.
- Conduct the free vibration test as in section 5.3 and record the results in the format given in table 5.7. To a first approximation take ξ to be the average of the values obtained in columns 4 and 5 of the table 5.7. In the analysis of the mathematical model (figure 5.6b) the two modes of the system may be assumed to have the same damping ratio of ξ.
- Run the forced vibration test on the combined system at different motor RPM. For a given motor RPM, allow the system to oscillate for a few seconds so that the system reaches its steady state. At this stage measure the amplitudes of both primary beam and absorber beam responses by using the time history of displacement responses acquired on the oscilloscope and record the amplitude data as in tables 5.8 and 5.9. Note that the frequency of driving and the frequency of structural response can be assumed to be equal and this can be measured from the trace of displacement response on the oscilloscope.
- Plot *Y/F* versus *f* and *Z/F* versus *f*. Compare these results with that obtained from mathematical model of the structure shown in figure 5.9 (see equations 5.2 and 5.4).

5.4 Report submission

1. Document the experimental observations as per format given in tables 5.2-5.9.
2. Develop the experimental model as per the simplifications suggested in figures 5.6 and 5.7.
3. Compare the experimentally observed plots of *X/F* versus *f, Y/F* versus *f* and *Z/F* versus *f* with corresponding predictions from the mathematical model.

Discuss the qualitative features of these plots and explain the mutual agreement/disagreement between theoretical and experimental results.

4. Respond to the following questions:
   (a) How do you assess the effectiveness of the vibration absorber in the present study?
   (b) Comment on the design of the absorber system and point out deficiencies, if any.
   (c) Do you think the principle of vibration absorber has potential application in earthquake engineering? Discuss.
   (d) Give a few examples of engineering systems in which the principle of DVA has been used.

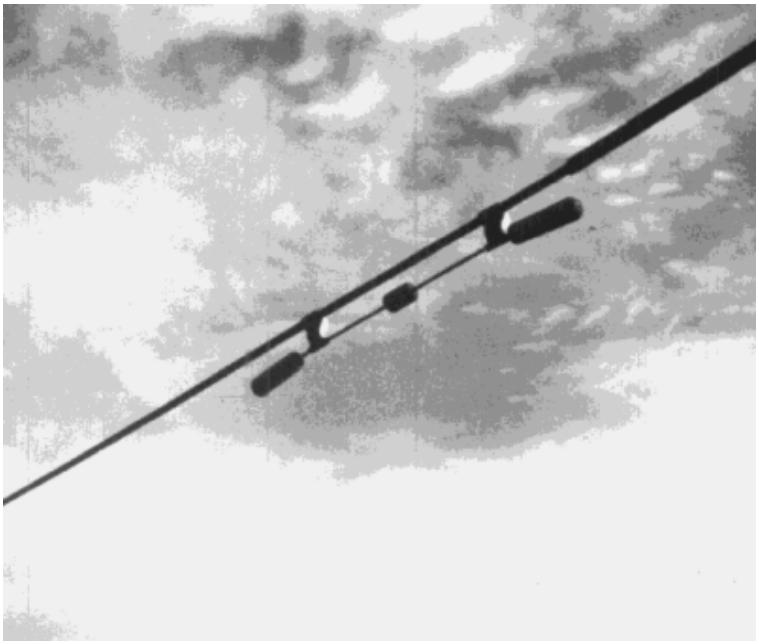

Figure 5.1 Stockbridge damper attached to a transmission cable line
(*http://www.dulhunty.com/an5.htm*)

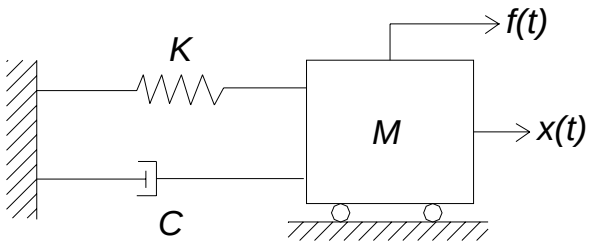

Figure 5.2 Harmonically driven sdof system: $f(t)=Fe^{i\omega t}$

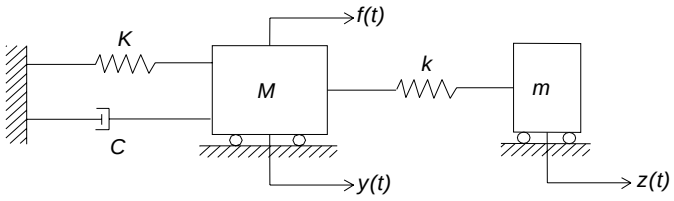

Figure 5.3 Addition of auxiliary spring and mass elements to the primary system: $f(t)=Fe^{i\omega t}$

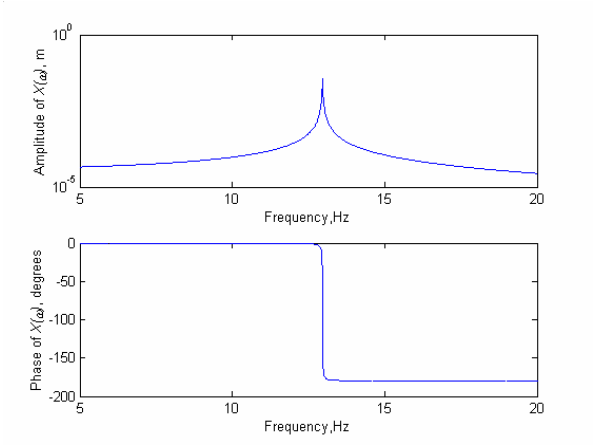

(a)

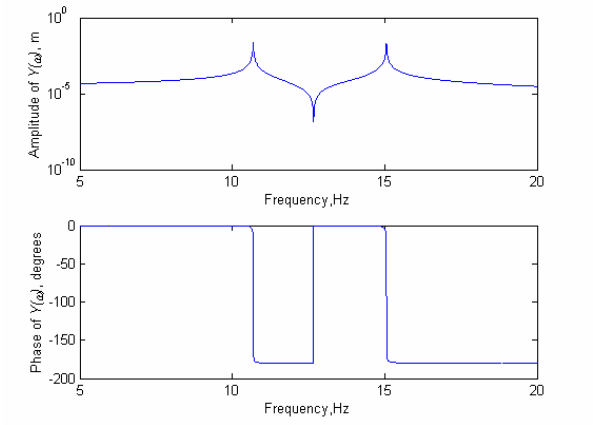

(b)

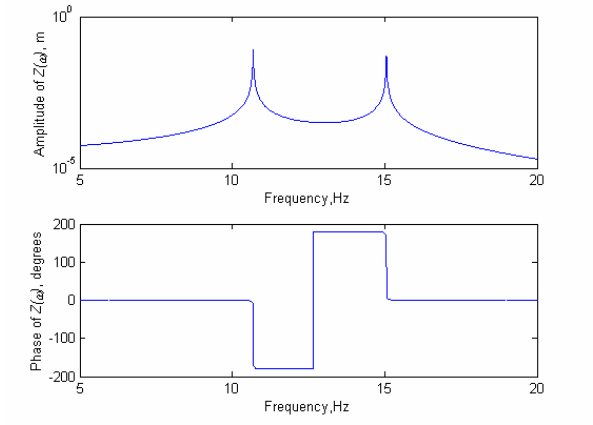

(c)

Figure 5.4 Amplitude and phase spectra of response of harmonically driven systems; (a) response of sdof system; (b) response of primary system in the 2-dof system; (c) response of secondary system in the 2-dof system.

Figure 5.5a Experimental setup for DVA

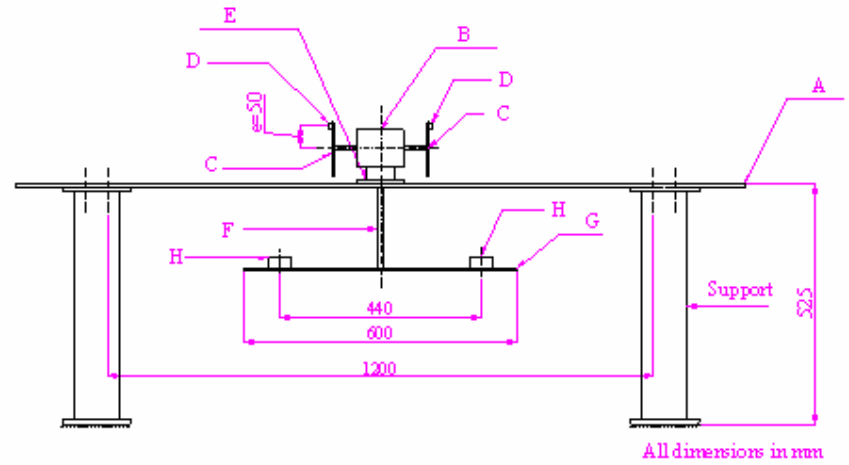

A-Main Beam; B-D.C. Motor; C-Fly Wheel; D-Eccentric mass; E-Plate welded to main beam to facilitate mounting of motor with nut and bolts; F-Connecting Rod, G-Absorber Beam; H-Mass attached to the absorber beam; the support is made up of I-section ISMB 200.

Figure 5.5b Schematic diagram of experimental setup for DVA

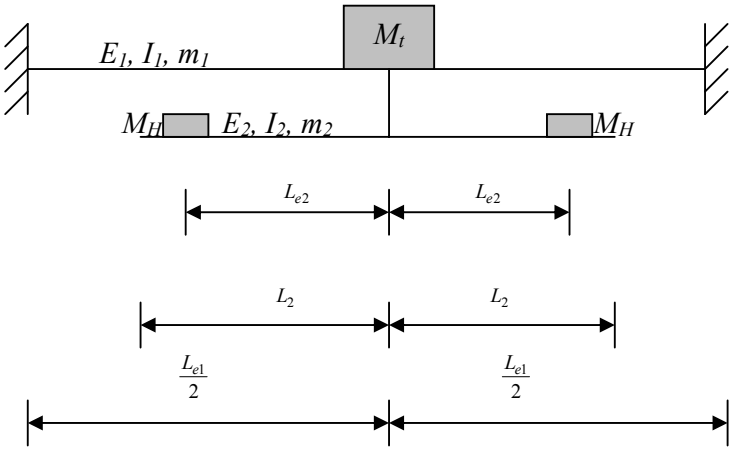

(a)

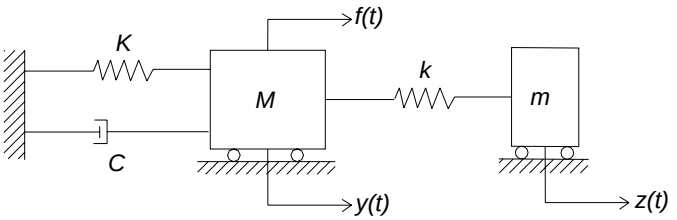

(b)

Figure 5.6 Modeling of the primary beam and absorber beam system; (a) physical model; M_t: mass of motor assembly and connecting rod; (b) a 2-dof mathematical model.

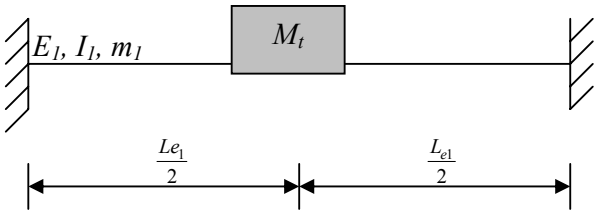

(a)

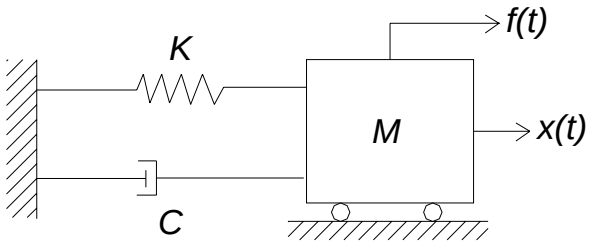

(b)

Figure 5.7 Modeling of the primary beam alone; (a) physical model; M_t: mass of motor assembly; (b) sdof mathematical model

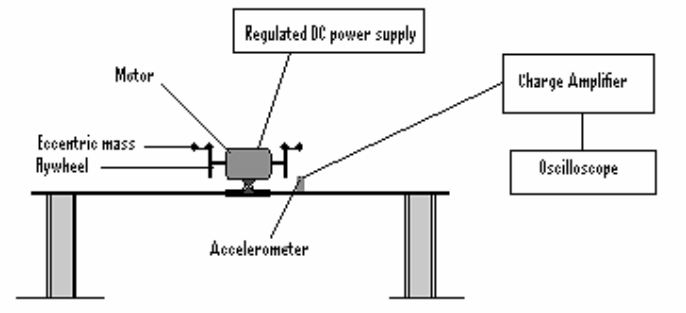

Figure 5.8. Setup for studies on primary beam (without absorber beam).

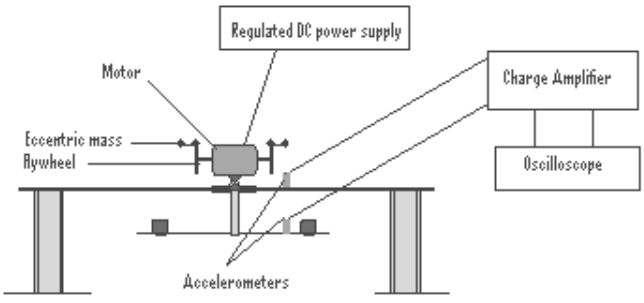

Figure 5.9. Setup for studies on combined system of primary beam and absorber beam.

Table 5.1 Equipments used in free vibration and forced vibration test of DVA

S.No.	Equipments	Quantity
1	Oscilloscope	1
2	Accelerometers	2
3	Transducers conditioning amplifiers	2
4	Regulated DC power supply	1

Table 5.2 Physical properties of parts of the structure

Notation	Part	Material	Mass kg		Material Properties	
			Formula	Value	Young's Modulus (E) N/m^2	Mass density (ρ) kg/m^3
A	Main Beam	Mild Steel	$\rho*D_1*B_1*Le_1$	M_A =	2.10E+11	7800
B	D.C. Motor	-	-	M_B+M_C =	0.69E+11	2700
C	Fly wheel	Aluminum				
D	Eccentric mass	Mild Steel	-	M_D =	2.10E+11	7800
E	Connecting plates	Mild Steel	-	M_E =	2.10E+11	7800
F	Connecting rod	Mild Steel	$\rho*D_c*B_c*Lc$	M_F =	2.10E+11	7800
G	Absorber beam	Aluminum	$\rho*D_2*B_2*L_2$	M_G =	0.69E+11	2700
H	Mass on absorber beam	Mild Steel	$\rho*(pi*D_G^2/4)*T_G$	M_H =	2.10E+11	7800
ac1	Accelrometer1	-	-	M_{ac1}=	-	-
ac2	Accelrometer2	-	-	M_{ac2}=	-	-

Table 5.3 Geometric data of the structure

Part	Dimensions in mm			
	Depth (D)	Width (B)	Length (L)	Effective Length (L_e)
Main beam	D_1=	B_1 =	L_1 =	$L_{e\,1}$=
Absorber beam	D_2=	B_2 =	$^{\#}L_2$=	$L_{e\,2}$ =
Connecting rod	D_c =	B_c =	L_c =	-
Mass on absorber beam	Diameter (D_G)			
	Thickness (T_G)			
Eccentricity of eccentric mass on the flywheel, e=50 mm				
$^{\#}$The absorber is modeled as a cantilever beam. The total length of the absorber beam is 2*L_2				

Table 5.4 Details of the sensors used; *CF*: conversion factor

Sl. No.	Sensor	Sensitivity, S		*CF*	Mass kg
		pC/ms^{-2}	pC/g		
1					
2					

Table 5.5 Free vibration test data on primary beam (without absorber)

S.No.	Quantity	Notation	Observations
1	Amplitude of 0th peak	A_0	
2	Amplitude of nth peak	A_n	
3	Number of cycles	n	
4	Logarithmic decrement	δ	
5	Damping ratio	ζ	

Table 5.6 Forced vibration test data on primary beam (without absorber)

S.No.	Frequency, f (Hz)	Frequency $\omega=2\pi f$ (rad/s)	Amplitude σ rms (mV)	Amplitude $X=\sqrt{2}\ (CF)\ \sigma$ (m)	Force, $F=2M_D e\omega^2$ (N)	Receptance X/F (m/N)
1						
2						
3						
4						
5						
6						
7						
8						
9						
10						
11						
12						
13						
14						
15						
16						
17						
18						
19						
20						

Table 5.7 Free vibration test data on combined system.

S.No.	Quantity	Notation	Observations on primary beam	Observations on absorber beam
1	Amplitude of 0^{th} peak	A_0		
2	Amplitude of n^{th} peak	A_n		
3	Number of cycles	n		
4	Logarithmic decrement	δ		
5	Damping ratio	ζ		
Average value of damping ratio, ζ=				

Table 5.8 Forced vibration test data on combined system; measurement made on main beam

S.No.	Frequency, f (Hz)	Frequency $\omega=2\pi f$ (rad/s)	Amplitude σ rms (mV)	Amplitude $Y=\sqrt{2}\ (CF)\ \sigma$ (m)	Force, $F=2M_D e\omega^2$ (N)	Receptance Y/F (m/N)
1						
2						
3						
4						
5						
6						
7						
8						
9						
10						
11						
12						

13						
14						
15						
16						
17						
18						
19						
20						
21						
22						
23						
24						
25						

Table 5.9 Forced vibration test data on combined system; measurement made on absorber beam

S.No.	Frequency, f (Hz)	Frequency $\omega=2\pi f$ (rad/s)	Amplitude σ rms (mV)	Amplitude $Z=\sqrt{2}\ (CF)\ \sigma$ (m)	Force, $F=2M_D e\omega^2$ (N)	Receptance Z/F (m/N)
1						
2						
3						
4						
5						
6						
7						
8						
9						
10						
11						
12						
13						
14						
15						
16						
17						
18						
19						
20						
21						
22						
23						
24						
25						

EXPERIMENT 6

Dynamics of a four storied building model with and without an open ground floor

6.0 Background

IS 1893 2002 defines a soft story as the story in which lateral stiffness is less than 60% of that in the story above or lass than 70% of the average lateral stiffness of the three stories above. Buildings with soft stories often occur in practice in multi-storied buildings in which the ground floor has an *open* configuration so as to facilitate vehicle parking. Such buildings are often vulnerable to earthquakes [see C V R Murty, 2005, IITK BMTPC Earthquake Tip 21, Why are open-ground storey buildings vulnerable in earthquakes, NICEE Publication, Kanpur]. There have been a large number of instances in which such structures have suffered severe damage or even collapsed during major earthquakes.

The objective of the present experiment is to understand the dynamical behavior of a four-storied building frame model with an open ground floor. To achieve this we consider two frames that are identical in all aspects excepting the fact that one of them has an open ground floor and the other not. Figure 6.1 shows the two frames under study. We use a set of aluminum plates to mimic the action of walls. In frame 6.1a the ground floor has no partition walls while in 6.1b they are present. Because of the absence of walls in 6.1a the lateral stiffness of the ground floor becomes much less than that in other floors and hence the floor is considered to be a soft floor. Figure 6.2 provides the details of the frame structure under consideration. In this experiment we study the natural frequencies, mode shapes and dynamic response under harmonic base motion of the two frames shown in figure 6.1 and analyze the difference in their behavior.

6.1 Mathematical model

The frames shown in figure 6.1 are approximated by a four-dof shear beam models as shown in figure 6.3. It may be noted that the two frames in figure 6.1 can be modeled mathematically by using similar models. The parameters m_1, k_1 and c_1 however, would be different for the two models. Based on the free body diagrams shown in figure 6.3b the following equations of motion can be setup for the system in figure 6.3a:

$$\begin{aligned}
&m_1\ddot{x}_1 + c_1(\dot{x}_1 - \dot{x}_g) + c_2(\dot{x}_1 - \dot{x}_2) + k_1(x_1 - x_g) + k_2(x_1 - x_2) = 0\\
&m_2\ddot{x}_2 + c_2(\dot{x}_2 - \dot{x}_1) + c_3(\dot{x}_2 - \dot{x}_3) + k_2(x_2 - x_1) + k_3(x_2 - x_3) = 0\\
&m_3\ddot{x}_3 + c_3(\dot{x}_3 - \dot{x}_2) + c_4(\dot{x}_3 - \dot{x}_4) + k_3(x_3 - x_2) + k_4(x_3 - x_4) = 0\\
&m_4\ddot{x}_4 + c_4(\dot{x}_4 - \dot{x}_3) + k_4(x_4 - x_3) = 0
\end{aligned} \qquad \ldots(6.1)$$

The equation can be cast in the matrix form as

$$\begin{bmatrix} m_1 & 0 & 0 & 0 \\ 0 & m_2 & 0 & 0 \\ 0 & 0 & m_3 & 0 \\ 0 & 0 & 0 & m_4 \end{bmatrix}\begin{Bmatrix} \ddot{x}_1 \\ \ddot{x}_2 \\ \ddot{x}_3 \\ \ddot{x}_4 \end{Bmatrix}+\begin{bmatrix} c_1+c_2 & -c_2 & 0 & 0 \\ -c_2 & c_2+c_3 & -c_3 & 0 \\ 0 & -c_3 & c_3+c_4 & -c_4 \\ 0 & 0 & -c_4 & c_4 \end{bmatrix}\begin{Bmatrix} \dot{x}_1 \\ \dot{x}_2 \\ \dot{x}_3 \\ \dot{x}_4 \end{Bmatrix}+\begin{bmatrix} k_1+k_2 & -k_2 & 0 & 0 \\ -k_2 & k_2+k_3 & -k_3 & 0 \\ 0 & -k_3 & k_3+k_4 & -k_4 \\ 0 & 0 & -k_4 & k_4 \end{bmatrix}\begin{Bmatrix} x_1 \\ x_2 \\ x_3 \\ x_4 \end{Bmatrix}= \quad \ldots(6.2)$$
$$\begin{bmatrix} c_1+c_2 & -c_2 & 0 & 0 \\ -c_2 & c_2+c_3 & -c_3 & 0 \\ 0 & -c_3 & c_3+c_4 & -c_4 \\ 0 & 0 & -c_4 & c_4 \end{bmatrix}\begin{Bmatrix} 1 \\ 1 \\ 1 \\ 1 \end{Bmatrix}\dot{x}_g+\begin{bmatrix} k_1+k_2 & -k_2 & 0 & 0 \\ -k_2 & k_2+k_3 & -k_3 & 0 \\ 0 & -k_3 & k_3+k_4 & -k_4 \\ 0 & 0 & -k_4 & k_4 \end{bmatrix}\begin{Bmatrix} 1 \\ 1 \\ 1 \\ 1 \end{Bmatrix}x_g$$

In a more compact form, the equation reads

$$[M]\{\ddot{x}\}+[C]\{\dot{x}\}+[K]\{x\}=[C]\{\Gamma\}\dot{x}_g+[K]\{\Gamma\}x_g \quad \ldots(6.3)$$

Here Γ is a column vector of ones of size 4×1. It may be recalled that in Experiment 1 we have analyzed this type of models and also have discussed the methods to determine the parameters of the models. Here, while the analysis procedure remains the same, the method for determination of model parameters, especially, the stiffness parameters $\{k\}_{i=1}^{4}$, becomes complicated due to presence of the stiffeners that represent the partition walls. To circumvent this difficulty, we propose to evaluate the inter-storey stiffness by studying a single storey frames as shown in figure 6.4 and 6.5. Here we excite the single storey frames by harmonic base motions and determine the frequency ω_n at which the resonance occurs. By estimating the mass participating in vibration, the inter-storey stiffness can be evaluated by using the formula $K=\omega_n^2 M$. Clearly, in evaluating the mass participating in vibration, the presence (or absence) of partition walls need to be taken into account. Thus, by denoting the stiffness of a frame with open storey as K_{open} and frame with closed storey as K_{close}, we can determine now the parameters of the model in equation 6.2. Thus one gets, for frame with open ground floor $k_1=k_{open}; k_2=k_3=k_4=k_{close}$ and for frame with closed ground floor, $k_i=k_{close}; i=1,2,3,4$. Similarly, m_1 = $M_c+M_s+0.5(M_{sa}+M_{sb})$ or m_1 = M_c+M_s+ $(M_{sa}+M_{sb})$ depending on whether the structure has soft first storey or not. The other mass parameters are determined as

$m_2 = M_c+M_s+ (M_{sa}+M_{sb})$;
$m_3 = M_c+M_s+ (M_{sa}+M_{sb})$;
$m_4 = 0.5M_c+M_s+0.5(M_{sa}+M_{sb})$ …(6.4)

Here M_c=mass of columns, M_s=mass of slabs, M_{sa}=mass of stiffner A, M_{sb}=mass of stiffener B; see figure 6.2 and Table 6.1.

The undamped natural frequencies and modal vectors can be computed for the mathematical model by solving the eigenvalue problem $K\phi=\omega^2 M\phi$. These solutions, in turn, can be used to evaluate the forced response analysis by assuming that the undamped modal matrix would diagonalize the damping matrix also. Alternatively, solution to equation 6.3 can also be constructed by noting that, under harmonic excitations, the system would respond harmonically at the driving frequency as time becomes large. Accordingly, when $x_g(t)=X_g \exp[i\omega t]$ we can take the solution to be of the form $x(t)=X(\omega)\exp[i\omega t]$ as $t\to\infty$. This leads to

$$\{X(\omega)\} = \left[-\omega^2 M + i\omega C + K\right]^{-1}\left[i\omega C + K\right]\{\Gamma\}X_g \quad \ldots(6.5)$$

The matrix $\left[-\omega^2 M + i\omega C + K\right]$ can be thought of as the stiffness matrix of the structure that includes the effects of mass and damping and therefore, is referred to as the dynamic stiffness matrix. Refer to Appendix A for details on response analysis using normal mode expansion.

The evaluation of damping matrix generally presents greater difficulty. Here one could estimate the modal damping values by performing either the logarthimic decrement test or by using the half-power bandwidth method.

Figure 6.6 illustrates the first mode shape for the frame structure with and without open ground floor. From the mode shapes it could be observed that, for frame with open ground floor, the deformation is mainly concentrated in the ground floor. Consequently, the columns in the ground floor would attract higher loads. If these columns are not adequately designed to take into account these increased demands, they are susceptible to failure. The failure of ground floor columns has catastrophic consequence to the building no matter how strong the building parts are at higher elevations. In contrast, the mode shape for frame without open ground floor shows no abrupt changes in the mode shape thereby indicating no likelihood of load concentration in columns at different floors.

6.2 Experimental procedure

6.2.1 Instruments and sensors

Table 6.1 provides the details of instruments to be used in the experimental study.

6.2.2 Preliminary measurements and analysis

1) Collect the data pertaining to geometric and material properties of the two frames (tables 6.2 and 6.3). Parts of data in table 6.2 have to be obtained from the instructor/handbooks.
2) Study the charts/manuals that accompany the sensors and the charge amplifiers and note down the sensor sensitivities, sensor mass and factors to convert the measured electrical signal into mechanical units; this depends upon the amplifier settings used- see table 6.4.
3) Mount the one-storey frames on the shake table as shown in figure 6.4 and 6.5. Excite the frames by harmonic base motion by varying the driving frequency. At every instance of change in frequency ensure that the system reaches steady state by allowing the frame to oscillate for about 30-50 cycles. Determine the frequency at which resonance occurs. A simpler alternative would be to set the frame structures into free vibration by gently pulling the slab and releasing it. From the trace of the free vibration decay one could not only estimate damping but also approximately determine the natural frequency. If you use this alternative record your observations as per format in Table 6.5a and b. The damping value obtained in this step, could, to a first approximation, be

used as modal damping values for the four storied frame structures under study.

4) Estimate the inter-story stiffness for open and closed stories using the data on natural frequency obtained in the previous step.

5) Determine all the parameters of the stiffness and mass matrices for the two four storied frames. Perform the free vibration analysis and determine the natural frequencies and mode matrix.

6.2.3 Four storied frames under harmonic base motion

1) Arrange the experimental setup as shown in figures 6.7a and b; also see figure 6.1. Note that the accelerometer needs to be placed on the slab in such a way that displacement along *x*-direction is picked up.
2) Set the frame into free vibration by applying an initial displacement. This can be achieved by gently pulling the frame at about the top slab and releasing it. Evaluate the logarithmic decrement and hence the damping ratio. One model for the damping can be obtained by assuming that the damping ratio so determined would remain constant for all the modes.
3) Run the base motion test on the frame at different values of motor RPM making sure that readings at resonant frequencies are not missed. For a given motor RPM, allow the frame to oscillate for a few seconds so that the frame reaches its steady state. At this stage measure the amplitude of the frame response by using time history of displacement response acquired on the oscilloscope and record the amplitude data as in tables 6.6 and 6.7. Note that the frequency of driving and the frequency of structural response can be assumed to be equal and this can be measured from the trace of displacement response on the oscilloscope. It may be noted that the test could be conducted even if only two channel measurements are possible, in which case, the above steps need to be repeated suitably.
4) The frequencies at which the structure undergoes resonance can be identified by observing the variation of response amplitudes as motor RPM is varied. At resonant conditions, in addition to noting the amplitude of slab oscillations, also note if the slabs are vibrating in phase or not. Based on this information the modal vectors for the first three modes could be established. Compare these mode shapes with the analytical mode shapes obtained in step 6.2.2.5.
5) Plot $\{X\}_{i=1}^{4}$ versus *f*.
6) From the plots in the previous step estimate the modal damping either by half-power bandwidth method or by relating the peak amplitude to the modal damping (see M Paz, 1984, Structural dynamics, CBS Publishers, New Delhi, for details).
7) Using the modal damping ratios obtained in steps (c),(g) or (k) determine the C matrix using the relation $C = \left[\Phi^t\right]^{-1}[\Xi]\left[\Phi\right]^{-1}$ where Ξ is a diagonal matrix with entry on the n^{th} row being $2\eta_n\omega_n$. It cn be shown that $\left[\Phi^t\right]^{-1} = M\Phi$ and $\left[\Phi\right]^{-1} = \Phi^t M$, and, therefore, one gets $C = M\Phi\Xi\Phi^t M$ (see Appendix A). Using this C matrix and equation 6.3, solve the mathematical model to determine analytically the amplitude of floor responses as a function of the

driving frequency. Compare these analytical predictions with the measured frequency response functions.

6.2.4 Report submission

1. Document the experimental observations and the deductions as per the format given in tables 6.2-6.9.
2. Develop the mathematical model as per the simplifications suggested in figure 6.3.
3. Document the plots of floor response amplitudes as a function of the driving frequency obtained using analysis as well as experiment. Discuss the qualitative features of these plots. Explain the mutual agreement/disagreement between theoretical and experimental results.
4. Discuss the difference in the displacement behavior of the frames with and without open ground floor.
5. Estimate the forces in the different columns (that is, spring forces in figure 6.3) as a function of driving frequency for the two frames. Discuss the nature of these forces.
6. Respond to the following questions

    a. In the present study we have studied the effect of having a soft storey in the ground floor. What would happen if intermediate stories happen to be soft stories?
    b. Often soft stories also tend to be weak stories. That is, just as they are deficient in stiffness they could also be deficient in strength. Discuss qualitative nature of seismic response of a frame that has a weak and a soft ground floor.
    c. Do you foresee any problems in the frame behavior if instead of stiffness being irregularly distributed, the mass is irregularly distributed.
    d. In this experiment we have studied the effect of irregular distribution of stiffness in building elevation. In experiment 2 we have studied the effect of irregular distribution of stiffness and/or mass in plan. Discuss qualitative behavior under earthquake loads of a multi-storey frame that has unsymmetric plan and has soft ground storey.

(a) (b)

Figure 6.1 Model for a four-storied building frame; (a) frame with a open ground floor; (b) frame with a “closed” ground floor.

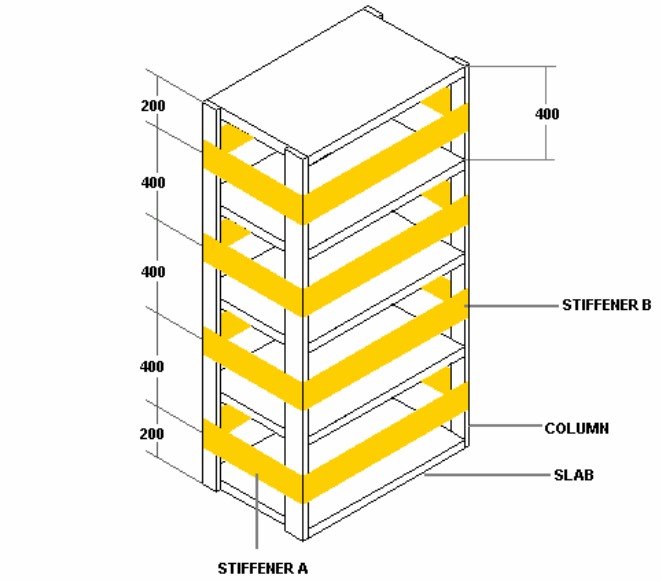

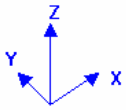

Sl.no.	Description	Material	Dimension	Quantity
1	Slab	Aluminum	300*150*12.7	5
2	Column	Aluminum	1600*25.1*6	4
3	Stiffener A	Aluminum	150*160*2	8
4	Stiffener B	Aluminum	312*160*2	8

All dimensions in mm
Note: The slabs are equally spaced

Figure 6.2 Details of the building frame.

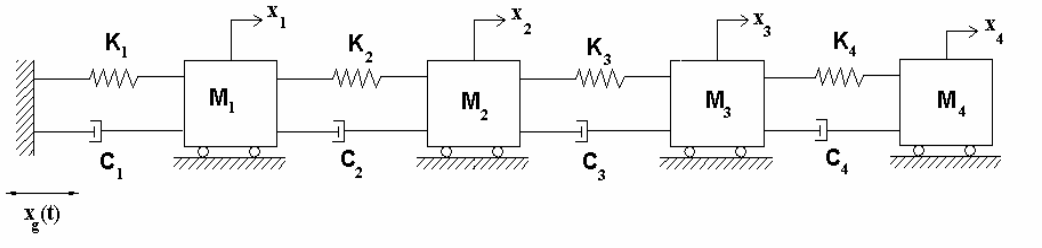

(a)

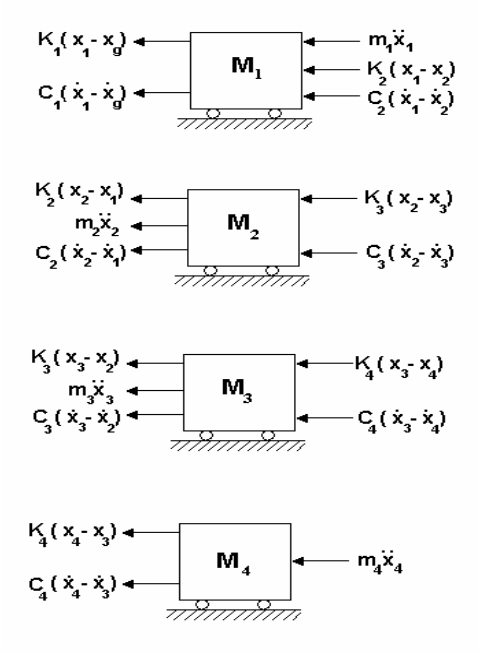

(b)

Figure 6.3 Model for the dynamics of frames (a) a four dof shear beam model; (b) free body diagrams.

(a)

(b)

Figure 6.4 Setups for measuring inter-storey stiffness; (a) open floor; (b) closed floor.

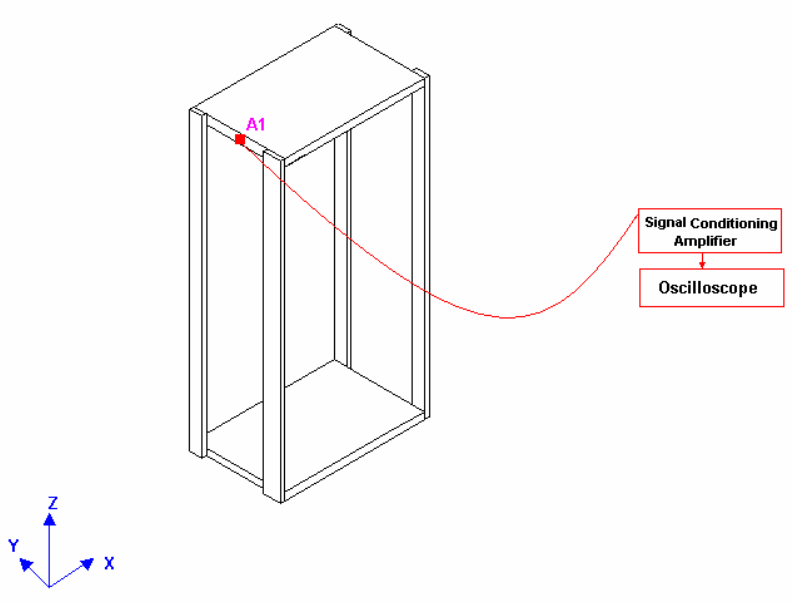

(a)

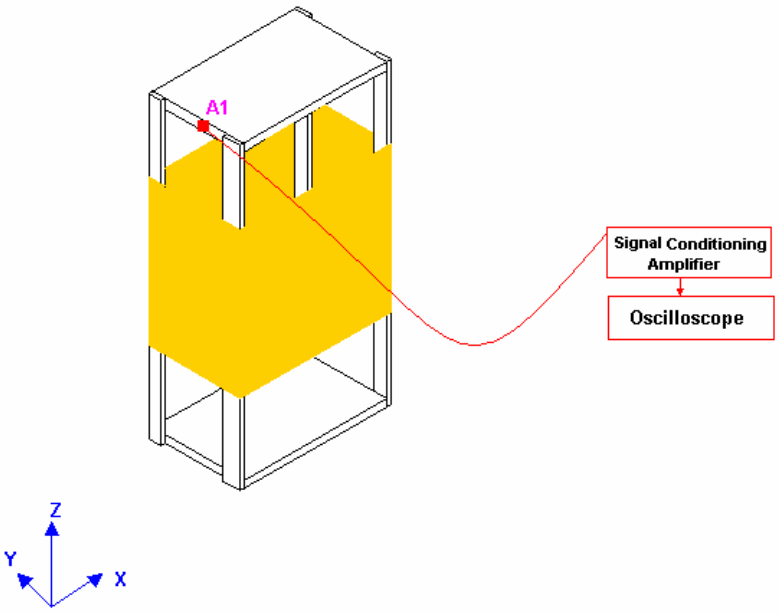

(b)

Figure 6.5 Measurement of inter-storey stiffness by measuring first natural frequency; (a) open floor; (b) closed floor; the frames would be subjected to harmonic base motions in the *x*-direction.

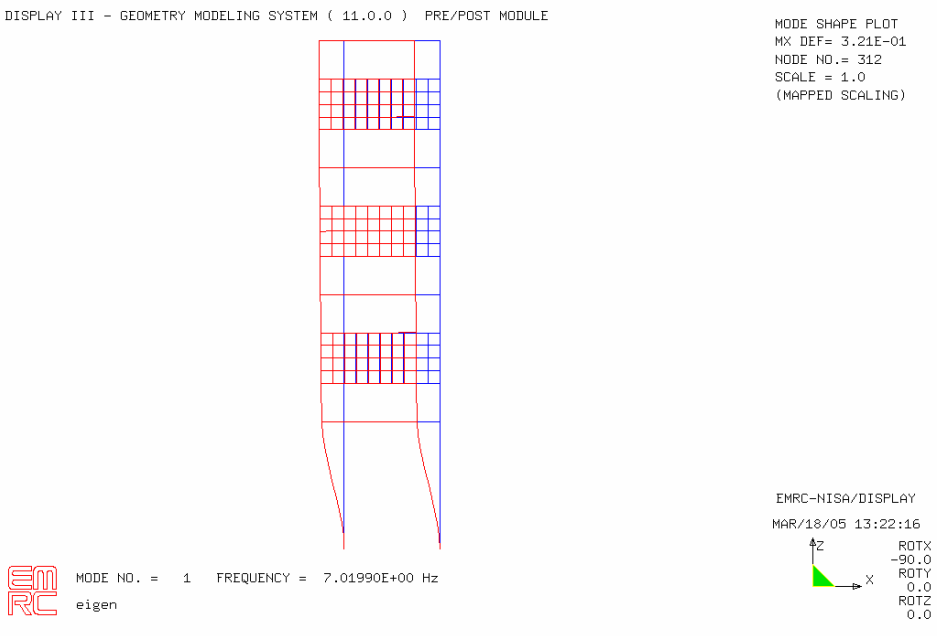

(a)

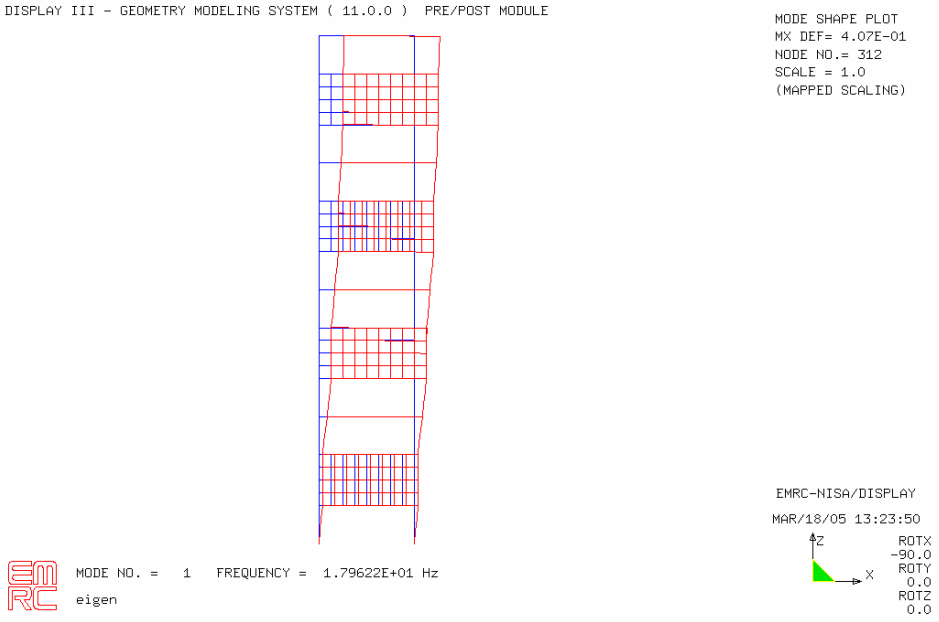

(b)

Figure 6.6 Fundamental mode shape of the four storey frame using finite element analysis; (a) structure with soft first storey; (b) structure without soft first storey; note that the stiffeners here have been modeled using shell elements.

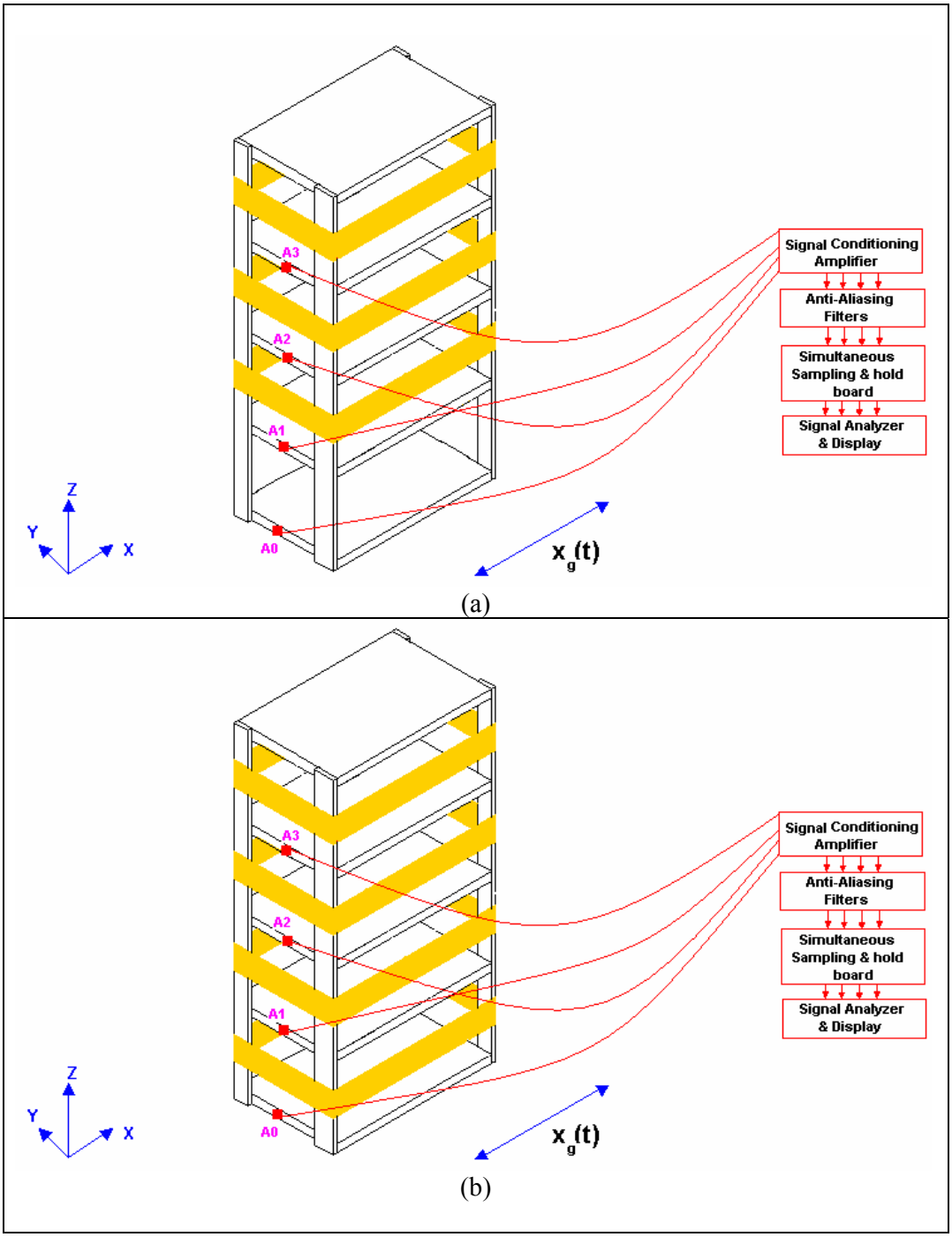

Figure 6.7 Setup for harmonic base motion test (a) frame with open ground floor; (b) frame with closed ground floor.

Table 6.1 Equipments used in forced vibration test of four-story shear building frame

Sl.No.	Equipments	Quantity
1	Accelerometers	4
2	Nexus conditioning amplifier	1
3	Shake Table	1
4	Data Acquisition System	1

Table 6.2 Physical properties of parts of the structure

Sl. No.	Part	Material	Mass kg	Material Properties	
				Young's Modulus (E) N/m^2	Mass density (ρ) kg/m^3
1	Column	Aluminum	M_c =		
2	Slab	Aluminum	M_s =		
3	Stiffener A	Aluminum	M_{sa} =		
4	Stiffener B	Aluminum	M_{sb} =		

Table 6.3 Geometric data of the structure

Sl. No.	Part	Dimensions in mm		
		Depth	Width	Length
1	Slab			
2	Column			
3	Stiffener A			
4	Stiffener B			

Table 6.4 Details of the sensors used

Sl. No.	Sensor	Sensitivity, S		Mass gm
		mV/ms^{-2}	mV/g	
1				
2				
3				
4				

Table 6.5a Free vibration test data for the one storey structure without walls

S.No.	Quantity	Notation	Observations
1	Amplitude of 0^{th} peak	A_0	
2	Amplitude of n^{th} peak	A_n	
3	Number of cycles	n	
4	Logarithmic decrement	δ	
5	Damping ratio	ζ	
6	Experimental Frequency	f	
7	Total mass (SDOF approximation)	M_1	
8	Stiffness (from experiment)	K_{exp}	

Table 6.5b Free vibration test data for the one storey structure with walls

S.No.	Quantity	Notation	Observations
1	Amplitude of 0^{th} peak	A_0	
2	Amplitude of n^{th} peak	A_n	
3	Number of cycles	n	
4	Logarithmic decrement	δ	
5	Damping ratio from modal analysis	ζ	
6	Experimental Frequency	f_s	
7	Total mass (SDOF approximation)	M_2	
8	Stiffness (from experiment)	K_{exps}	

Table 6.6 Base motion test data on four storey building frame with soft first storey

Sl.no	Frequency (Hz)	Base motion Amplitude $\sigma_x * 10^{-4}$ rms (V)	First floor Amplitude $\sigma_{x1} * 10^{-4}$ rms (V)	Second floor Amplitude $\sigma_{x2} * 10^{-4}$ rms (V)	Third floor Amplitude $\sigma_{x3} * 10^{-4}$ rms (V)	Base motion Displacement Amplitude $X = \sqrt{2}\ \sigma x$ (m) $*10^{-4}$	First floor Displacement Amplitude $X_1 = \sqrt{2}\ \sigma x_1$ (m) $*10^{-4}$	Second floor Displacement Amplitude $X_2 = \sqrt{2}\ \sigma x_2$ (m) $*10^{-4}$	Third floor Displacement Amplitude $X_3 = \sqrt{2}\ \sigma x_3$ (m) $*10^{-4}$
1									
2									
3									
4									
5									
6									
7									
8									
9									
10									
11									
12									
13									
14									
15									
16									
17									
18									
19									
20									

Table 6.7 Base motion test data on four storey building frame without soft first storey

Sl.no	Frequency (Hz)	Base motion Amplitude $\sigma_x * 10^{-4}$ rms (V)	First floor Amplitude $\sigma_{x1} * 10^{-4}$ rms (V)	Second floor Amplitude $\sigma_{x2} * 10^{-4}$ rms (V)	Third floor Amplitude $\sigma_{x3} * 10^{-4}$ rms (V)	Base motion Displacement Amplitude $X = \sqrt{2}\ \sigma x$ (m) $*10^{-4}$	First floor Displacement Amplitude $X_1 = \sqrt{2}\ \sigma x_1$ (m) $*10^{-4}$	Second floor Displacement Amplitude $X_2 = \sqrt{2}\ \sigma x_2$ (m) $*10^{-4}$	Third floor Displacement Amplitude $X_3 = \sqrt{2}\ \sigma x_3$ (m) $*10^{-4}$
1									
2									
3									
4									
5									
6									
7									
8									
9									
10									
11									
12									
13									
14									
15									
16									
17									
18									
19									
20									

Table 6.8 Estimate of the first natural frequency of the building frame with and without soft first story

Frame with soft first story		Frame without soft first story	
Analytical	Experimental	Analytical	Experimental

Table 6.9 Estimate of the fundamental mode shape of the building frame with and without soft first story

Frame with soft first story		Frame without soft first story	
Analytical	Experimental	Analytical	Experimental

Experiment 7

Dynamics of one-span and two-span beams.

7.0 Background

The study of behavior of bridge structures subjected to dynamic effects of moving loads, wind and earthquake loads is of considerable interest in civil engineering. Similarly, vibration analysis of piping structures in industrial plants subjected to earthquake loads is also of significant interest. These structures can be idealized as simple beam structures for the purpose of preliminary studies. In the present experiment we study the responses of one span and two span simply supported beams to harmonic excitations. The treatment of dynamic behavior of such beams, as distributed parameter dynamical systems, is contained in many books: see, for instance, the book by Paz (1984), in which singe-span beams, modeled as Euler-Bernoulli beams, with different boundary conditions (free, simply supported or clamped), is discussed in detail. Figures 7.1 and 7.2 show the structure under study. For the purpose of this study, we model these two structures as systems with two-degrees of freedom. The degrees of freedom considered are the translations at quarter points of the single-span beam and mid-span points for the two-span beam. The mass matrix is obtained by lumping the masses at the quarter points (for simple supported beam) and at mid-span points (for two-span beam). For the purpose of evaluating the stiffness matrix, you would need to employ one of the methods for computing deflections of beam structures under concentrated loads.

7.1 Experimental set-up

The beam structures shown in figures 7.1 and 7.2 are supported on special clamping devices that are designed to simulate simple support conditions. The intermediate support (figure 7.1b and 7.2b) is detachable so that, upon the removal of the support, the structure reduces to a one-span beam structure shown in figures 7.1a and 7.2a. In both these cases the beam is driven at a distance of 300 mm from the right hand support by an electric motor with eccentric mass and whose speed can be controlled. An auxiliary dummy mass equal to the mass of the motor is placed at 300 mm from the left end support so as to achieve a structure which is symmetric about x=600 mm. The setup used for conducting the experiment is depicted in figure 7.3. The force transmitted by the motor is deduced by measuring the motor RPM and knowing the eccentric mass and its eccentricity.

7.2 Mathematical models

As has been already noted, we propose to model the two beam structures using two-dof models. The governing equations in this case would be of the form

$$\begin{bmatrix} m_{11} & 0 \\ 0 & m_{22} \end{bmatrix} \begin{Bmatrix} \ddot{x}_1 \\ \ddot{x}_2 \end{Bmatrix} + \begin{bmatrix} c_{11} & c_{12} \\ c_{12} & c_{22} \end{bmatrix} \begin{Bmatrix} \dot{x}_1 \\ \dot{x}_2 \end{Bmatrix} + \begin{bmatrix} k_{11} & k_{12} \\ k_{12} & k_{22} \end{bmatrix} \begin{Bmatrix} x_1 \\ x_2 \end{Bmatrix} = \begin{Bmatrix} 0 \\ F \end{Bmatrix} \exp(i\omega t) \qquad \ldots(7.1)$$

The mass matrix coefficients for one span beam is given by,

$m_{11} = 0.5*M_A + M_E + M_F$

$m_{22} = 0.5*M_A + M_B + M_C + 2*M_{D1} + M_F$

and for two span beam,

$m_{11} = 0.25*M_A + M_E + M_F$

$m_{22} = 0.25*M_A + M_B + M_C + 2*M_{D2} + M_F$

Here M_A = Mass of main beam, M_B = Mass of motor, M_C = mass of flywheel, M_{D1} and M_{D2} = eccentric mass on the flywheel, M_E = mass of lumped mass and M_F = base plate mass.

It may be noted that, for one span beam, the contribution to mass due to distributed mass of the beam is evaluated by assuming $y(x,t) = \sin(\pi x / L)\,\phi(t)$ leading to

$$\frac{1}{2}\int_0^L m\left\{\sin^2\frac{\pi x}{L}\right\}\dot{\phi}^2(t)\,dx = 2\times\frac{1}{2}M^*\left\{\sin\left(\frac{\pi}{L}\cdot\frac{L}{4}\right)\right\}^2\dot{\phi}^2(t)\,dx$$

$$M^* = \frac{mL}{2}$$

$$= 0.5 * M_A$$

Similarly, for the two span beam, it is assumed that $y(x,t) = \sin(2\pi x / L)\,\phi(t)$ leading to

$$\frac{1}{2}\int_0^{L/2} m\left\{\sin^2\frac{2\pi x}{L}\right\}\dot{\phi}^2(t)\,dx = \frac{1}{2}M^*\left\{\sin\left(\frac{2\pi}{L}\cdot\frac{L}{4}\right)\right\}^2\dot{\phi}^2(t)\,dx$$

$$M^* = \frac{mL}{4}$$

$$= 0.25 * M_A$$

To construct the stiffness matrix for the case of single span beam, we consider the loading configurations as shown in figure 7.4a and 7.4b. With reference to the notations used in this figure, the flexibility and stiffness matrices for the system are given respectively by

$$S = \begin{bmatrix} y_{11} & y_{12} \\ y_{21} & y_{22} \end{bmatrix} \;\&\; K = S^{-1} = \begin{bmatrix} y_{11} & y_{12} \\ y_{21} & y_{22} \end{bmatrix}^{-1} \qquad \ldots(7.2)$$

The same expression would be valid for the two-span beam with the modifications that the deflections $y_{ij}, i,j=1,2$ are now interpreted with reference to figure 7.4c and 7.4d. The evaluation of the damping matrix would be based on experimental results and this would be elaborated later in this document. Once the structural matrices have been formulated the solution of equation 7.1 proceeds along the lines outlined in Appendix A. Thus, one can either use the normal mode expansion method or the dynamic stiffness matrix

approach to obtain the solutions. The latter solution would be valid only in the steady state and will be of the form

$$x(t) = X(\omega)\exp(i\omega t)$$
$$X(\omega) = [-\omega^2 M + i\omega C + K]^{-1}\{f\} \quad \ldots(7.3)$$

Here *M,C* and *K* are, respectively, the mass, damping and stiffness matrices and *f* is the force vector. It is of interest to note that the mode shapes of the two-span beam has interesting resemblance to the mode shapes of simply supported beams and propped cantilever beams. This feature can be observed from figure 7.5, wherein, the first five mode shapes for a single-span simply supported beam, a single-span propped cantilever beam and a two span continuous beam with simple supports and equal spans, are shown. It may be noted that the span of the two single-span beams are equal and are two times the individual spans of the continuous beam. It can be seen that the first mode of the two-span beam is identical to the second mode of the simply supported one-span beam. Similarly, in the second mode of the continuous beam, the deflected profile of the individual spans resembles the mode shape of the single span propped cantilever beam. Similar features associated with the higher modes of the beams could also be deduced. It may be noted that the mode shapes shown in figure 7.5 have been obtained using finite element method and these models take into account the presence of concentrated masses at the quarter points of the beams.

7.3 Experimental Procedure

7.3.1 Instruments and sensors

Table 7.1 provides the details of the instruments and sensors used in this experiment.

7.3.2 Initial measurements

- Collect the data pertaining to geometric and material properties of the vibrating system (tables 7.2 and 7.3). Parts of data in table 7.2 have to be obtained from instructor/handbooks.
- Study the charts/manuals that accompany the sensors and the charge amplifiers and note down the sensor sensitivities, sensor mass and factors to convert the measured electrical signal into mechanical units; this depends upon the amplifier settings used- see table 7.4.

7.3.3 Studies on one-span beam

- Arrange the experimental setup as shown in figure 7.3a.
- Set the beam into free vibration by applying an initial displacement. This can be achieved by gently pulling down the beam at about the mid-span and releasing it. Observe the free vibration decay on the oscilloscope and record the results as per the format given in table 7.5. Evaluate the logarithmic decrement and hence the damping ratio. As a first

approximation this value of damping could be assumed to be valid for all the modes.

- Run the forced vibration test on the beam at different values of motor RPM. Vary the RPM so that you cross the first two resonances of the beam. Under the resonant conditions observe if the two masses are oscillating in phase or not.
- For a given motor RPM, allow the beam to oscillate for a few cycles so that the beam reaches its steady state. At this stage, measure the amplitude of the beam responses by using time history of displacement response acquired on the oscilloscope and record the amplitude data as in table 7.6. Note that the frequency of driving and the frequency of structural response can be assumed to be equal and this can be measured from the trace of displacement response on the oscilloscope.
- Using the modal damping ratios obtained in the above step determine the C matrix using the relation $C = \left[\Phi^t\right]^{-1}[\Xi]\left[\Phi\right]^{-1}$ where Ξ is a diagonal matrix with entry on the n^{th} row being $2\eta_n\omega_n$. It can be shown that $\left[\Phi^t\right]^{-1} = M\Phi$ and $\left[\Phi\right]^{-1} = \Phi^t M$, and, therefore, one gets $C = M\Phi\Xi\Phi^t M$ (see Appendix A). Using this C matrix, solve the mathematical model to determine analytically the amplitude of floor responses as a function of the driving frequency (see equations 7.1 and 7.2). Compare these analytical predictions with the measured frequency response functions.
- Plot the variations of X_1/F and X_2/F versus f and compare this plot with the results from mathematical model of the structure.

7.3.4 Studies on two-span beam

These steps are essentially similar to the steps adopted for studying the one-span beam (see section 7.3.3). Here the set-up needs to be according to figure 7.3b. The measurements on damping and forced response need to be recorded as per the formats given in Tables 7.5 and 7.7.

7.4 Report preparation

1. Evaluate the 2×2 flexibility matrices for the one-span and two-span beams using any method of structural analysis that you are familiar with. Derive equation 7.1.
2. Analyze the mathematical model and obtain predictions on variations of X_1/F and X_2/F versus f for the two beams.
3. Document the experimental observations as per format given in tables 7.2-7.7.
4. Compare the experimentally observed plots of X_1/F and X_2/F versus f for the two beams with corresponding predictions from the mathematical model. Discuss the qualitative features of these plots and explain the mutual agreement/disagreement between theoretical and experimental results.
5. Respond to the following questions:
   (a) Explain the mutual agreement/disagreement between the analytical predictions and experimental results on beam responses.

(b) Explain the relationship between the normal modes of the two-span beam with those of one span simple supported and propped cantilever beams. What would happen if the two-span beam had unequal spans?
(c) What modifications would you make to the mathematical model for the beam structures if the beams were to be subjected to dynamic support motions, and moving loads?
(d) List the features that you would expect in the earthquake response of bridges as their span becomes longer.
(e) Piping structures in industrial plants are supported at different levels within a civil structure. Discuss how you would analyze the response of such piping structures to earthquake loads.

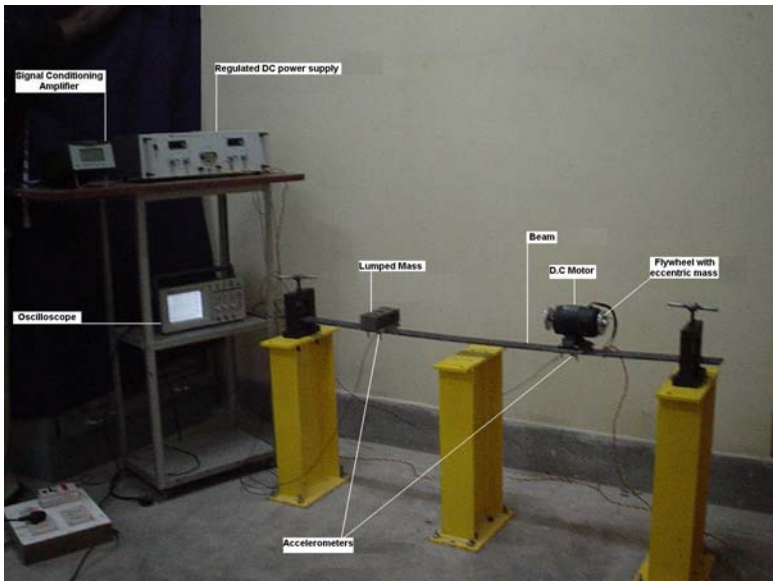

(a)

(b)

Figure 7.1 The test rig showing the beam structure under study; (a) one-span beam; (b) two-span beam. The intermediate support in figure (b) can be removed to obtain the one-span beam of figure (a).

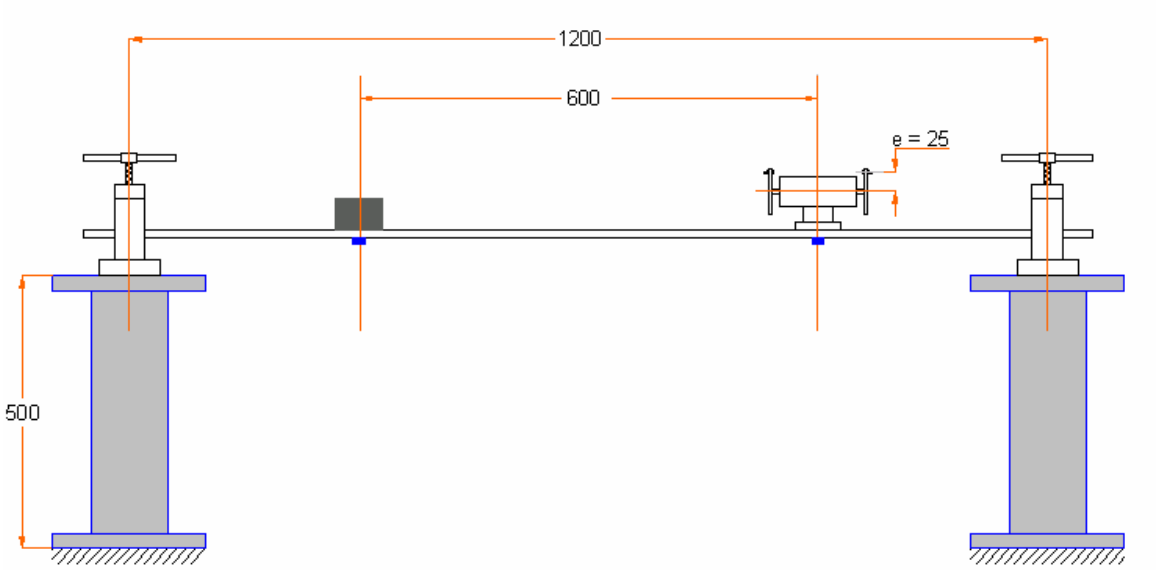

(a)

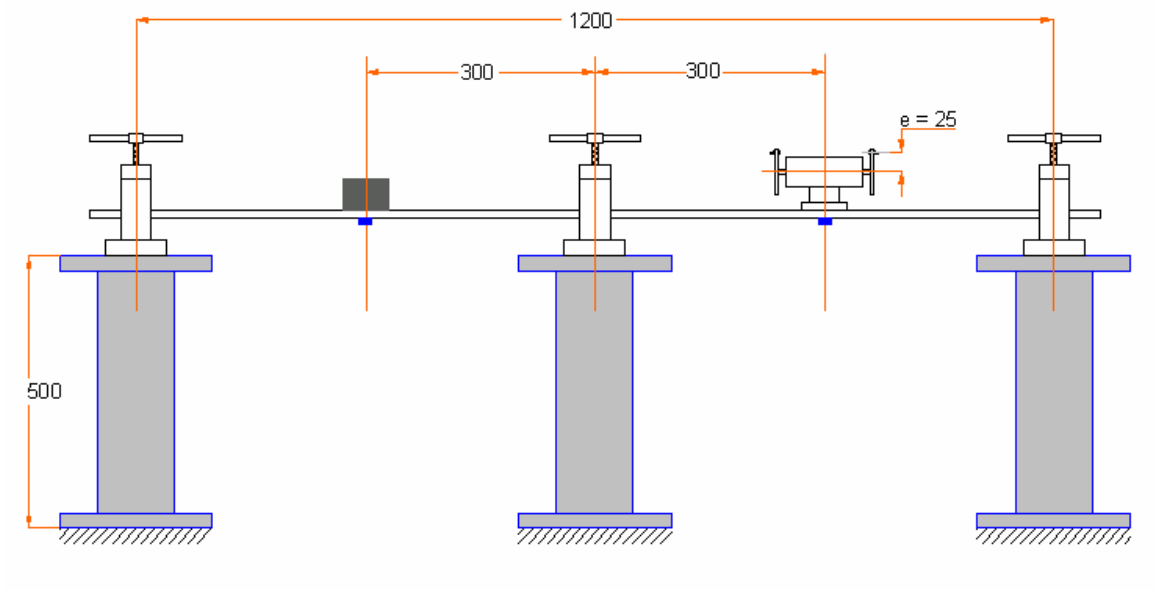

(b)

Figure 7.2 Details of the beam structure under study; (a) one-span beam; (b) two-span beam.

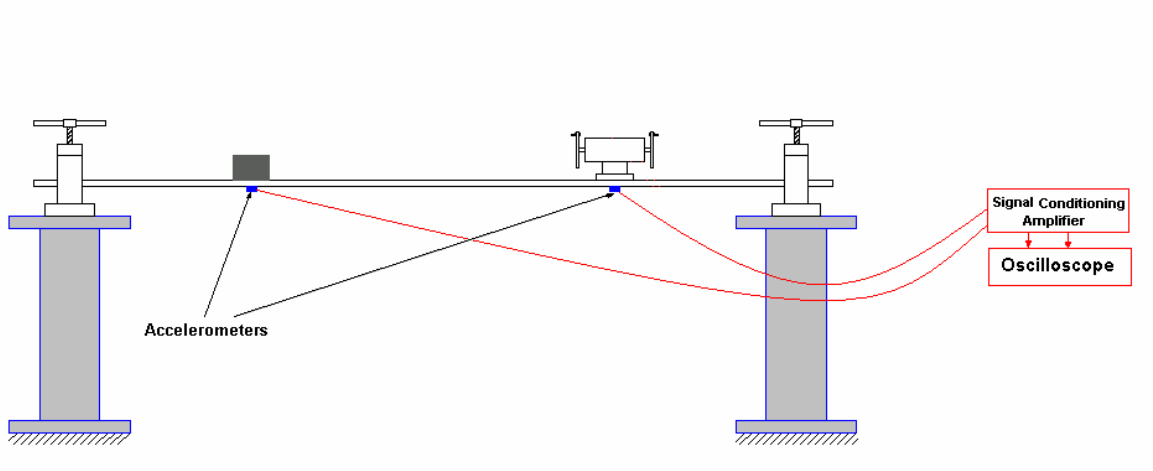

(a)

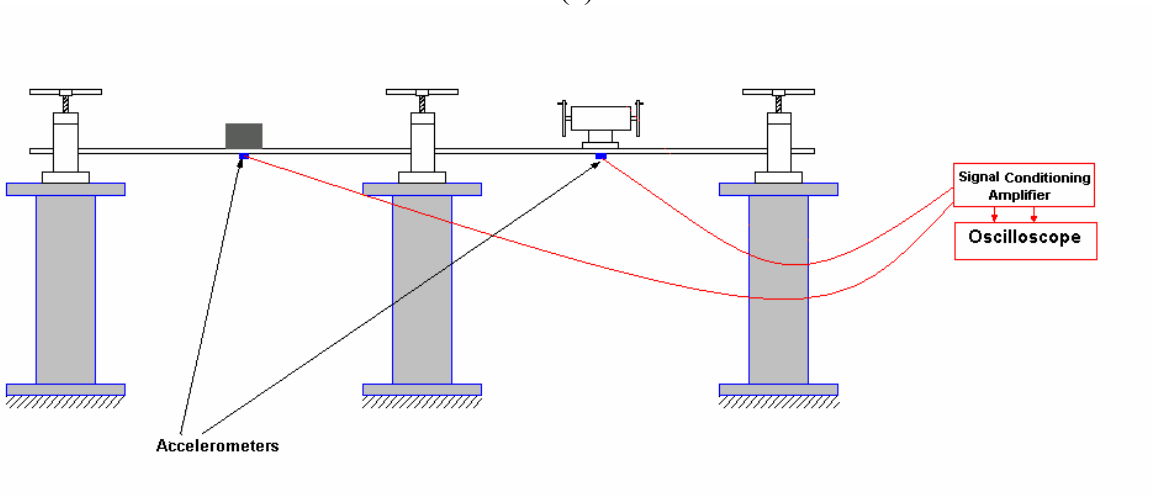

(b)

Figure 7.3 Setup for measurement; the force transmitted by the motor is deduced by measuring the motor RPM and knowing the eccentric mass.

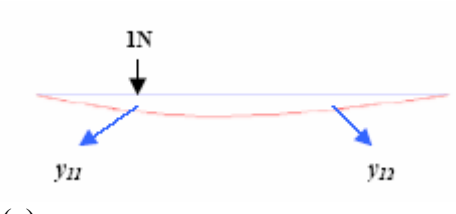

(a)

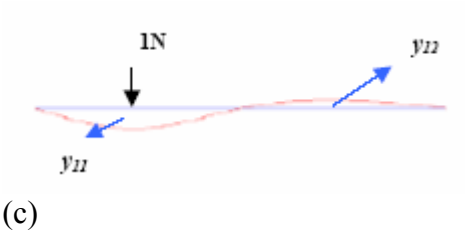

(c)

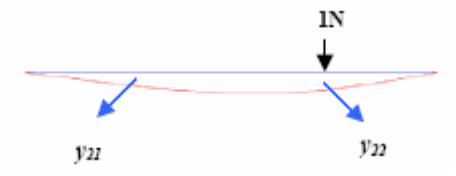

(b)

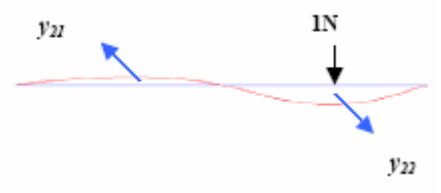

(d)

Figure 7.4 Calculation of flexibility matrix for the beam structures; (a) and (b): single-span beam; (c) and (d): two-span beam.

Figure 7.5 First five mode shapes of a single-span simply supported beam, a single-span propped cantilever beam and a two-span simply supported continuous beam.

Table 7.3 Equipment used in free vibration and forced vibration test of Simply supported beam & Continouos beam

S.No.	Equipments	Quantity
1	Oscilloscope	1
2	Accelerometers	2
3	Signal conditioning amplifier	1
4	Regulated DC power supply	1
5	D.C Motor	1

Table 7.4 Physical properties of parts of the structure

Part	Material	Mass Kg	Material Properties	
			Young's Modulus (E) N/m^2	Mass density (ρ) kg/m^3
Main Beam	Mild Steel	M_A =		
D.C. Motor	-	M_B+M_C=		
Fly wheel	Aluminum			
Eccentric mass (Simply supported beam)	Mild Steel	M_{D1} =		
Eccentric mass (Continuous beam)	Mild Steel	M_{D2} =		
Lumped Mass	Mild Steel	M_E =		
Base plate	Mild Steel	M_F =		

Table 7.3 Geometric data of the structure

Part	Dimensions in mm			
	Depth (D_A)	Width (B_A)	Length (L_A)	Effective Length (L_e)
Main beam				
Eccentricity of eccentric mass on the flywheel, e=				
Formula for calculating, $M_A = D_A * B_A * L_e * \rho$				

Table 7.4 Details of the sensors used

Sl. No.	Sensor	Sensitivity, S		Mass Gm
		mV/ms^{-2}	mV/g	
1				
2				

Table 7.5 Free vibration test data on simply supported beam (observations I) and continuous beam (observations II)

S.No.	Quantity	Notation	Observations I	Observations II
1	Amplitude of 0^{th} peak	A_0		
2	Amplitude of n^{th} peak	A_n		
3	Number of cycles	n		
4	Logarithmic decrement	δ		
5	Damping ratio	ζ		

Table 7.6 Forced vibration test data on simply supported beam

Sl. No.	Frequency, f (Hz)	Frequency $\omega=2\pi f$ (rad/s)	Amplitude σ_{x1} rms (mV)	Amplitude σ_{x2} rms (mV)	Conversion Factor CF (V/m)	Displacement Amplitude $X_1 = \sqrt{2}\ (CF)\ \sigma_{x1}$ (m)	Displacement Amplitude $X_2 = \sqrt{2}\ (CF)\ \sigma_{x2}$ (m)	Force, $F = 2M_{D\,2}\ e\omega^2$ (N)	Receptance X_1/F (m/N)	Receptance X_2/F (m/N)
1										
2										
3										
4										
5										
6										
7										
8										
9										
10										
11										
12										
13										
14										
15										
16										
17										
18										

19										
20										

Table 7.7 Forced vibration test data on Continuous beam

Sl. No.	Frequency, f (Hz)	Frequency $\omega=2\pi f$ (rad/s)	Amplitude σ_{x1} rms (mV)	Amplitude σ_{x2} rms (mV)	Conversion Factor CF (V/m)	Displacement Amplitude $X_1 = \sqrt{2}\ (CF)\ \sigma_{x1}$ (m)	Displacement Amplitude $X_2 = \sqrt{2}\ (CF)\ \boldsymbol{\sigma_{x2}}$ (m)	Force, $F = 2M_{D\,2}\ e\omega^2$ (N)	Receptance X_1/F (m/N)	Receptance X_2/F (m/N)
1										
2										
3										
4										
5										
6										
7										
8										
9										
10										
11										
12										
13										
14										
15										
16										
17										
18										
19										
20										

Experiment 8

Earthquake induced waves in rectangular water tanks

8.0 Background

The study of behavior of liquid storage tanks during an earthquake is one of the important problems in earthquake engineering. In the event of an earthquake there would be additional fluid pressures that would be created in the body of the liquid and an understanding of the nature of these pressure fields is vital for safe design of these tanks. It is of interest to note that water tanks need to be functional following a major earthquake since they would serve to control fires that often get triggered during a major earthquake. There have been several instances of failure of water tanks during the 1993 Latur earthquake and the 2001 Bhuj earthquake in India; see figure 8.1. The study of liquid storage tanks under earthquakes needs the application of principles of fluid and solid mechanics. The term sloshing is used to describe any motion of a free liquid surface inside its container. The liquid motion interacts with the motion of elastic containers thereby producing a rich variety of fluid-structure interactions.

In this experiment we study the phenomena of formation of standing waves on free surface of liquid inside a rectangular container. The setup used for this purpose is shown in figure 8.2. This consists of a rectangular tank whose walls are made up of perspex plates housed inside a steel cage. The wall thickness and the walls and the stiffness of the steel frame are so designed that the tank walls can be treated as being rigid at frequencies at which we expect to have standing waves formed on the liquid surface. The tank is mounted on an electro-mechanical shake table that supplies harmonic base motions to the tank base. This motion can be viewed, to a first approximation, as the earthquake induced motions on a rectangular tank mounted directly on the ground. The objective of the experiment is to excite the liquid volume inside the tank at different frequencies and detect the frequencies at which standing waves are formed on the liquid surface. A mathematical model based on fluid mechanics background is used to theoretically predict these frequencies and the wave patterns.

8.1 Mathematical model

Figure 8.3 shows a two-dimensional water tank of length *2l* containing water up to a height *h*. We assume that the liquid flow is inviscid, irrorational, and incompressible. We now consider the question as to what type of steady state waves may exist on the liquid surface. We use the notation $\phi(x,y,t), u(x,y,t), \& v(x,y,t)$ to represent, respectively, the velocity potential, velocity components in x and y directions. The following equation is known to govern the velocity potential (see, for example, L G Currie, 1974, Fundamentals of mechanics of fluids, McGraw-Hill, NY, pp. 201-205)

$$\frac{\partial^2 \phi}{\partial x^2} + \frac{\partial^2 \phi}{\partial y^2} = 0 \qquad \ldots(8.1)$$

with the boundary conditions given by

$$\frac{\partial^2 \phi}{\partial t^2}(x,h,t) + g\frac{\partial \phi}{\partial y}(x,h,t) = 0$$
$$\frac{\partial \phi}{\partial y}(x,o,t) = 0$$
$$\frac{\partial \phi}{\partial x}(\pm l,y,t) = 0$$

…(8.2)

The first of the above boundary conditions is obtained by applying the Bernoulli's equation on the free surface and the remaining set of boundary conditions reflects the fact that the normal fluid velocity components at the wall boundaries are zero. The symbol *g* in the above equation represents the acceleration due to gravity and the other notations are explained in figure 8.3. We seek a steady state wave solution of the form

$$\phi(x,y,t) = \psi(x,y)\cos\omega t$$

…(8.3)

This leads to the field equation

$$\frac{\partial^2 \psi}{\partial x^2} + \frac{\partial^2 \psi}{\partial y^2} = 0$$

…(8.4)

with the boundary conditions

$$-\omega^2 \psi(x,h) + g\frac{\partial \psi}{\partial y}(x,h) = 0$$
$$\frac{\partial \psi}{\partial y}(x,o) = 0$$
$$\frac{\partial \psi}{\partial x}(\pm l,y) = 0$$

…(8.5)

We seek the solution of equation 8.4 in the variable separable form $\psi(x,y) = X(x)Y(y)$. This leads to the equation

$$\frac{d^2 X}{dx^2}Y + X\frac{d^2 Y}{dy^2} = 0 \qquad \ldots(8.6)$$

Dividing both sides by *XY* one gets

$$\frac{1}{X}\frac{d^2 X}{dx^2} = -\frac{1}{Y}\frac{d^2 Y}{dy^2} \qquad \ldots(8.7)$$

Since the left hand side is a function of x alone and right hand side is a function of y alone it turns out that each of the two terms appearing in the above equation needs to be equal to the same constant. That is,

$$\frac{1}{X}\frac{d^2X}{dx^2} = -\frac{1}{Y}\frac{d^2Y}{dy^2} = -\lambda^2 \qquad \ldots(8.8)$$

This leads to

$$\begin{aligned} &\frac{d^2X}{dx^2} + \lambda^2 X = 0 \\ &\frac{d^2Y}{dy^2} - \lambda^2 Y = 0 \end{aligned} \qquad \ldots(8.9)$$

with boundary conditions

$$\frac{dX}{dx}(\pm l) = 0; \quad \frac{dY}{dy}(0) = 0; \quad g\frac{dY}{dy}(h) - \omega^2 y(h) = 0 \qquad \ldots(8.10)$$

From the first equation 8.9 one gets

$$X(x) = a\cos\lambda x + b\sin\lambda x \qquad \ldots(8.11)$$

Imposing the boundary conditions $\frac{dX}{dx}(\pm l) = 0$ one gets

$$\lambda\begin{bmatrix} -\sin\lambda l & \cos\lambda l \\ \sin\lambda l & \cos\lambda l \end{bmatrix}\begin{Bmatrix} a \\ b \end{Bmatrix} = 0 \qquad \ldots(8.12)$$

For nontrivial solution one gets the condition $\lambda\sin\lambda l\cos\lambda l = 0$. This leads to two families of solutions, namely,

$$\begin{aligned} &\lambda_n = \frac{n\pi}{l}; n = 1,2,3,\ldots,\infty \\ &\lambda_m = \frac{(2m+1)\pi}{2l}; m = 0,1,2,3,\ldots,\infty \end{aligned} \qquad \ldots(8.13a)$$

The corresponding solutions for *X(x)* are obtained as

$$\begin{aligned} &X(x) = a\cos\frac{n\pi x}{l}; n = 1,2,3,\ldots,\infty \\ &X(x) = b\sin\frac{(2m+1)\pi x}{2l}; m = 0,1,2,3,\ldots,\infty \end{aligned} \qquad \ldots(8.13b)$$

where a and b are arbitrary constants.

Considering now the second of the equation in (8.9) we get

$$Y(y) = c\cosh\lambda y + d\sinh\lambda y \qquad \ldots(8.14)$$

Imposing the boundary conditions on Y listed in (9) we get

$$\frac{dY}{dy}(0) = 0 \Rightarrow d\lambda = 0 \Rightarrow d = 0$$

$$g\frac{dY}{dy}(h) - \omega^2 y(h) = 0 \Rightarrow g\lambda\sinh\lambda h - \omega^2\cosh\lambda h = 0 \qquad \ldots(8.15)$$

$$\Rightarrow \omega^2 = g\lambda\tanh\lambda h$$

with the parameter c remaining arbitrary. Combining equations 8.13 and 8.15 one gets

$$\omega_n^2 = \frac{n\pi}{l}g\tanh\left(\frac{n\pi h}{l}\right); n = 1,2,...,\infty$$

$$\omega_m^2 = \frac{(2m+1)\pi}{2l}g\tanh\left(\frac{(2m+1)\pi h}{2l}\right); m = 0,1,2,...,\infty \qquad \ldots(8.16)$$

This leads to two families of standing wave patterns given by

$$\phi_n(x,y,t) = A_n\cos\frac{n\pi x}{l}\cosh\frac{n\pi y}{l}\cos\omega_n t$$

$$\phi_m(x,y,t) = B_m\sin\frac{(2m+1)\pi x}{2l}\cosh\frac{(2m+1)\pi y}{2l}\cos\omega_m t; m = 0,1,2,...,\infty \qquad \ldots(8.17)$$

The velocity components can subsequently obtained by using

$$u(x,y,t) = \frac{\partial\phi}{\partial x}\ \&\ v(x,y,t) = \frac{\partial\varphi}{\partial y} \qquad \ldots(8.18)$$

In particular one gets

$$v_n(x,h,t) = \alpha_n\cos\frac{n\pi x}{l}\cos\omega_n t; n = 1,2,...,\infty$$

$$v_m(x,h,t) = \beta_m\sin\frac{(2m+1)\pi x}{2l}\cos\omega_m t; m = 0,1,2,...,\infty \qquad \ldots(8.19)$$

It may be noted that the natural frequencies given by equation 8.16 and the velocity profiles at $y=h$ given by equation (8.19) can be observed and measured during experiments. Figure 4 shows plots of first few modes of surface oscillations as per equation 8.19 (with l=0.12 m and h=0.20 m). The variation of natural frequencies (equation 8.16) for l=0.12 m and for different values of h are shown in figure 8.5.

8.2 Experimental procedure

1. Mount the water tank on the shake table as shown in figure 8.2. See Table 8.1 for list of equipment and sensors needed to perform this experiment.
2. Measure the dimensions of the tank and the water level inside the tank. Add a color dye to the water so as to facilitate visual observations of the water surface oscillations.
3. Excite the tank harmonically starting with low values of frequency. At each frequency visually observe the behavior of the water surface.
4. At every value of the frequency allow sufficient time to pass so that oscillations of water reach steady state.
5. As the frequency of driving approaches one of the natural frequencies, the water surface begin to oscillate with perceptible amplitudes (see figure 8.6). Note down the frequency at which such oscillations occur. Record observations as in Tables 8.2 and 8.3.
6. The profile of the standing waves at resonance can be measured by a simple device as shown in figure 8.7. This consists of inserting a white sheet at the inner wall of the tank and allow the oscillating liquid surface to leave behind a tinted trace on the sheet. The shape of the standing waves could be inferred by measuring the heights from mean level of the tinted trace left on the paper by the oscillating liquid surface. Following this procedure, obtain the shape of the standing waves at the liquid surface for first few modes.
7. Predict the frequencies and shapes of the standing waves using the theoretical formulation provided in section 8.1.
8. Compare the theoretical and experimental results and draw conclusions on their mutual agreement/disagreement.
9. Repeat the experiment for different values of heights of water level inside the tank.
10. Remount the tank by swiveling it through 90 degrees about the vertical axis. Repeat the experiment as described above for this configuration.

8.3 Report submission

1. Tabulate the observed natural frequencies for different heights of water level and for the two alternative ways of mounting the tank. Include the results from theoretical analysis in this table.
2. Measure the water heights above the still surface level from the tinted trace obtained on the white sheet (see step 6 in section 8.2). Plot these observed surface profiles and super pose on it the theoretical predictions (equation 8.19).
3. Answer the following questions:

   (a) What modifications are needed to the governing equations derived in section 3.0 if the applied support motion also is to be included in the boundary conditions? What would be this modification if the tank is subjected to three-component support motion?

(b) What would happen if the tank had a square or cylindrical cross section instead of rectangular cross section?
(c) The tank walls have been assumed to be rigid in this study. Is this a realistic assumption? How can this assumption be relaxed in the analysis?
(d) Attention in this experiment has been limited to the study of formation of standing waves. How the study can be extended, analytically and experimentally, to obtain the fluid pressure distribution on the tank walls?

Figure 8.1 Failure of water tank in Manfera during the 2001 Bhuj earthquake

Figure 8.2 Experimental setup.

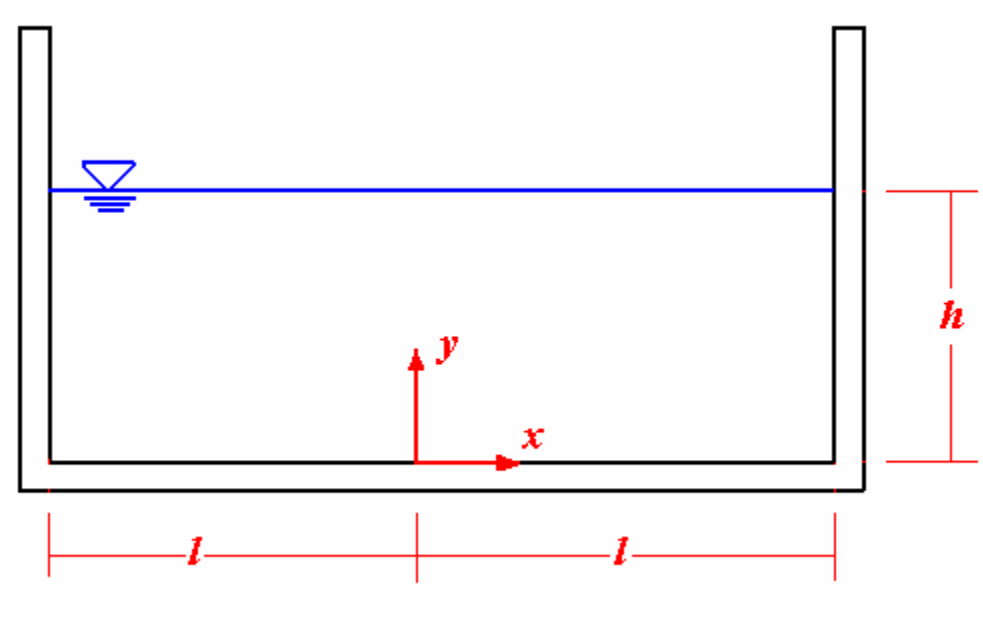

Figure 8.3 Geometry of water stored in a rectangular container.

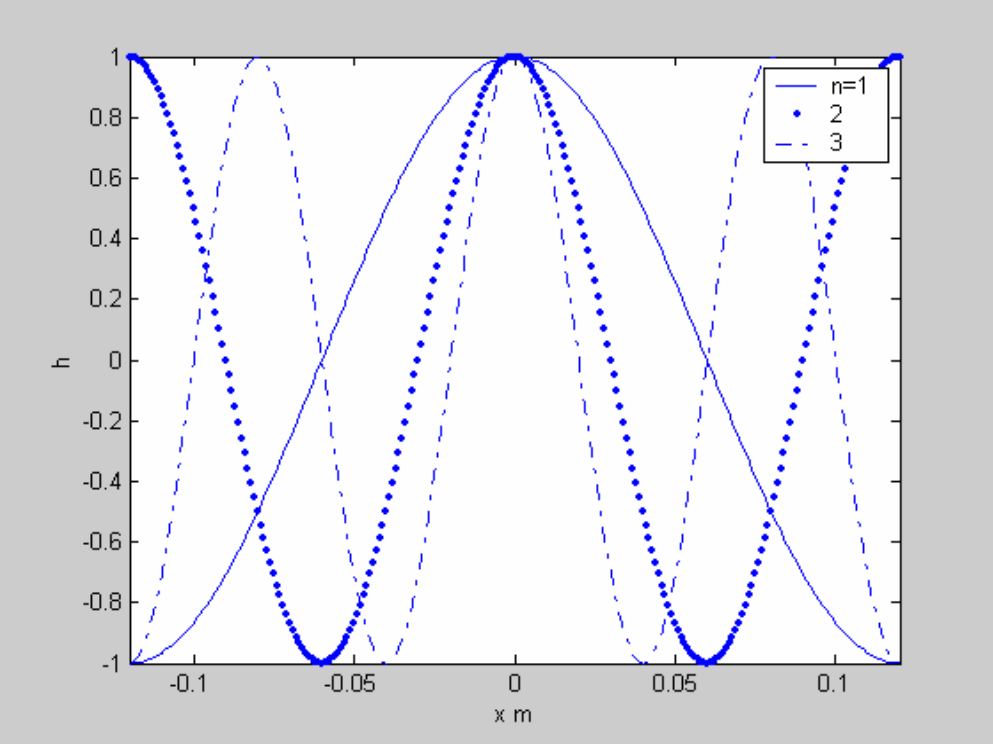

(a)

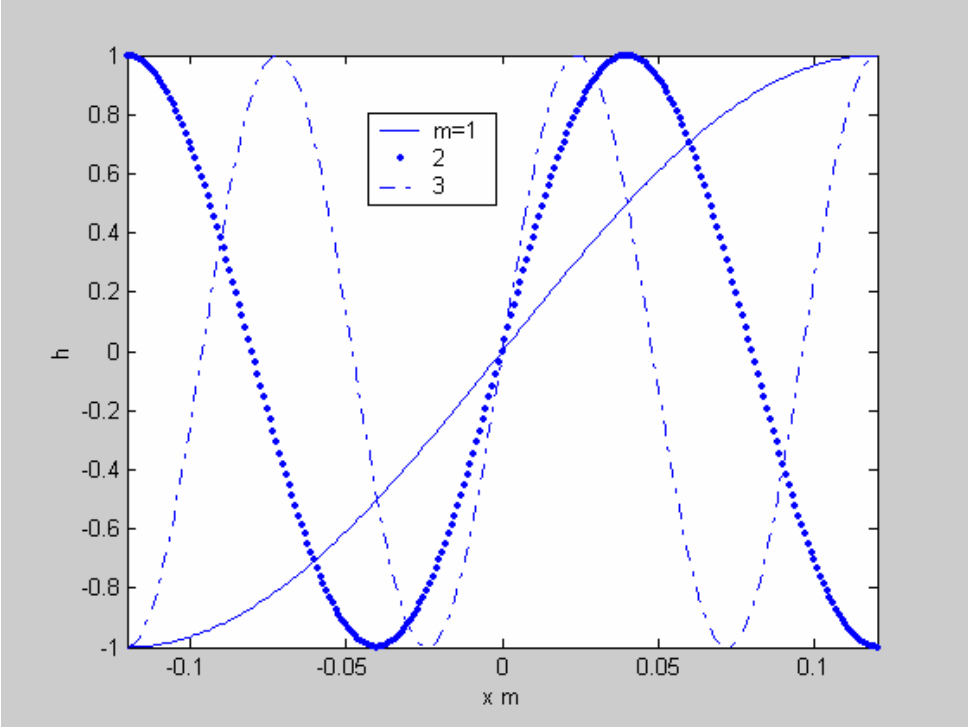

(b)

Figure 8.4 The first few modes of oscillations of the liquid surface estimated using theory.

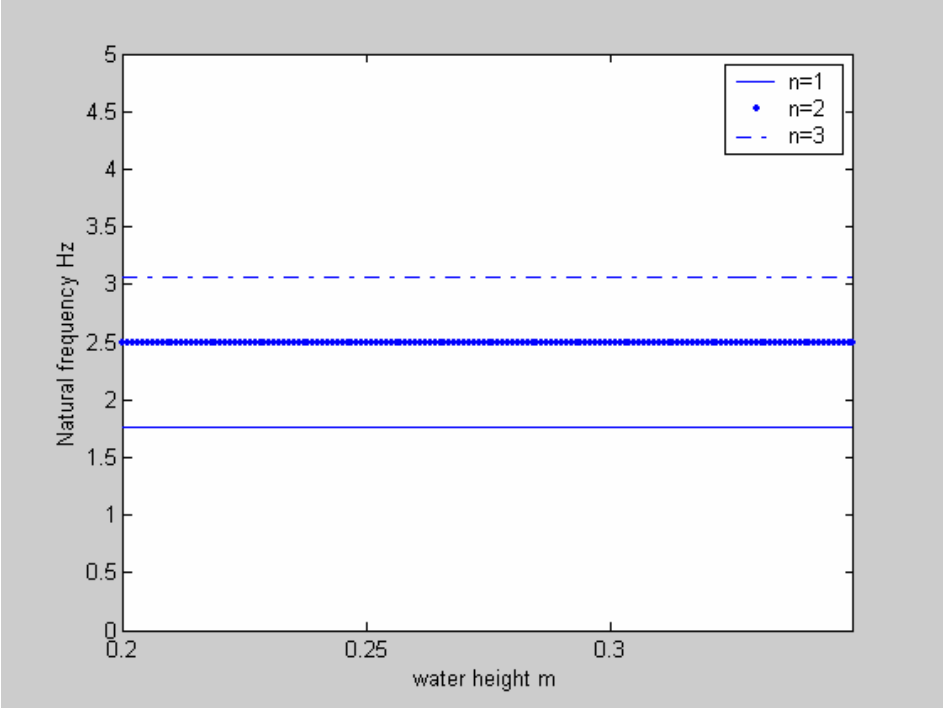

(a)

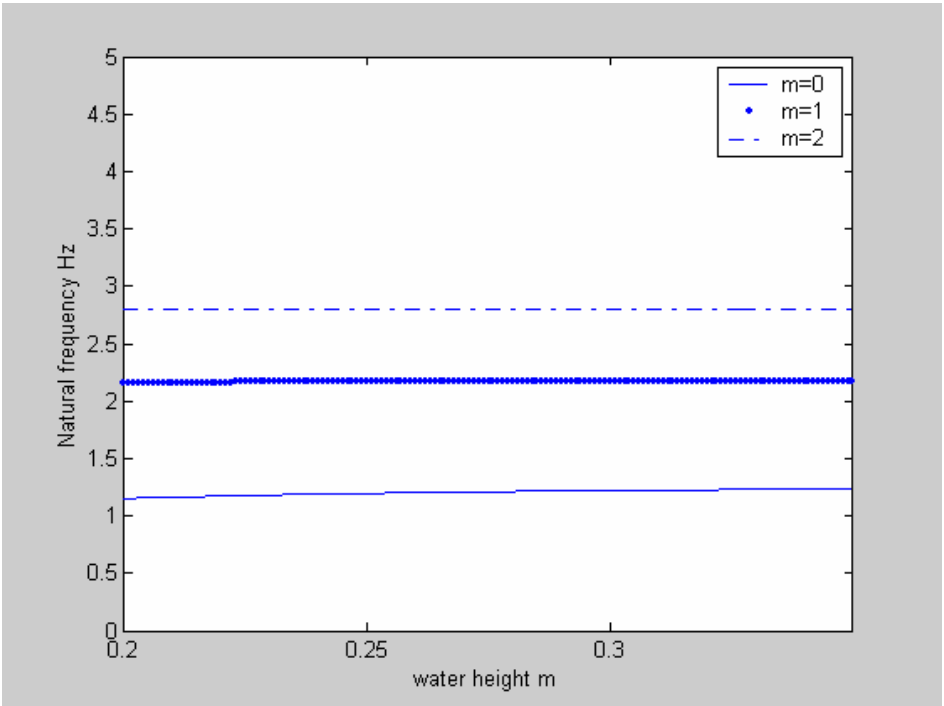

(b)

Figure 8.5 Estimates of natural frequencies with l=0.12 m and for different values of liquid column height.

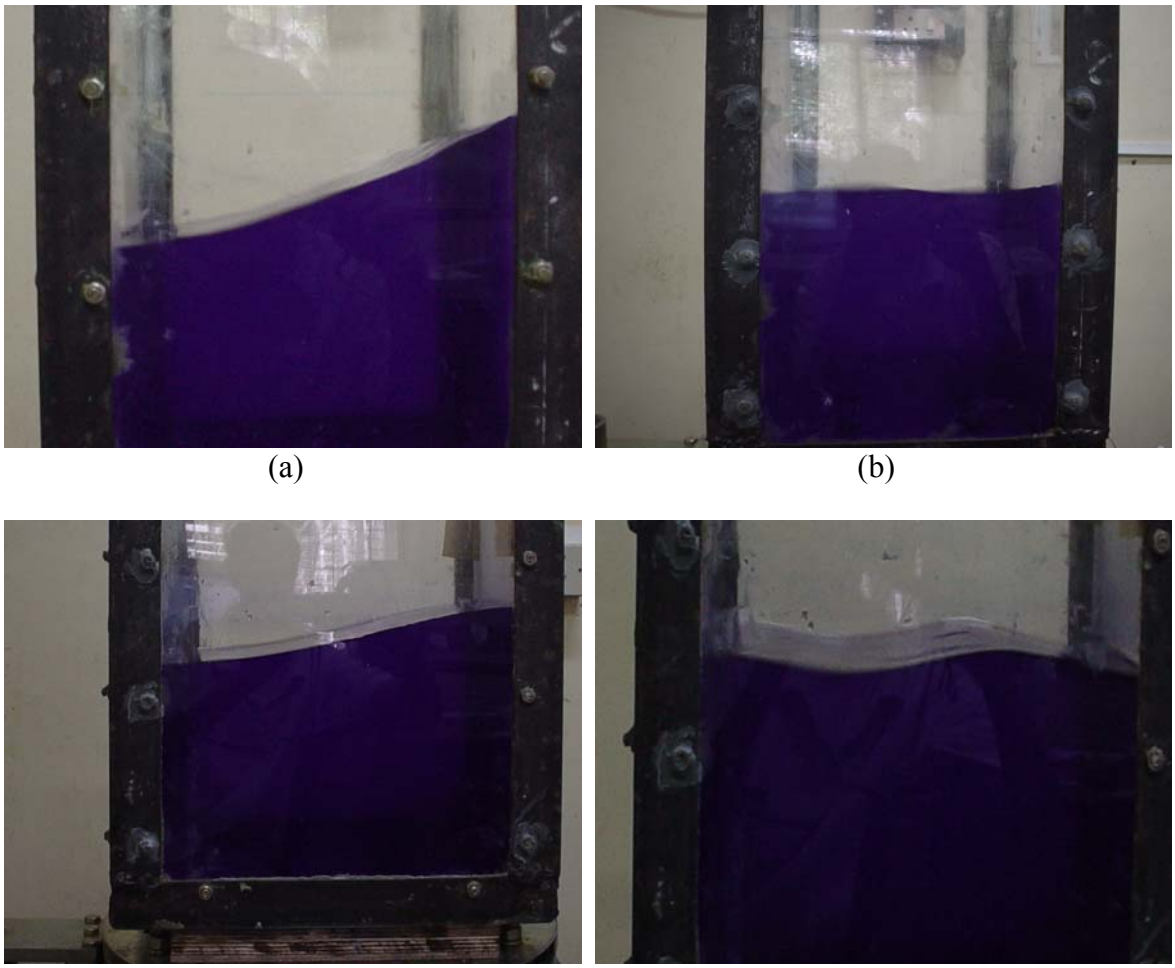

Figure 8.6 Liquid surface oscillations at resonance (a) *l*=0.12 m; mode 1 (b) *l*=0.12 m; 2 mode 2 (c) *l*=0.15 m mode 1 (d) *l*=0.15 m mode 2

Figure 8.7 Method for measuring the water surface profile at resonance; notice the blue trace left on the white paper by the oscillating liquid surface.

Table 1 Equipments used in conducting experiment on water tank

No.	Equipments	Quantity
1	Oscilloscope	1
2	Accelerometers	1
3	Signal conditioning amplifier	1
4	Shake table	1

Table 2 Natural frequencies of liquid column; l=0.12 m; h=0.20 m.

Mode Number	Analysis (Hz)	Experiment (Hz)
1		
2		
3		

Table 3 Natural frequencies of liquid column; l=0.15 m; h=0.20 m.

Mode Number	Analysis (Hz)	Experiment (Hz)
1		
3		
5		

Experiment 9

Dynamics of free-standing rigid bodies under base motions

9.0 Background

Studies of free-standing rigid blocks under dynamic base motion is of considerable interest in earthquake engineering, not only because of their relevance to the understanding of toppling of unrestrained systems, such as, battery racks, transformers, computer CPUs, refrigerators, cup boards, book cases, etc., but also, from the point of view of inferring the possible amplitude of ground accelerations based on observations on toppled objects in an earthquake hit area (see figure 9.1). Even for objects that are fixed to the supports, such as equipment bolted to the ground, in case the bolts yield during strong motion, the system would subsequently behave like a free standing object. It is evident that toppling of equipment would often result in loss of functionality and hence contribute to economic losses due to an earthquake. The free standing objects could have a variety of geometries (for example, rectangular, cylindrical, stacked objects) and under the action of multi-component dynamic base motions, these objects could display a rich variety of dynamic behavior. These motions are characterized by large displacements and energy dissipation mechanisms involving impacting and sliding. Consequently, mathematical models for such systems are nonlinear in nature and require numerical solution procedures.

In the present experiment we study the dynamics of a rectangular rigid block under one dimensional harmonic base motion. The setup for studying the initiation of rocking, rocking oscillations and possible toppling of rigid rectangular blocks is shown in figure 9.2. Here the energy dissipation takes place by impacts with the velocity after impact being a fraction less than the velocity before impact. In making a mathematical modeling, the block is assumed to be long in one direction so that attention could be focused on the study of planar rocking behavior. Furthermore, we neglect the possibility of sliding of the block in the direction of applied base motion. To capture the energy dissipation due to impacting in a numerical model, one needs to determine the time of impacts while integrating the governing equation of motion. This can be achieved by dividing the time interval into a sequence of subintervals with each of the subintervals representing episodes of rocking between two successive impacts. The lengths of these subintervals are not know *a prioi* and a termination criteria based on the zeros of the rotation response of the block needs to be built into the integration scheme. This exercise, in itself, would provide a good opportunity to appreciate the nuances of integrating nonlinear equations of motion.

9.1 Mathematical model and program for numerical simulations

A rigid rectangular block resting on a rigid base is shown in figure 9.3. We denote by W the weight of the block and by g the acceleration due to gravity; H and B are the block dimensions as shown in figure 9.3. The block is taken to be long in the direction normal to the plane of the paper. It is assumed that the block does not slide and when set into

rocking motions it rotates about axes passing through the points O and O'. The base acceleration *h(t)* is taken consist of a single horizontal component of harmonic signal. From figure 9.3 it can be deduced that the force $\frac{Wh}{g}$ tends to lift the block around the corner O' while the force *0.5WB* resists this action. Thus, whenever the condition

$$\frac{WB}{2} > \frac{Wh(t)H}{2g} \qquad \ldots(9.1)$$

is satisfied, there would be no uplift. Consequently it can be concluded that the minimum acceleration *h** needed to lift the block about the corner O' is given by

$$\frac{h^*}{g} = \frac{B}{H} \qquad \ldots(9.2)$$

Thus, if in an earthquake hit area we observe that a rectangular object of dimensions *B* and *H* has actually toppled or we find evidence that an object had lifted up during the earthquake, it is likely that the ground acceleration would have been at least *B/H* during the earthquake. Once the object lifts up about a corner, the equation of equilibrium can be deduced by considering the free body diagram of the object as shown in figure 4a and b. Thus when the body is rocking about O one gets

$$I\ddot{\theta} + WR\sin(\alpha - \theta) + \frac{Wh(t)}{g}R\cos(\alpha - \theta) = 0 \qquad \ldots(9.3)$$

Similarly, for rocking about O' one has

$$I\ddot{\psi} + WR\sin(\alpha - \psi) + \frac{Wh(t)}{g}R\cos(\alpha - \psi) = 0 \qquad \ldots(9.4)$$

Noting that $\theta = -\psi$, the above two equations can be combined into a single equation as

$$I\ddot{\theta} + WR\sin(\alpha\,\mathrm{sgn}\,\theta - \theta) + WR\cos(\alpha\,\mathrm{sgn}\,\theta - \theta)\frac{h(t)}{g} = 0 \qquad \ldots(9.5)$$

with specified initial conditions $\theta(0)$ and $\dot{\theta}(0)$. Here sgn(.) denotes the signum function defined as $\mathrm{sgn}(\theta) = 1$ for $\theta > 1$ and $\mathrm{sgn}(\theta) = -1$ for $\theta < 1$. Let us define *t*>0* such that $\theta(t^*) = 0$, that is, *t** denotes the time at which the block impacts the base. The velocity after impact is taken to be related to the velocity before impact through the relation $\theta(t^{*+}) = \eta\theta(t^{*-})$; here η is the coefficient of restitution between the block and the supporting base. The above equation is highly nonlinear both in terms of large rotations and also in terms of dissipation of energy through impacting. Furthermore, the excitation term *h(t)* appears as a parametric excitation term. This type of equations can only be solved numerically. To capture the energy dissipation due to impacting in a numerical model, one needs to determine the time *t** of impacts while integrating the governing equation of motion. This can be achieved by dividing the time interval into a sequence of subintervals with each of the subintervals representing episodes of rocking

between two successive impacts. The lengths of these subintervals are not know *a prioi* and a termination criteria based on the zeros of the rotation response of the block needs to be built into the integration scheme. To develop a numerical simulation scheme we re-write equation 9.5 in the form

$$\ddot{\theta} + \omega^2 \sin(\alpha \operatorname{sgn}\theta - \theta) + \omega^2 \cos(\alpha \operatorname{sgn}\theta - \theta)\frac{h(t)}{g} = 0 \qquad \ldots(9.6)$$

Here $\omega^2 = WR/I$. Furthermore, using the notation $(\theta, \dot{\theta}) = (\theta_1, \theta_2)$ the above equation can be written in terms of two first order differential equations as

$$\begin{aligned} \dot{\theta}_1 &= \theta_2 \\ \dot{\theta}_2 &= -\omega^2 \sin(\alpha \operatorname{sgn}\theta_1 - \theta_1) - \omega^2 \cos(\alpha \operatorname{sgn}\theta_1 - \theta_1) \end{aligned} \qquad \ldots(9.7)$$

The equation is now in a form suitable for numerical integration using procedures such as Runge-Kutta method. The following is a code that uses Matlab ODE45 routine along with provision for detecting the event of impacting.

```
clear all
close all

global g B H alpha w R eta amp alm
B=75e-03;
H=115e-03;
R=sqrt(B^2+H^2)/2;
g=9.81;
w=sqrt(0.75*g/R);
alm=63.14;
amp=0.00287;
eta=.43;
alpha=atan(B/H);
period=2*pi/alm;
npts=10000;
ncyc=10;
nimpacts=100;


dt=period/npts;
%theta0=alpha/100;
theta0=0.03;
thetadot0=0;
t0=0;
icount=1;
for j=1:nimpacts;
```

```
tspan=t0:dt:t0+ncyc*period;

z0=[theta0;thetadot0];
options=odeset('events','on');
[t,z,te,ze,ie]=ode45('eom',tspan,z0,options);

nlast=size(z,1)
time(icount:icount+nlast-1)=t;
th(icount:icount+nlast-1)=z(:,1);
thdot(icount:icount+nlast-1)=z(:,2);
icount=icount+nlast;

t0=t(nlast);
theta0=0;
thetadot0=z(nlast,2)*eta;
end;
figure(1)
plot(time,th);
xlabel('time s')
ylabel('rotation rad')
title('Rotation as predicted by numerical integration')
axis([0 6 -0.12 0.12])
figure(2)
plot(time,thdot);
xlabel('time s')
ylabel('rotation velcoity rad/s/s')
title('Rotation velocity as predicted by numerical integration')
axis([0 6 -4 4])
figure(3)
% comet(th,thdot)
plot(th,thdot)
xlabel('rotation rad')
ylabel('rotation velocity rad/s/s')
title('Phase plane plot')
axis([-.12 .12 -4 4])
function [value,isterminal,dircn]=eom(t,z,flag);
global g B H alpha w R eta amp alm
if nargin<3|isempty(flag)
   value=[z(2);                -w*w*sin(alpha*sign(z(1))-z(1))+w*w*cos(alpha*sign(z(1))-
z(1))*amp*alm*alm*sin(alm*t)/g];
else
   switch flag;
   case 'events'
      value=z(1);
      isterminal=1;
      dircn=0;
```

```
   otherwise
      error('function not programmed for this event')
   end;
end;
```

9.2 Experimental procedure

At the outset we need to note that in this experiment it is required to measure the angle of rotation and rotational velocity of the rocking block. Table 9.1 lists the sensors and data acquisition system needed to conduct this experiment. The measurements on rotation and rotational velocity can be accomplished by using displacement and velocity sensors meant for measuring translational displacements and velocities. Thus, in figure 9.5 we show the path traced by a displacement/velocity sensor mounted on the lateral face of the block as the block rocks. Clearly, in order to obtain the rotational displacement/velocity the sensor measurement needs to be divided by the radius of the arc of circle that the senor traces as the block rocks.

1. Measure B and H for the block and deduce R and α .
2. Place the block on the table as shown in figure 9.2 and fix the sensors as shown.
3. Calculate the minimum acceleration needed for the block to lift up using equation 9.2. Run the shake table by varying the driving frequency in small steps. In doing so, for a fixed value of table displacement, we would be increasing the base acceleration in small increments. Make sure that the block starts from rest at every increment of the driving frequency. Verify if the criterion given by equation 9.3 for lift up is satisfied or not.
4. Select a driving frequency above the critical frequency and run the shake table. Record the displacement and velocity time histories and subsequently deduce the rotational displacement and velocity.
5. The coefficient of restitution η can be estimated by zooming the velocity plot and measuring the reduction in velocity before and after impacts (see figure 9.6). The coefficient can be estimated a t a set of about 10 points and an average value over these impacts could be used as the estimate.
6. For the block configuration under study run the Matlab code (listed in section 9.1) to numerically simulate the block rocking. The input to this program consists of B, H, η and details of *h(t)*.
7. Compare the measured time histories of rotational displacement and velocity with the corresponding numerical predictions. Also plot the phase plane plot, that is, plot of $\theta(t)$ versus $\dot{\theta}(t)$. Comment on the mutual agreement/disagreement between experimental observations and numerical predictions..
8. By varying the frequency/amplitude of the base motion, thereby varying the peak base acceleration, observe when the block would topple. (Caution: do not mount sensors on the block when you are trying to simulate toppling of the block if not sensors could get damaged when the block topples).

9.3 Report submission

1. Document the observations on steps 1-8 as in section 9.2.
2. Include the print outs of the Matlab plots and the Matlab m-file.
3. Respond to the following questions
   (a) Construct the moment-rotation diagram for the rectangular block under study.
   (b) What are the limitations of the mathematical model developed in section 9.2?
   (c) Do you think study of toppled/lifted objects indeed provide a reliable means to estimate the peak ground acceleration in an earthquake hit area?
   (d) Re-derive the governing equation of motion for the block by including simultaneous action of horizontal and vertical components of the ground motion and also by including the possibility of sliding in addition to rocking.

Figure 9.1 Overturned and tilted rigid objects observed at Bhuj subsequent to the 2001 Gujarath earthquake. Based on such observations one could estimate a lower bound on peak ground acceleration that might have occurred during the earthquake.

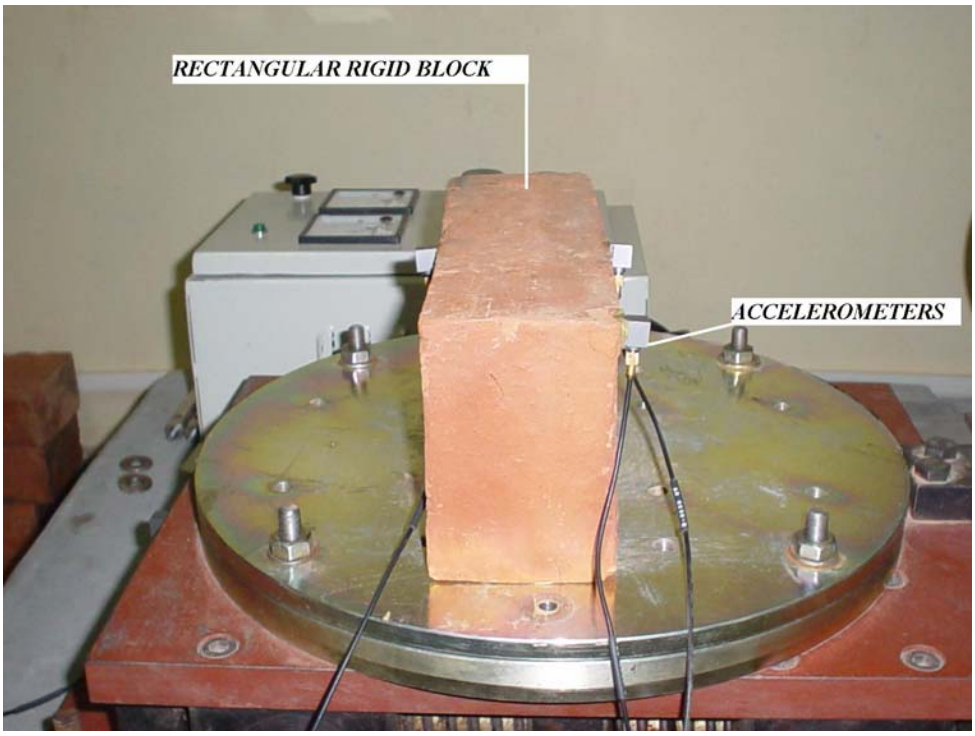

(a)

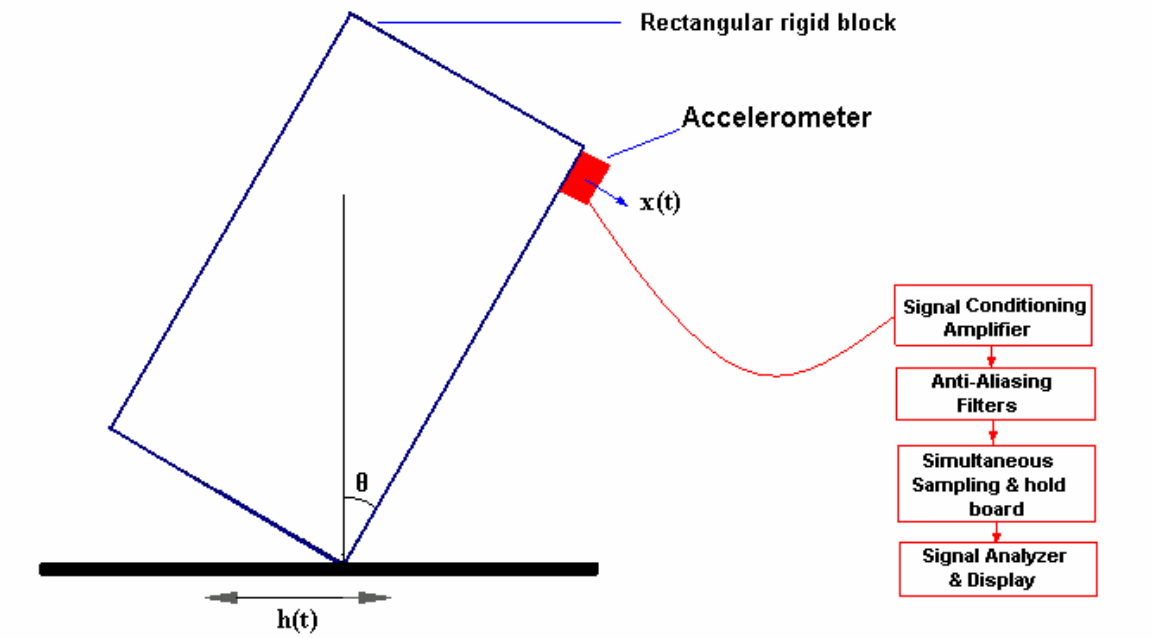

(b)

Figure 9.2 Rectangular rigid block placed freely on a shake table and subject to harmonic base motion; (a) view of block placed on the table; (b) Measurement setup.

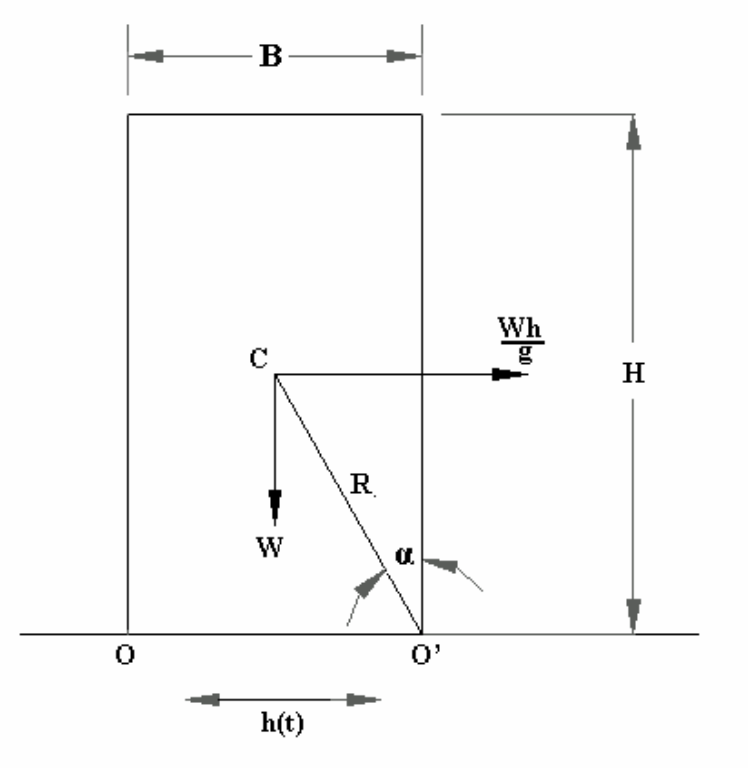

Figure 9.3 Rectangular rigid block under harmonic base acceleration

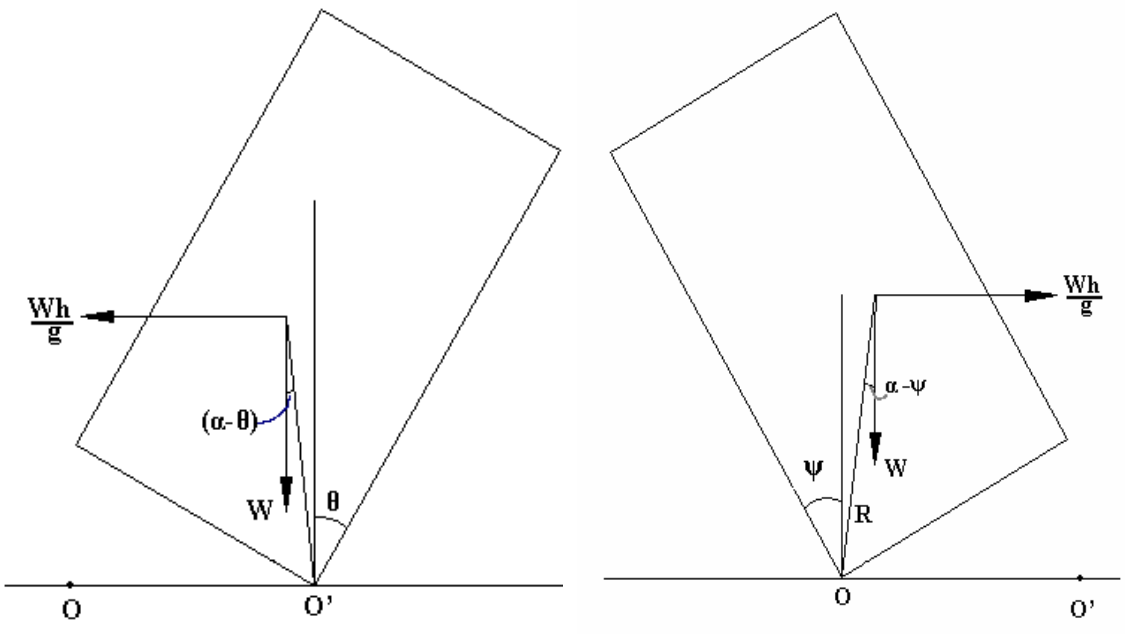

(a) (b)

Figure 9.4 Free body diagram of the block under base acceleration.

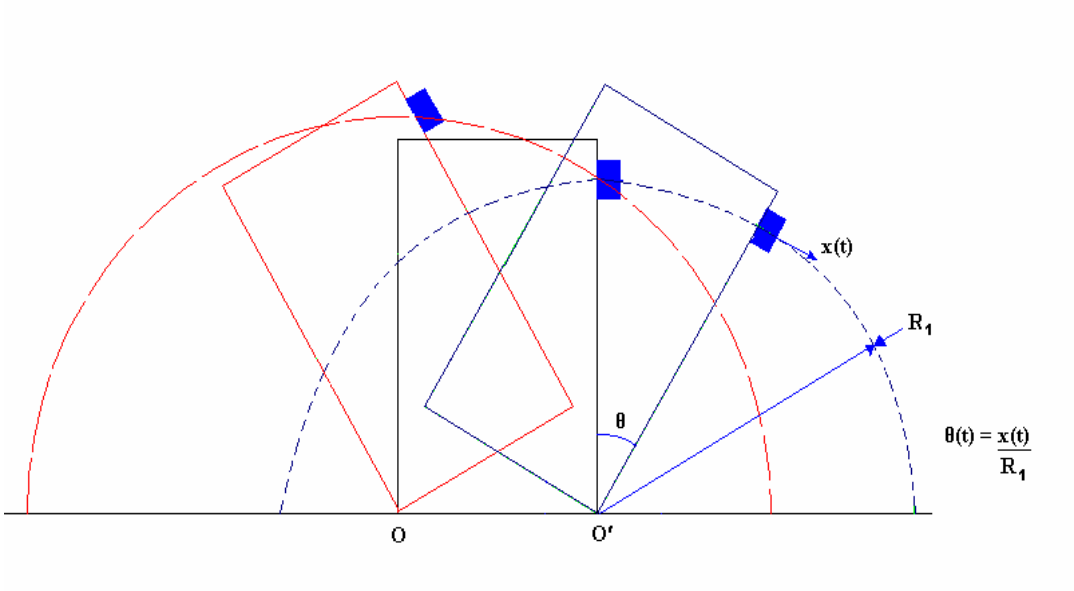

Figure 9.5 Paths traced by sensors in a rocking block.

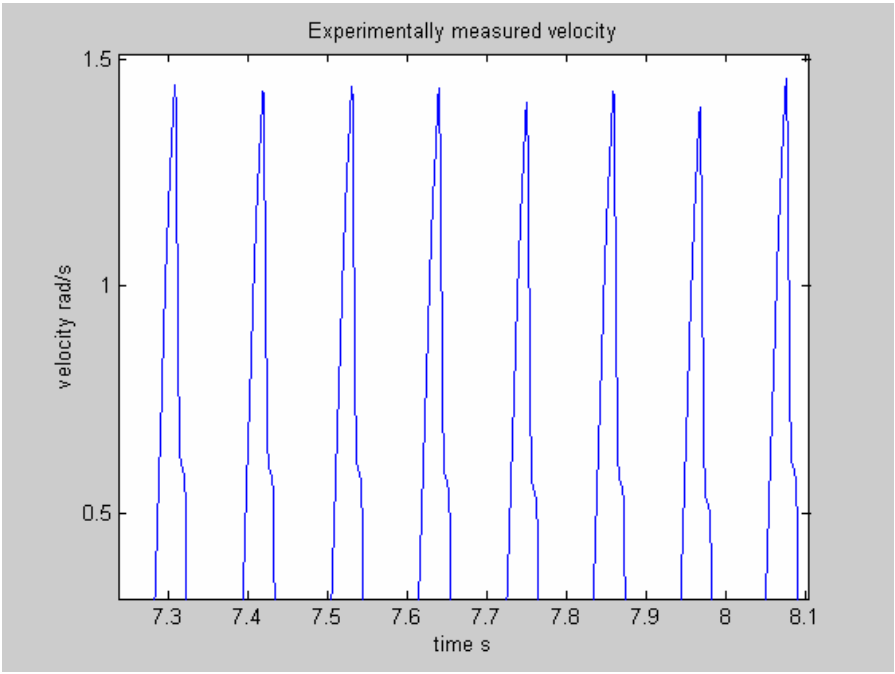

Figure 9.6 Zoomed trace of rotational velocity time histories showing the loss of velocity upon impacts.

Table 9.1 Equipments used in conducting the experiment

No.	Equipments	Quantity
1	PC Based Data Acquisition system (2 Channels)	1
2	Accelerometers	2
3	Signal conditioning amplifier (two channels)	1
4	Shake table	1

EXPERIMENT 10

Seismic wave amplification, liquefaction and soil-structure interactions

10.0 Background

Most often civil engineering structures are founded on soil layers. Exception to this occurs when rock outcrops are available on which the structures could be directly supported. Consequently, the ground motions that act on the structure supports are often filtered through the soil layers on which they are founded. This leads to several questions pertaining to modifications caused by the soil layers to the seismic waves, the response of soil itself to such wave passages and the possible interaction between soil layer and the structure in which case the soil and structural systems need to be analyzed together as mutually interacting systems. Figure 10.1 show the schematic of the problem of seismic wave amplification. Here the amplitude and frequency content of the motion at the ground surface level get modified due to the passage of the motions at the bedrock level through the soil-layer. The response of structures founded on soft soil deposits is also characterized by the following features (S L Kramer, 2004, Geotechnical earthquake engineering, Pearson Education, Singapore):

(a) The inability of the foundation to conform to the deformations of the free-field motion would cause the motion of the base of structure to deviate from the free-field motion.
(b) The dynamic response of the structure itself would induce deformation of the supporting soil.

This process, in which the response of the soil influences the motion of the structure and response of the structure influences the motion of the soil, is referred to as soil-structure interaction. The error due to the neglect of these effects could be unconservative and this could be established only after analyzing problems on case-by-case basis. The term liquefaction refers to drastic reduction in strength of saturated cohesionless soil deposits to the point where the deposits flow as fluids. Consequently, the soil would no longer be able to support engineering structures, thereby, leading to dramatic structural failures. Such damages have been observed to occur during several major earthquakes in the past. Such failures are most commonly observed near rivers, bays and other bodies of water (Kramer 2004).

In the present experiment we study the problem of seismic wave amplification through a shear layer and also the problem of soil-structure interactions. We also demonstrate the phenomenon of liquefaction. The setup shown in figure 10.2 is used to mimic the behavior of a soil layer. This consists of a thick layer of foam (commonly used for upholstery) enclosed inside a set of four Perspex plates that are connected to each other via a set of hinges. When subject to horizontal base motion (figure 10.2a), the system behavior closely resembles that of a soil layer. For the purpose of studying soil structure interactions, the setup shown in figures 10.3 and 10.5 is used. This consists of a one storied building frame that can be mounted on the soil layer (figure 10.3a, 10.5c) or

directly on to the shake table (figure 10.3b, 10.5b). Two frames have been designed to demonstrate the phenomenon of soil structure interactions. When mounted on the soil layer shown in figure 10.2, for one of these frames, the effect of soil structure interactions would be important than for the other frame. The setup shown in figure 10.4 is used to demonstrate the occurrence of liquefaction in dynamically loaded soil layers. These setups fashioned after the models proposed by Berton *et al*, 2004 (S Berton, T C Hutchinson, and J E Bolander, 2004, Dynamic behavior of simple soil-structure systems, University of California at Davis, http://ucist.cive.wustl.edu/).

10.1 Mathematical model

10.1.1 Seismic wave amplification

We adopt a one dimensional shear beam analysis to study the system shown in figure 10.1. It is assumed that

(a) the boundaries at $x=0$ and $x=l$ are horizontal ,
(b) the boundary at $x=0$ represents the rigid rock level and the boundary at $x=l$ represent the free-ground surface,
(c) the soil layer is modeled as a shear beam,
(d) the applied motion at the base is horizontal and the response of the shear layer is predominantly caused by waves propagating vertically upwards from the base, and
(e) the soil and the bedrock level extend to infinity in the horizontal direction.

Denoting by G the shear modulus of the soil layer and by ρ the mass density, the governing equation of motion can be shown to be given by (see the book by Kramer cited above)

$$G\frac{\partial^2 u}{\partial x^2}+\eta\frac{\partial^3 u}{\partial x^2\partial t}=\rho\frac{\partial^2 u}{\partial t^2} \qquad \ldots(10.1)$$

with boundary conditions

$$u(0,t)=h(t) \quad \& \quad \frac{\partial u}{\partial x}(l,t)=0. \qquad \ldots(10.2)$$

The second term on the left hand side in equation 10.1 represents the strain rate dependent viscous damping. It is assumed that the base motion is harmonic in nature given by $h(t)=h_0\exp(i\omega t)$. Since the system is linear, the solution in the steady state can be taken to be of the form $u(x,t)=\phi(x)\exp(i\omega t)$. It follows that the unknown function $\phi(x)$ is governed by the equation

$$\phi''(x)+\lambda^2\phi=0 \qquad \ldots(10.3)$$

with $\phi(0)=h_0$ and $\phi'(l)=0$. Here a prime denotes differentiation with respect to x and

$$\lambda^2=\frac{\rho\omega^2}{G+i\eta\omega} \qquad \ldots(10.4)$$

The solution of equation 10.3 is of the form

$$\phi(x) = A\cos\lambda x + B\sin\lambda x \qquad \ldots(10.5)$$

After imposing the boundary conditions $\phi(0) = h_0$ and $\phi'(l) = 0$ one gets

$$\varphi(x) = h_0\cos\lambda x + h_0\tan\lambda l\sin\lambda x \qquad \ldots(10.6)$$

Thus the motion at the top of the soil layer is given by

$$u(l,t) = h_0\sec\lambda l\exp(i\omega t) \qquad \ldots(10.7)$$

The ratio $u(l,t)/h(t)$ can be interpreted as the dynamic magnification ratio and this given by

$$\Xi(\omega) = \sec\lambda l \qquad \ldots(10.8)$$

Figure 10.6 shows the typical variation of the amplitude and phase of the amplification factor. It can be observed that the amplification factor depends upon the frequency and the damping and it reaches its maximum values at the soil layer natural frequencies.

An alternative way to derive the above result is to employ method of normal mode expansion. This method cannot be applied directly to equation 10.1 since it is associated with time varying boundary conditions. To proceed further we introduce the transformation

$$u(x,t) = v(x,t) + h(t) \qquad \ldots(10.9)$$

and the equation for the new dependent variable *v(x,t)* is given by

$$G\frac{\partial^2 v}{\partial x^2} + \eta\frac{\partial^3 v}{\partial x^2\partial t} = \rho\frac{\partial^2 v}{\partial t^2} + \rho\ddot{h}(t) \qquad \ldots(10.10)$$

with boundary conditions given by

$$v(0,t) = 0\ \&\ \frac{\partial v}{\partial x}(l,t) = 0 \qquad \ldots(10.11)$$

To analyze equations 10.10 and 10.11 we begin by considering the undamped free vibration problem given by

$$G\frac{\partial^2 v}{\partial x^2} = \rho\frac{\partial^2 v}{\partial t^2} \qquad \ldots(10.12)$$

and seek the solution in the form $v(x,t) = \phi(x)\exp(i\Omega t)$. This leads to the eigenvalue problem

$$\phi'' + \mu^2\phi = 0$$
$$\phi(0) = 0\ \&\ \phi'(l) = 0 \qquad \ldots(10.13)$$

Here a prime denotes differentiation with respect to *x*. This leads to the definition of the eigenvalues and eigenfunctions given by

$$\mu_n = \frac{(2n+1)\pi}{2l}; \phi_n(x) = \sqrt{\frac{2}{\rho l}} \sin \mu_n x; n = 0,1,2,...,\infty \quad \ldots(10.14)$$

The mode shapes satisfy the orthogonality conditions

$$\int_0^l \rho \phi_n(x)\phi_k(x)dx = \delta_{nk} \quad \ldots(10.15)$$

Here δ_{nk} is the Kronecker delta function such that $\delta_{nk} = 1$ for $n=k$ and $\delta_{nk} = 0$ for $n \neq k$. We now assume the solution of equation 10.10 in the form

$$v(x,t) = \sum_{k=0}^{\infty} a_k(t)\phi_k(x) \quad \ldots(10.16)$$

where $\{a_k(t)\}_{k=0}^{\infty}$ are the generalized coordinates. By substituting equation 10.16 in 10.10 and using the orthogonality relations, the equations governing the generalized coordinates can be shown to be given by

$$\ddot{a}_n + 2\varsigma_n \Omega_n \dot{a}_n + \Omega_n^2 a_n = \gamma_n \ddot{h}(t) \quad \ldots(10.17)$$

with

$$\gamma_n = \int_0^l \rho \phi_n(x)dx \quad \& \quad \varsigma_n = \frac{\eta \Omega_n}{2G} \quad \ldots(10.18)$$

For $h(t) = h_0 \exp(i\omega t)$ the steady state solution of equation 10.17 is given by

$$a_n(t) = \frac{-h_0 \gamma_n \omega^2}{\Omega_n^2 - \omega^2 + i2\varsigma_n \omega \Omega_n} \exp(i\omega t) \quad \ldots(10.19)$$

If one uses a one mode approximation, the displacement at the top of the soil layer is obtained as

$$u(l,t) = h_0 \exp(i\omega t) + \sqrt{\frac{2}{\rho l}} \frac{h_0 \gamma_n \omega^2}{\Omega_n^2 - \omega^2 + i2\varsigma_n \omega \Omega_n} \exp(i\omega t)\phi(l) \quad \ldots(10.20)$$

This leads to the approximation to the amplification factor given by

$$\tilde{\Xi}(\omega) = 1 + \frac{\omega^2 \gamma \phi(l)}{\Omega_n^2 - \omega^2 + i2\varsigma_n \omega \Omega_n}; \quad \phi(l) = \sqrt{\frac{2}{\rho l}}; \quad \gamma = \frac{2\rho l}{\pi}\sqrt{\frac{2}{\rho l}} \quad \ldots(10.21)$$

Figure 10.7 shows the comparison of magnification factor obtained using equation10.8 and the above equation over the frequency range that encompasses the first mode frequency. Clearly, for this frequency range, a one mode approximation would suffice and this assumption is made in the subsequent part of the study.

10.1.2 Soil-structure interaction

In analyzing the soil-structure system shown in figures 10.3a and 10.5c two approaches are possible. In the first, we model the soil layer as a sdof system that is uncoupled from

the building model. The response of this soil layer is first analyzed by treating the system as a sdof system under support motion *h(t)*; the response of the soil layer is then fed as the input to the model for building frame which, again, is modeled as another single degree of freedom system; see figure 10.8a. In the second model, the soil layer and the building frame model are considered to be a two dof coupled system; see figure 10.8b. Let us compute the ratio of amplitude of response of the building floor and the amplitude of base motion at the bed rock level using the two models.

According to the model shown in figure 10.8a, the equations governing the soil and structure system are given by

$$\begin{aligned} &m_s\ddot{u} + c_s\dot{u} + k_s u \;\; = -m_s\ddot{h} \\ &u_T(t) = u(t) + h(t) \\ &m_b\ddot{y} + c_b\dot{y} + k_b y = -m_b\ddot{u}_T \\ &y_T(t) = y(t) + u_T(t) \end{aligned} \qquad \ldots(10.22)$$

Similarly, for the coupled system shown in figure 10.8b, the governing equations are given by

$$\begin{aligned} &m_S^* \;\; \ddot{u}_T + c_s(\dot{u}_T - \dot{h}) + c_b(\dot{u}_T - \dot{y}_T) + k_s(u_T - h) + k_b(u_T - y_T) = 0 \\ &m_b\ddot{y}_T + c_b(\dot{y}_T - \dot{u}_T) + k_b(y_T - u_T) = 0 \end{aligned} \qquad \ldots(10.23)$$

where $m^*_s = 0.5*(m_s+m_b)$

By using the notation $u = u_T - h \;\&\; y = y_T - h$, the above equation can be recast in the form

$$\begin{bmatrix} m_S^* & 0 \\ 0 & m_b \end{bmatrix}\begin{Bmatrix} \ddot{u} \\ \ddot{y} \end{Bmatrix} + \begin{bmatrix} c_s + c_b & -c_b \\ -c_b & c_b \end{bmatrix}\begin{Bmatrix} \dot{u} \\ \dot{y} \end{Bmatrix} + \begin{bmatrix} k_s + k_b & -k_b \\ -k_b & k_b \end{bmatrix}\begin{Bmatrix} u \\ y \end{Bmatrix} = -\begin{bmatrix} m_S^* & 0 \\ 0 & m_b \end{bmatrix}\begin{Bmatrix} 1 \\ 1 \end{Bmatrix}\ddot{h}(t) \qquad \ldots(10.24)$$

Since the excitation is harmonic in nature, the steady state solution of the above equation can be derived as

$$\begin{Bmatrix} u \\ y \end{Bmatrix} = \begin{Bmatrix} U \\ Y \end{Bmatrix}\exp(i\omega t)$$

$$\begin{Bmatrix} U \\ Y \end{Bmatrix} = \left[-\omega^2\begin{bmatrix} m_S^* & 0 \\ 0 & m_b \end{bmatrix} + i\omega\begin{bmatrix} c_s + c_b & -c_b \\ -c_b & c_b \end{bmatrix} + \begin{bmatrix} k_s + k_b & -k_b \\ -k_b & k_b \end{bmatrix}\right]^{-1}\begin{bmatrix} m_S^* & 0 \\ 0 & m_b \end{bmatrix}\begin{Bmatrix} 1 \\ 1 \end{Bmatrix}\omega^2 h_0 \qquad \ldots(10.25)$$

The amplification factors at the soil surface level and the building slab level can be deduced to be respectively given by U/h_0 and Y/h_0. Figure 10.9a shows the results of coupled and uncoupled analysis of soil-structure system for a typical case in which the

interactions are important and figure 10.9b shows the results for the case in which the interactions are relatively less important.

To obtain parameters of the equivalent sdof model for the soil layer one can compare the first of equation 10.22 with one term approximation in equation 10.16 and 10.17. The equivalent model for the frame models could be established by assuming that the frame behaves as a shear beam with the slab deforming parallely to the direction of base motion with no joint rotations.

10.1.3 Phenomenon of soil liquefaction

We limit of our objective here to demonstrate the occurrence of liquefaction. The setup shown in figure 10.4 consists of a rigid rectangular box filled with saturated sand. The soil here is taken to support a rectangular object (a brick in this case). The box is mounted on the shake table that provides harmonic base motion. The test consists of driving the box by varying the driving frequency in small steps. At each frequency value the system is oscillate for about 25-30 cycles. At a certain value of the driving frequency (about 5 Hz in the present instance), the soil deposits liquefies and the block topples as shown in figure 10.10. Notice the ponding of the water at the surface consequent to the occurrence of liquefaction.

10.2 Experimental procedure

10.2.1 Instruments and sensors

Table 10.1 provides the details of instruments to be used in the experimental study.

10.2.1 Studies on seismic wave amplification

1. Weigh the system consisting of Perspex enclosure and the sponge block. Record the geometric details of the model as per the format in Table 10.1. Estimate the volume of the sponge and Perspex material. Determine an equivalent density.
2. Mount the soil layer block on the shake table as shown in figure 10.2a. Perform the logarithmic decrement test and estimate the damping in the system shown in figure 10.2a. Record the results as in Table 10.5a.
3. Vibrate the soil layer system by applying harmonic base motion at different frequencies. Record the steady state amplitude of response and the amplitude and frequency of the base motion in the format given in Table 10.7. Deduce the seismic amplification factor.
4. Determine the first natural frequency based on the data obtained in the previous step. Use this information and estimate the value of the shear modulus of the soil layer by using equation 10.14 with $n=0$.
5. Obtain the parameters of the sdof model shown in figure 10.8a; see the first of the equation 10.22 with one term approximation in equation 10.16 and 10.17.

6. Predict the seismic wave amplification factor analytically using the sdof approximation. Compare this theoretical prediction with the experimentally measured amplification factor.

10.2.2 Studies on soil structure interactions

1. Record the geometric details of the two frames (figures 10.3c and 10.3d) in the format given in Table 10.2. Some of the details (on elastic constants) may have to be obtained from the instructor/handbooks.
2. First mount the frames on the shake table as shown in figure 10.3b. Measure the damping in the system by using logarithmic decrement test. Record the results as in Table 10.5a.
3. Excite the structure by harmonic base motions of varying frequencies and, for each value of the driving frequency, record the steady amplitude of the slab motion and the frequency and amplitude of the applied base motion. Ensure that the system starts from rest at every change in the driving frequency and also that the system reaches steady state before recording the response amplitude. Tabulate the results as shown in tables 10.6a and 10.6b.
4. Now mount the frames on the soil layer as shown in figure 10.3a (10.5c). Measure the damping in the system by using logarithmic decrement test. Record the results as in Table 10.5a.
5. Repeat step 3 above on the frame-soil layer structure and record the results as in table 10.8a and 10.8b. Notice that measurements on the response at the base of the frame (that is, at the top of the soil layer) and at the slab level need to be made.
6. Based on the observations made in tables 10.6 and 10.8 deduce the amplification factors for the soil-structure system.
7. Evaluate the model parameters for the configurations shown in figure 10.8. A sdof model for the building frame could be made by using the shear beam approximation. This model for the frame can be combined with the sdof model for the soil layer obtained in step 10.2.1.5 above. This leads to the combined soil-structure model shown in figure 10.8b.
8. Predict analytically the response of the frame slab by using coupled and uncoupled analyses as described in section 10.1.2. Compare the analytical predictions with the corresponding experimental observations.

10.2.3 Studies on liquefaction of soil

1. Mount the plywood box containing saturated sand on the shake table as shown in figure 10.4a. Place a brick on the sand surface as shown.
2. Apply harmonic base motion with varying frequencies. At every value of the driving frequency allow the system to vibrate for about 25-30 cycles.
3. When the system is driven at a frequency of about 5 Hz, you would notice that the sand would begin to liquefy and water would start ponding at the surface. This would be accompanied by sinking and toppling of the brick block.

10.3 Report submission

1. Document the experimental observations and the deductions as per the format given in tables10.1-10.9.
2. Develop the mathematical models for the soil layer, building frame and soil-structure system as per simplifications suggested in figure 10.8
3. For the soil layer system, compare the theoretical predictions on the wave amplification with corresponding observations from experiments and comment.
4. For the combined soil-structure system, compare the theoretical predictions using coupled and uncoupled analyses for the two frames with corresponding observations from experiments and comment on
    (e) need for performing coupled analysis, and
    (f) mutual agreement/disagreement between theoretical and experimental results especially in the frequencies around the second mode of the combined system.
5. Respond to the following questions.
    - What are the limitations of the setup shown in figure 10.2a *vis-à-vis* its ability to mimic the soil layer behavior?
    - In the present study we have replaced the soil layer by an equivalent sdof system. Suppose we wish to replace by a 2-dof system. How this can be accomplished?
    - How could the questions of seismic wave amplification, soil-structure interactions and liquefaction be included in seismic design of structures? How are these issues addressed in the IS 1893 code?
    - It is often observed that buildings founded on filled-up land suffer severe damage during major earthquakes. Why is this so?
    - Search the web and obtain information on failure of a building, a dam and a bridge due to earthquake induced liquefaction of soil layer.

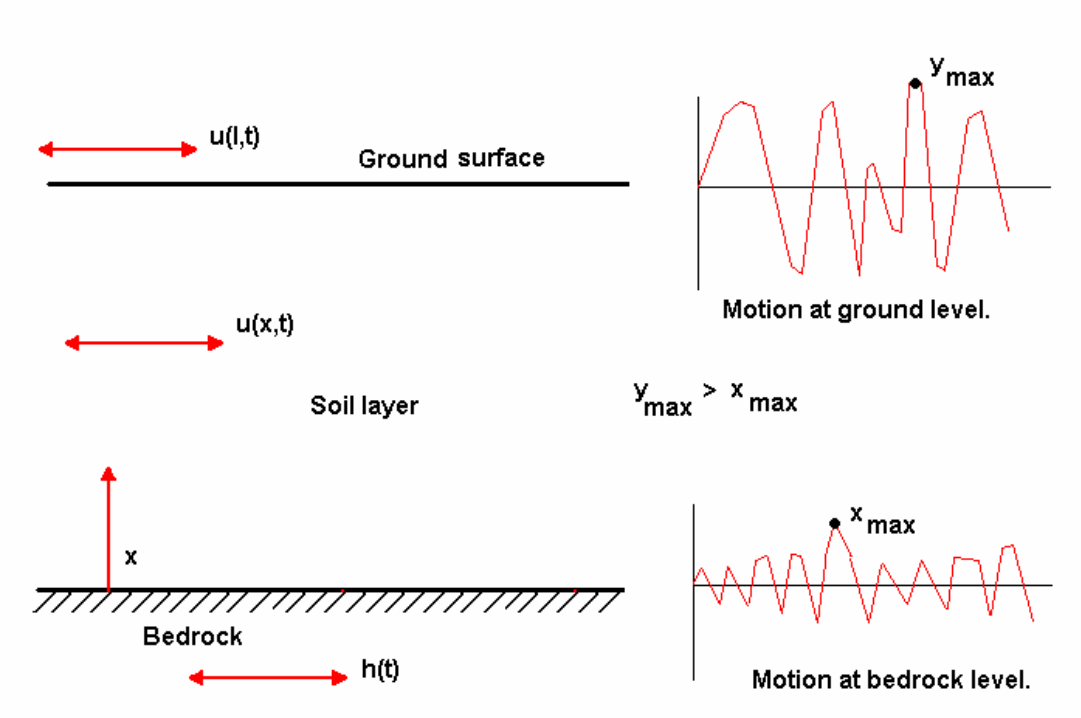

Figure 10.1 Schematic of wave amplification.

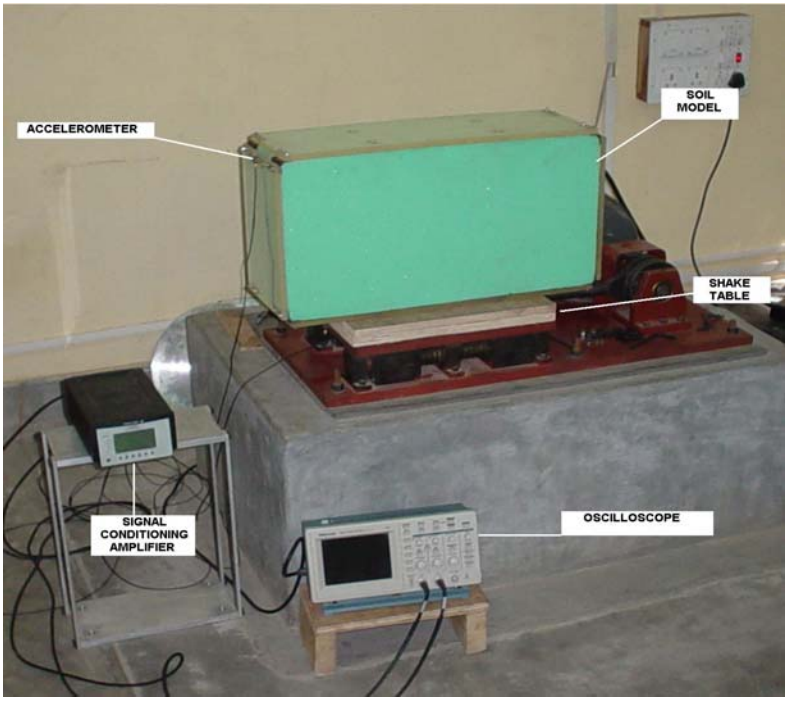

(a)

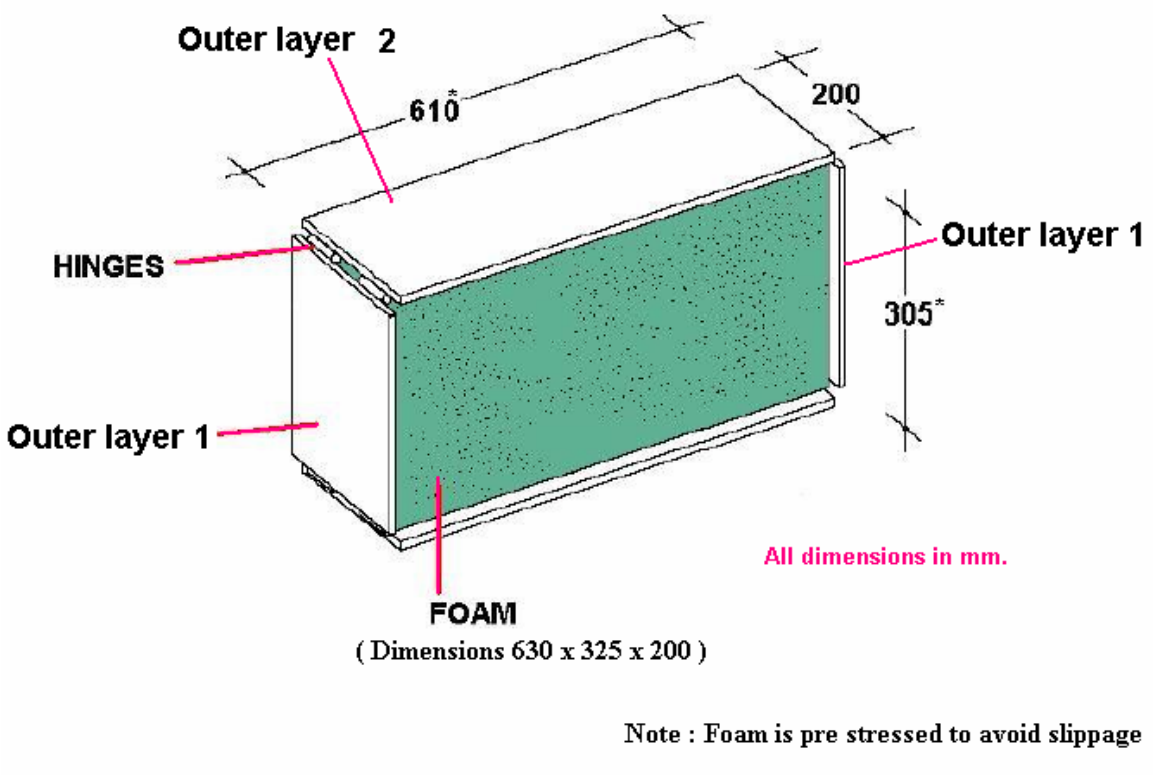

(b)

Figure 10.2 Setup for the study of seismic wave amplification; (a) Details of experimental setup; (b) Details of the shear layer model.

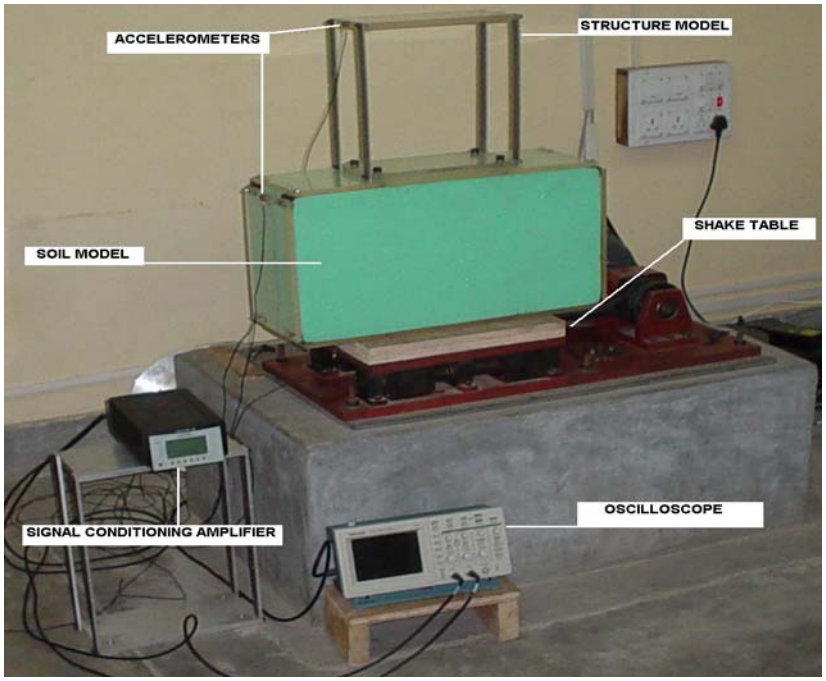

(a)

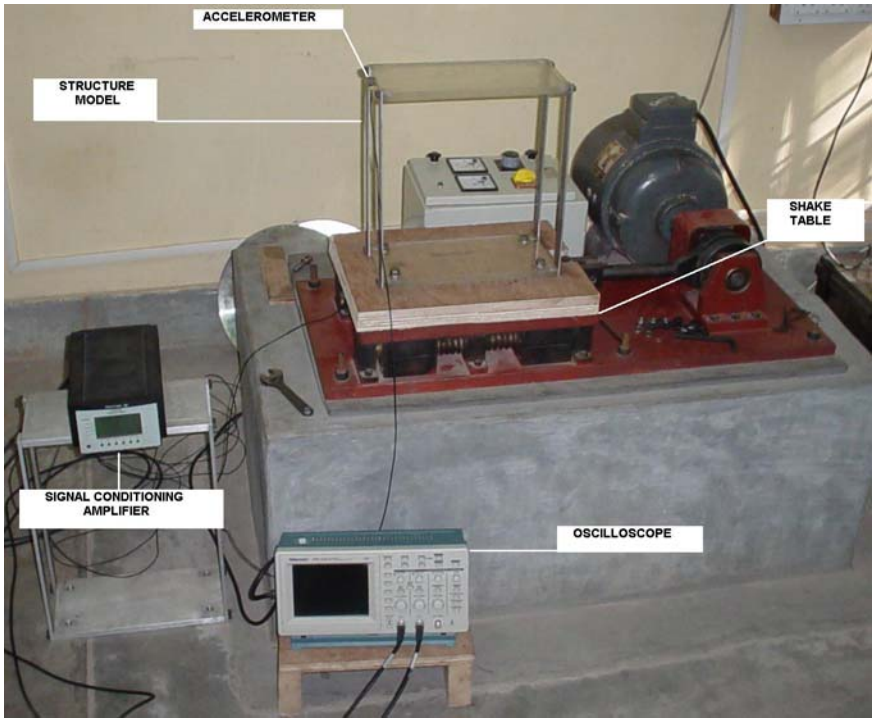

(b)

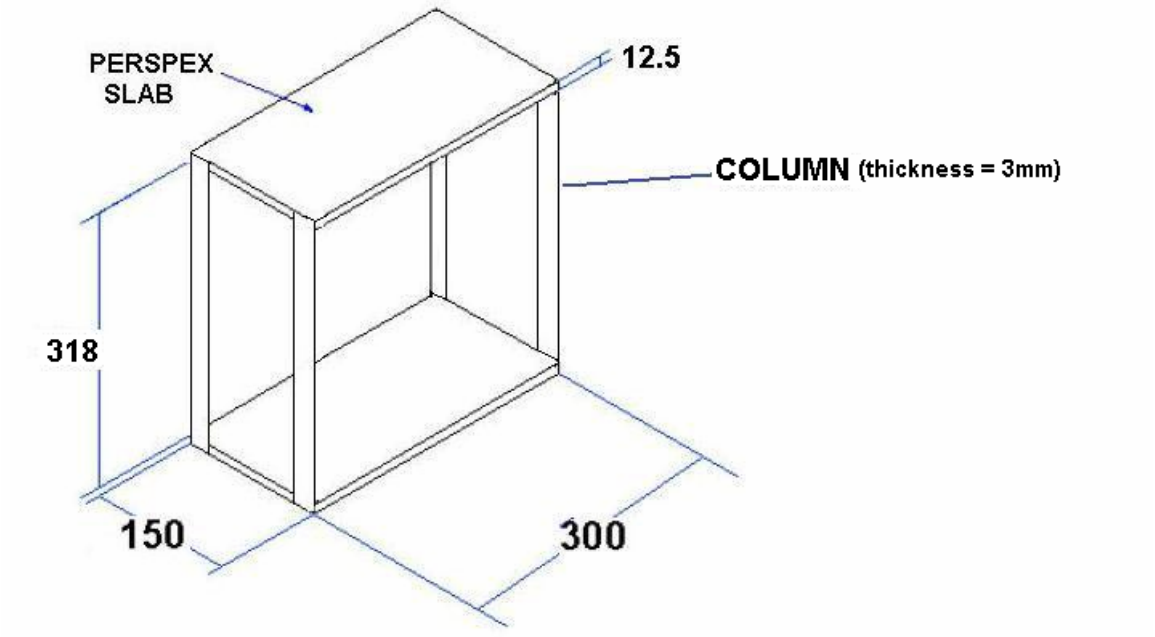

Column	Width (mm)
Aluminum	25

All dimensions in mm

(c)

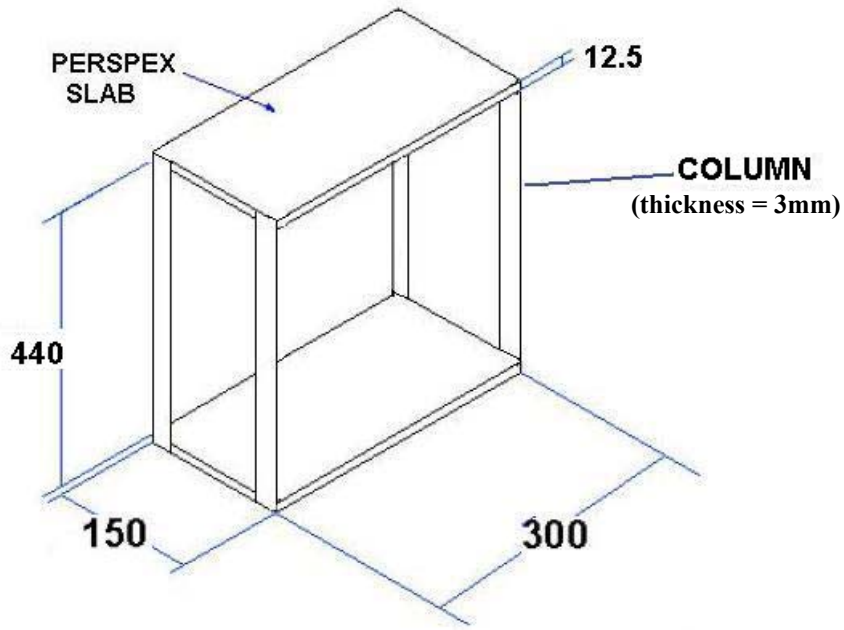

Column	Width (mm)
Aluminum	25

All dimensions in mm

(d)

Figure 10.3 Setup for the study of soil structure interaction (a) Combined shear layer building frame system; (b) Building frame model; (c) Details of the frame model I.
(d) Details of frame model II.

Figure 10.4a Setup for demonstration of phenomenon of liquefaction.

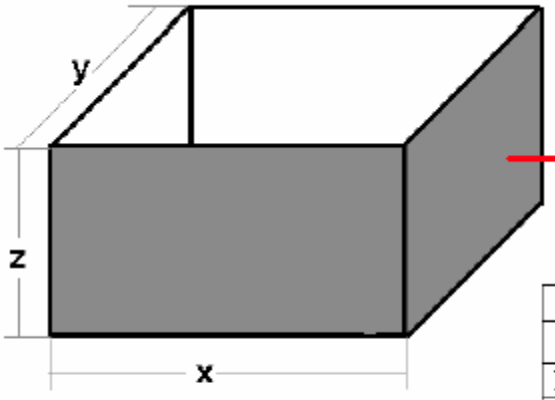

Dimensions		
	Box 1	Box 2
X	540	485
Y	440	380
Z	170	160

All dimensions in mm.
Inner dimensions given. Ply wood thickness = 18.75mm

Figure 10.4b Details of the ply wood box.

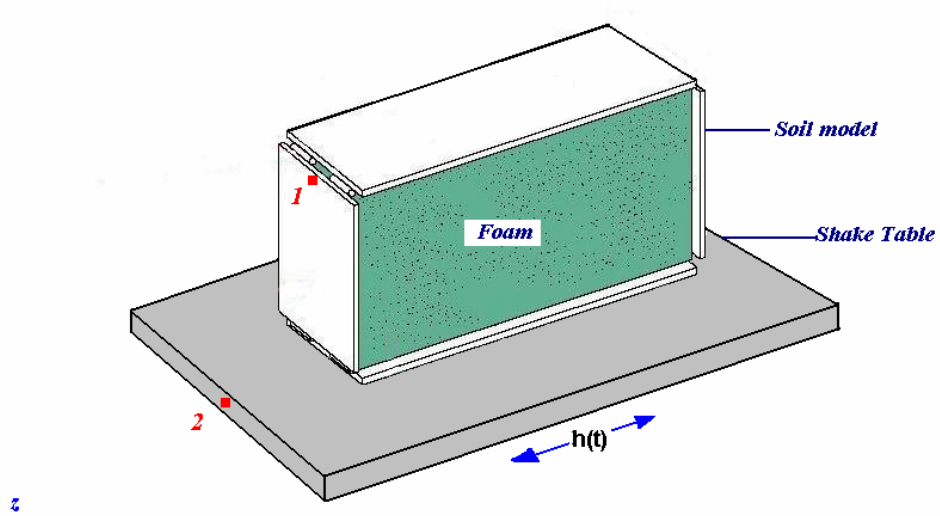

Accelerometers	Notation	Measurement
1	U_T	Response of soil model along X direction
2	H	Base motion along X direction

(a)

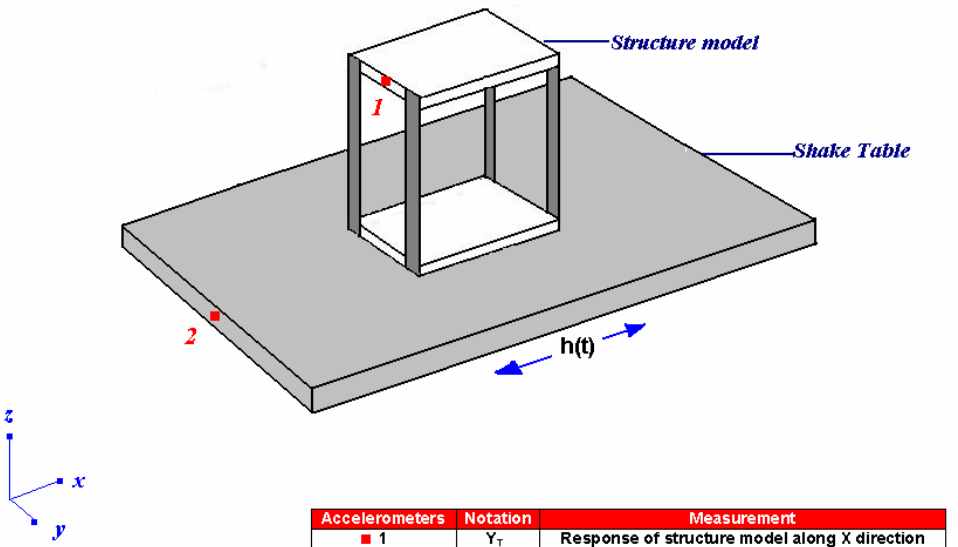

Accelerometers	Notation	Measurement
1	Y_T	Response of structure model along X direction
2	H	Base motion along X direction

(b)

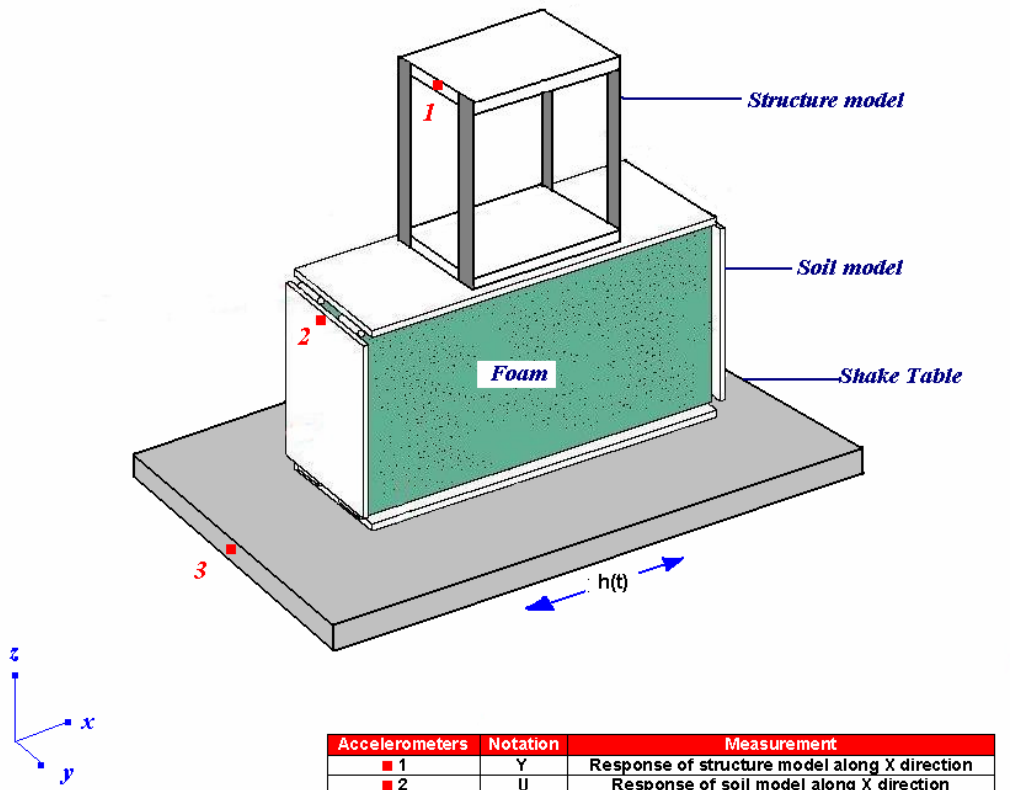

Accelerometers	Notation	Measurement
1	Y	Response of structure model along X direction
2	U	Response of soil model along X direction
3	H	Base motion along X direction

(c)

Fig 10.5 Schematic diagram of experimental setup (a) Soil model subjected to base motion; (b) Structure model subjected to base motion; (c) Soil-structure model subjected to base motion.

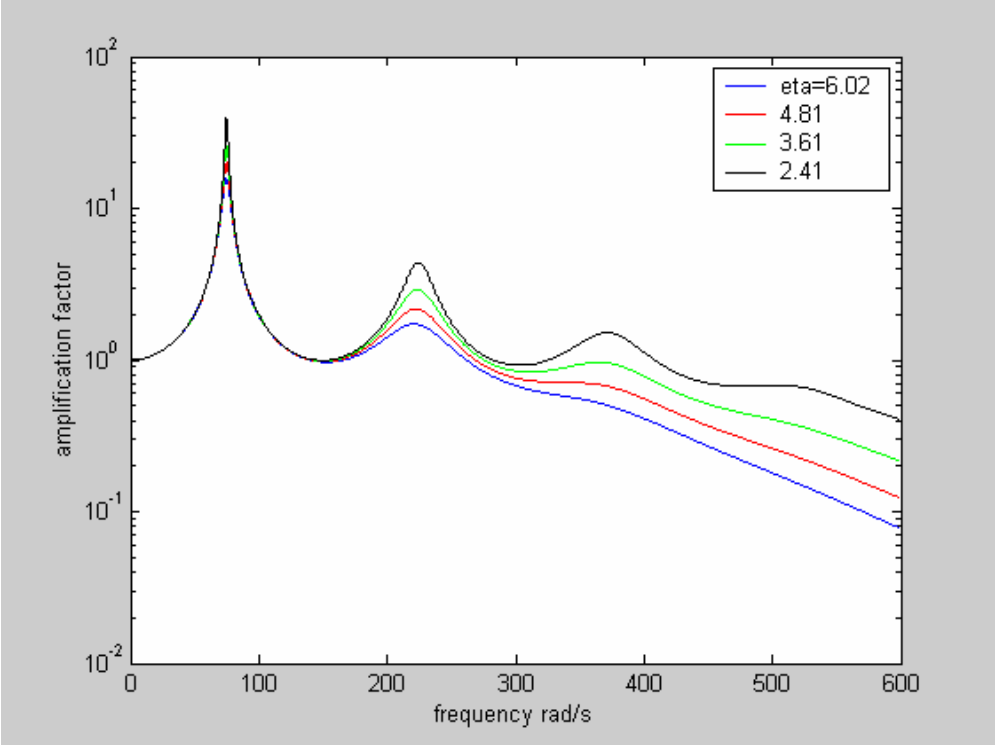

(a)

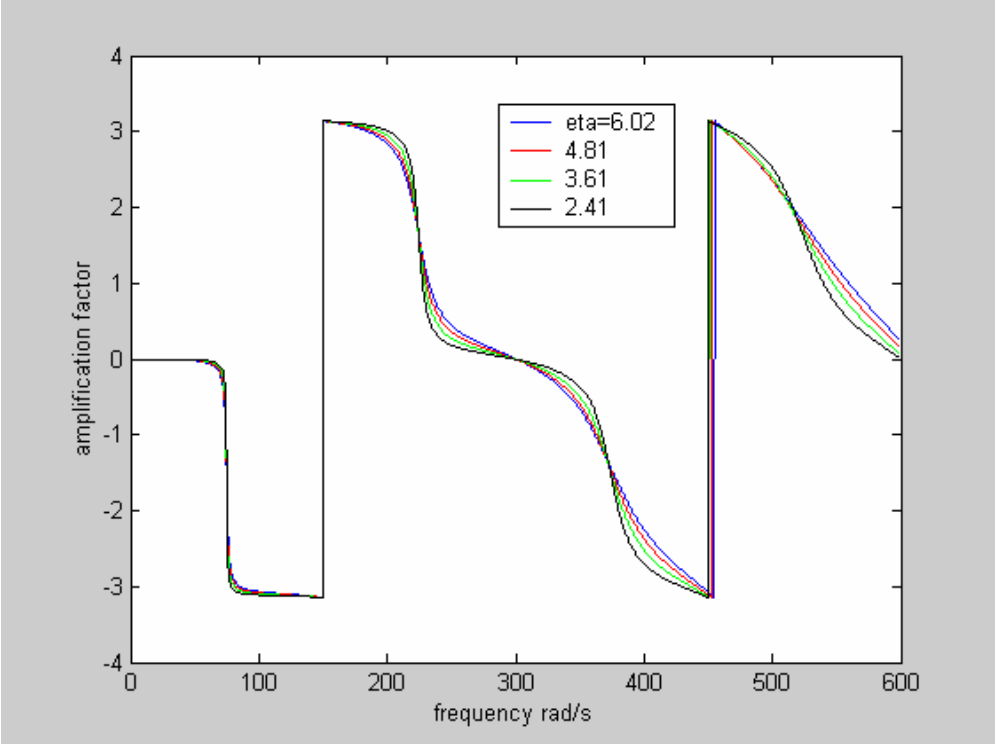

(b)

Figure 10.6 Typical variation of the amplification factor (a) amplitude; (b) phase.

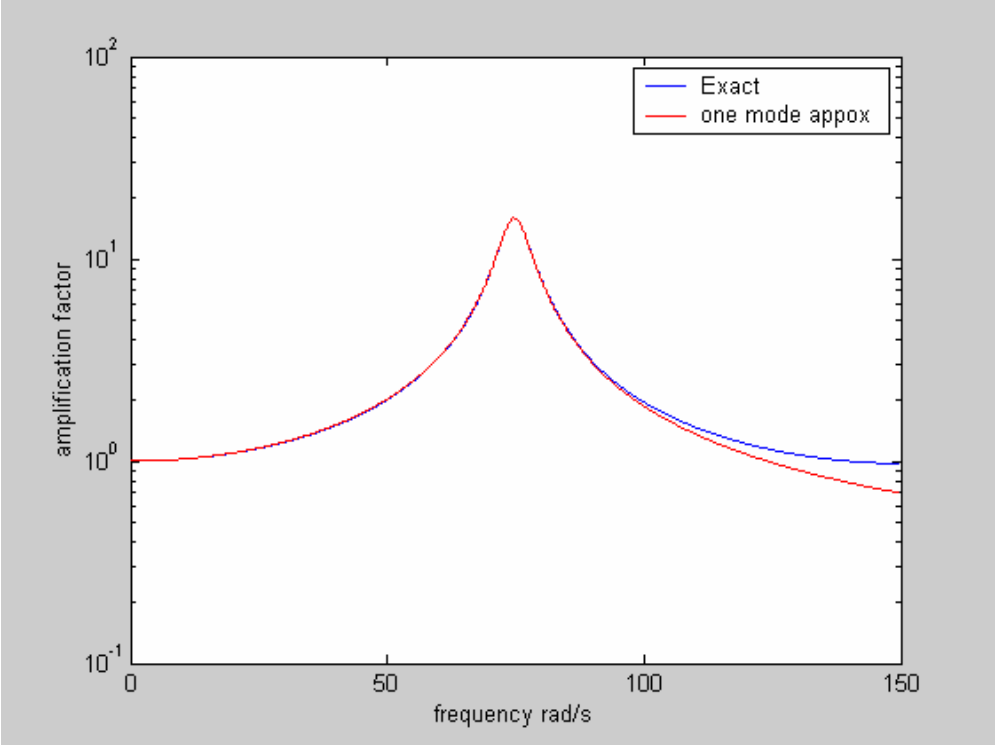

Figure 10.7 Amplification factor obtained using one mode approximation and the exact solution

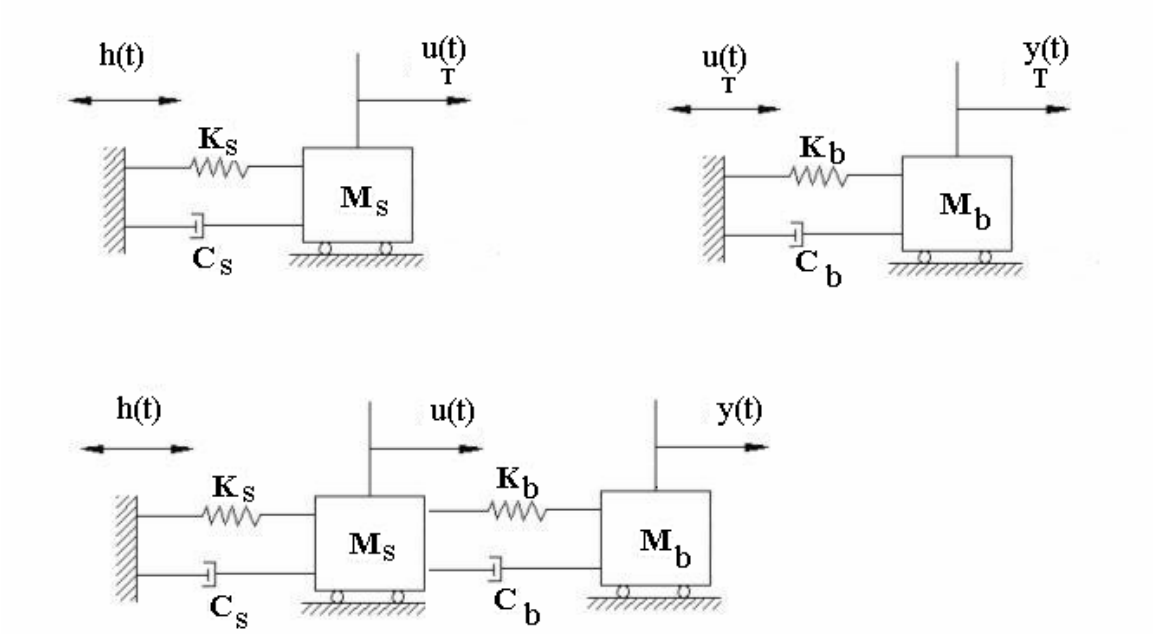

Figure 10.8 Models for soil-structure systems (a) Uncoupled analysis (b) Coupled analysis

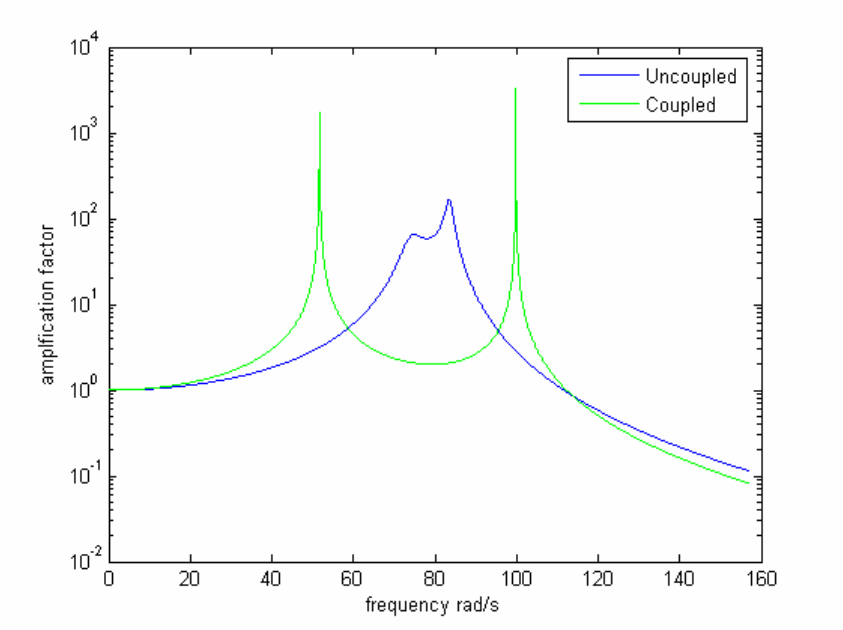

Figure 10.9a Coupled and uncoupled analysis of soil-structure system I.

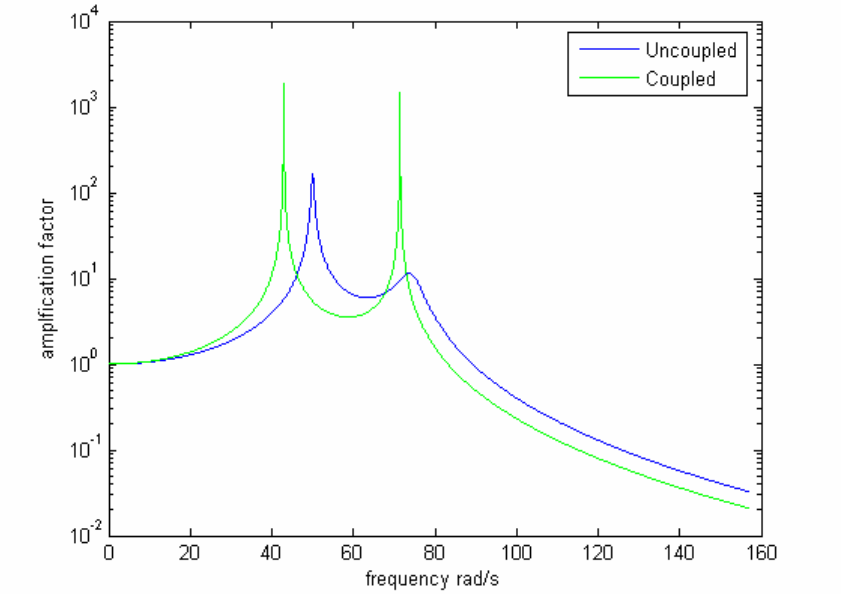

Figure 10.9b Coupled and uncoupled analysis of soil-structure system II.

Figure 10.10 The state of the brick block after liquefaction has occurred; notice the ponding of water at the surface. Figure 10.4a shows the state of the system before the dynamic base motions are applied.

Table 10.1 Equipments used in soil structure interaction

S.No.	Equipments	Quantity
1	Oscilloscope	1
2	Accelerometers	2
3	Transducers conditioning amplifiers	1

Table 10.2 Physical properties of parts of the soil-structure model I and II

Sl. No.	Part		Notations	Material	Quantity (Q)	Mass	Mass density (ρ) Kg/m^3	Young's Modulus (E) N/m^2
1	Structure 1	Column	M_{C1}	Aluminum	4			
		Slab	M_{S1}	Perspex	1			
		Bottom slab	M_{BS1}	Perspex	1			
		Screws	$M_{screws1}$	Mild steel	-		-	
2	Structure 2	Column	M_{C2}	Aluminum	4			
		Slab	M_{S2}	Perspex	1			
		Bottom slab	M_{BS2}	Perspex	1			
		Screws	$M_{screws2}$	Mild steel	-		-	
3	Soil model	Soil	M_F	Foam	1			-
		Outer layer 1	M_{OL1}	Perspex	2			
		Outer layer 2	M_{OL2}	Perspex	1			
		Hinges	M_H	Mild steel	-		-	
4	Assembling Parts	Allen screw	M_{AP1}	Mild steel	-		-	
		Allen nuts	M_{AP2}	Mild steel	-		-	

Table 10.3 Geometric data of the soil-structure models I and II

Sl. No.	Part		Material	Quantity (Q)	Dimensions in mm		
					Depth (D)	Width (B)	Length (L)
1	Structure 1	Column	Aluminum	4			
		Slab	Perspex	1			
		Bottom slab	Perspex	1			
		Screws	Mild steel	-	-	-	-
2	Structure 2	Column	Aluminum	4			
		Slab	Perspex	1			
		Bottom slab	Perspex	1			
		Screws	Mild steel	-	-	-	-
3	Soil model	Soil	Foam	1			
		Outer layer 1	Perspex	2			
		Outer layer 2	Perspex	1			
		Hinges	Mild steel	-	-	-	-
4	Assembling Parts	Allen screw	Mild steel	-	-	-	-
		Allen nuts	Mild steel	-	-	-	-
5	Height of soil model H_S = 0.305m						

Table 10.4 Details of the sensors used

Sl. No.	Sensor	Sensitivity, S		Mass kg
		pC/ms^{-2}	pC/g	
1				
2				
3				

Table 10.5a CASE 1-Free vibration test data on soil-structure model I

S.No.	Quantity	Notation	Observations		
			Soil model	Structure model 1	Soil structure model
1	Amplitude of 0^{th} peak	A_0			
2	Amplitude of n^{th} peak	A_n			
3	Number of cycles	n			
4	Damping ratio	ζ			

Table 10.5b CASE 2- Free vibration test data on soil-structure model II

S.No.	Quantity	Notation	Observations		
			Soil model	Structure model 2	Soil structure model2
1	Amplitude of 0^{th} peak	A_0			
2	Amplitude of n^{th} peak	A_n			
3	Number of cycles	n			
4	Damping ratio	ζ			

Table 10.6a Base motion test data on single-story shear building frame1

Sl.no.	Frequency (Hz)	Structure model Amplitude σ_1 rms (mV)	Conversion Factor CF (V/m)	Structure model displacement $Y_T = \sqrt{2}$ (CF) σ_1 (m)	Ratio Of Y_T / H
1					
2					
3					
4					
5					
6					
7					
8					
9					
10					
11					
12					
13					
14					
15					
16					
17					
18					
19					
20					
21					
22					
23					
24					
25					

Where ‘H’ is the base motion displacement =

Table 10.6b Base motion test data on single-story shear building frame II

Sl.no.	Frequency (Hz)	Structure model Amplitude σ_1 rms (mV)	Conversion Factor CF (V/m)	Structure model displacement $Y_T = \sqrt{2}$ (CF) σ_1 (m)	Ratio Of Y_T / H
1					
2					
3					
4					
5					

6					
7					
8					
9					
10					
11					
12					
13					
14					
15					
16					
17					
18					
19					
20					
21					
22					
23					
24					
25					

Table 10.7 Base motion test data on soil model

Sl.no.	Frequency (Hz)	Soil model Amplitude σ_1 rms (mV)	Conversion Factor CF (V/m)	Soil model displacement $U_T = \sqrt{2}$ (CF) σ_1 (m)	Ratio Of U_T / H
1					
2					
3					
4					
5					
6					
7					
8					
9					
10					
11					
12					
13					
14					
15					
16					
17					
18					

19					
20					
21					
22					
23					
24					
25					

Where 'H' is the base motion displacement =

Table 10.8a Base motion test data on soil-structure model I

Sl. No.	Frequency (Hz)	Structure model Amplitude σ_1 rms (mV)	Conversion Factor CF(V/m)	Soil model Amplitude σ_2 rms (mV)	Conversion Factor CF(V/m)	Structure model displacement $Y=\sqrt{2}$ (CF) σ_1 (m)	Soil model displacement $U=\sqrt{2}$ (CF) σ_2 (m)	Ratio Of Y/H	Ratio Of U/H
1									
2									
3									
4									
5									
6									
7									
8									
9									
10									
11									
12									
13									
14									
15									
16									
17									
18									
19									
20									
21									
22									
23									
24									
25									

Where 'H' is the base motion displacement

Table10.8b Base motion test data on soil-structure model II

Sl. No.	Frequency (Hz)	Structure model Amplitude σ_1 rms (mV)	Conversion Factor CF(V/m)	Soil model Amplitude σ_2 rms (mV)	Conversion Factor CF(V/m)	Structure model displacement $Y=\sqrt{2}$ (CF) σ_1 (m)	Soil model displacement $U=\sqrt{2}$ (CF) σ_2 (m)	Ratio Of Y/H	Ratio Of U/H
1									
2									
3									
4									
5									
6									
7									
8									
9									
10									
11									
12									
13									
14									
15									
16									
17									
18									
19									
20									
21									
22									
23									
24									
25									

Table 10.9a Case 1 Estimate of the natural frequencies of soil-structure model I.

Mode No.	Natural frequencies in Hz					
	Structure model I		Soil model		Soil-structure model I	
	Theory	Experiment	Theory	Experiment	Theory	Experiment
1						
2	-	-	-	-		

Table 10.9b Case 2 Estimate of the natural frequencies of soil-structure model II.

Mode No.	Natural frequencies in Hz					
	Structure model II		Soil model		Soil-structure model II	
	Theory	Experiment	Theory	Experiment	Theory	Experiment
1						
2	-	-	-	-		

Appendix A

Analysis of linear multi-degree of freedom vibrating systems

A.1 The search for a benign coordinate system

The generic form of equation of motion of externally driven linear multi-degree of freedom (mdof) vibrating systems with viscous damping model is given by

$$M\ddot{x} + C\dot{x} + Kx = f(t)$$
$$x(0) = x_0; \dot{x}(0) = \dot{x}_0$$

…(A.1)

Here *M, C* and *K* are, respectively, the mass, damping and stiffness matrices of size $n \times n$; $x, \dot{x}$ & $\ddot{x}$, are respectively, the displacement, velocity and acceleration vectors of size $n \times 1$; *f(t)* is the $n \times 1$ external forcing vector; and, x_0 & $\dot{x}_0$ are, respectively, the initial displacement and velocity vectors of size $n \times 1$. We take in this discussion that the structural matrices *M, C* and *K* are all symmetric. This equation represents the condition of equilibrium of the system. The equation of motion, for a given system, is not unique and it depends upon the coordinate system in which the analyst chooses to represent the dofs. This would mean that we can assume that the equation of motion has been formulated in a coordinate system that appeals to the analyst.

It may be noted that while dealing with static problems, the choice of coordinate system is often dictated by geometry of structure and applied loads. Thus, in the analysis of a circular plate under axi-symmetric loads, it would be most convenient to formulate the problem in cylindrical coordinate system; similarly, for a rectangular plate, the problem is easy to handle in Cartesian coordinate system. Of course, the use of polar coordinates for a rectangular plate or Cartesian coordinate system for a circular plate in itself is perfectly admissible: but then, we would be complicating the formulation unnecessarily. The response variables in such cases would get *coupled* with the details of this coupling governed by the choice of coordinate system used. While this issue is somewhat simple to understand in a static problem, in a dynamic problem, however, the coupling between dofs occurs in a much more subtle manner. For instance, even when we use polar cylindrical coordinates for the vibration analysis a circular plate, the equations of motion governing various dofs get mutually coupled! This coupling itself would be manifest in one or more of the structural matrices, namely, *M, C* or *K,* being *non-diagonal*. Now, if one were to introduce a new coordinate system, defined through the transformation $x = \Phi z$, where, $\Phi =$ an $n \times n$ matrix and z is the $n \times 1$ vector representing the new dofs, the structural matrices in the new coordinate system would be different from *M, C* and *K*. To see this, we can write the equation of motion in the *z*-coordinate system as

$$M\Phi\ddot{z} + C\Phi\dot{z} + K\Phi z = f(t)$$
$$x(0) = \Phi z(0); \dot{x}(0) = \Phi\dot{z}(0)$$

…(A.2)

By pre-multiplying by Φ^t one gets

$$\Phi^t M\Phi\ddot{z} + \Phi^t C\Phi\dot{z} + \Phi^t K\Phi z = \Phi^t f(t)$$
$$z(0) = \Phi^{-1}x(0); \dot{z}(0) = \Phi^{-1}\dot{x}(0)$$

…(A.3)

One can now think that the matrices $\overline{M} = \Phi^t M\Phi, \overline{C} = \Phi^t C\Phi, \& \overline{K} = \Phi^t K\Phi$ can be thought of the structural matrices in the new z-coordinate system. Clearly these matrices depend upon the definition of the coordinate transformation matrix Φ. If one or more of the matrices *M, C* and *K* are non-diagonal, it may be expected that one or more of the matrices $\overline{M}, \overline{C}$, or $\overline{K}$ would also be non-diagonal, *unless,* we choose the transformation matrix Φ intelligently! For a moment, let us imagine that we have indeed found out a magic Φ that makes all the three matrices $\overline{M}, \overline{C}$, and $\overline{K}$ diagonal. The upshot of this would be that, the equation of motion in the new z-coordinate system would get mutually uncoupled. That is, a *n*-dof system simply becomes a collection of *n* mutually uncoupled sdof systems. From the point of view of solving equation A.1, this is a major simplification. Therefore, it makes perfect sense to seek the transformation matrix Φ that uncouples the equation of motion. Indeed, the search for this coordinate system is a major theme is the subject of structural dynamics.

A.2 The modal matrix and orthogonality

We begin the search for the coordinate system by considering a seemingly unrelated problem of undamped free vibration analysis. The governing equation of motion here is given by

$$M\ddot{x} + Kx = 0$$

…(A.4)

Furthermore, we seek a special solution to this problem in the form

$$x = \phi \exp(i\omega t)$$

…(A.5)

Here ω is an unknown scalar quantity and ϕ is a $n \times 1$ vector. By substituting this solution in equation A.4, we get

$$K\phi = \omega^2 M\phi$$

…(A.6)

Clearly, $\phi = 0$ is a valid solution but we are not interested in this trivial solution since it does not teach us anything about the system under study. At this stage it is to be remembered that ω is an unknown still to be determined. Therefore, we are lead to the question: can we find ω for which $\phi \neq 0$ is a possible solution to equation A.6? This would mean that equation A.6 represents an algebraic eigenvalue problem. As is well known, the condition for non-trivial solution for A.6 is that

$$\left|K - \omega^2 M\right| = 0$$

…(A.7)

By noting that K and M are real valued, symmetric, and are associated, respectively, with potential and kinetic energies, which are, themselves, non-negative, the roots of the above equation would be real valued and nonnegative. Thus we could arrange all the eigenvalues in an ascending order as

$$\omega_1^2 \le \omega_2^2 \le \cdots \le \omega_n^2$$

…(A.8)

with the associated eigenvectors designated by $\{\phi_i\}_{i=1}^n$. Furthermore we could assemble all the eigenvectors in a single $n \times n$ matrix as

$$\Phi = \begin{bmatrix} \phi_1 & \phi_2 & \cdots & \phi_n \end{bmatrix}$$

…(A.9)

This matrix is termed as the modal matrix and it possesses special properties known as orthogonality properties. To see this we write equation of motion A.6 for two different values of eigenvalues as

$$K\phi_r = \omega_r^2 M\phi_r$$
$$K\phi_s = \omega_s^2 M\phi_s$$

…(A.10, A.11)

We pre-multiply the first of the above equations by ϕ_s^t and the second by ϕ_r^t to get

$$\phi_s^t K\phi_r = \omega_r^2 \phi_s^t M\phi_r$$
$$\phi_r^t K\phi_s = \omega_s^2 \phi_r^t M\phi_s$$

…(A.12, A.13)

Transposing both sides of equation A.13, and noting that $K = K^t$ & $M = M^t$, we get

$$\phi_s^t K\phi_r = \omega_s^2 \phi_s^t M\phi_r$$

…(A.14)

Now, subtracting equation A.12 from equation A.14, we get

$$\left(\omega_r^2 - \omega_s^2\right)\phi_s^t M\phi_r = 0$$

…(A.15)

Thus, for $r \ne s$, if $\omega_r^2 \ne \omega_s^2$, it follows that

$$\phi_s^t M\phi_r = 0 \; if \; r \ne s.$$

…(A.16)

From equation A.12, it would also follow that,

$$\phi_s^t K\phi_r = 0 \; if \; r \ne s.$$

…(A.17)

Equations A.16 and A.17 are true for all $r, s = 1,2,\cdots n$. This fact can be succinctly stated by saying that the matrices $\overline{K} = \Phi^t K \Phi \,\&\, \overline{M} = \Phi^t M \Phi$ are both diagonal. We say that the modal matrix Φ is orthogonal with respect to the mass and stiffness matrices. In fact, our search for the transformation matrix that simultaneously *diagonalizes* both *M* and *K* matrices is over! This matrix is indeed the modal matrix Φ.

It may be recalled that the eigenvectors associated with equation A.6 are not unique, in the sense that, if ϕ is a eigenvector, a constant multiplier of ϕ, namely, $\alpha\phi$, is also an eigenvector. It is a common practice to scale the eigenvectors such that the matrix $\Phi^t M \Phi$ becomes an identity matrix. In this case we get

$$\Phi^t M \Phi = I \;\&\; \Phi^t K \Phi = Diag\left[\omega_i^2\right]$$

…(A.18)

When the modal matrix has been made unique by scaling the eigenvectors as above, we say that the modal matrix has been mass normalized and we call these scaled eigenvectors as normal modes. The quantity ω_i is called the i^{th} natural frequency of the system. It follows that an *n*-dof system would possess *n* natural frequencies and *n* normal modes.

A.3 Undamped forced response analysis

We now consider a slightly modified version of equation A.1, namely,

$$M\ddot{x} + Kx = f(t)$$
$$x(0) = x_0 ; \dot{x}(0) = \dot{x}_0$$

…(A.19)

We begin by performing the free vibration analysis, as outlined in the previous section, and obtain the natural frequencies $\omega_i, i = 1,2,\cdots n,$ and the mass normalized modal matrix Φ. Next, we introduce the transformation, $x = \Phi z$, and derive the equation of motion in the new coordinate system as (see equation A.3)

$$\Phi^t M \Phi \ddot{z} + \Phi^t K \Phi z = \Phi^t f = F(t)$$

…(A.20)

By the virtue of orthogonality property of the modal matrix (equation A.18) it turns out that the generalized mass and stiffness matrices, $\overline{M} = \Phi^t M \Phi$, & $\overline{K} = \Phi^t K \Phi$ are both diagonal. If the modal matrix is normalized as in equation A.18, it follows that, equation A.20 is equivalent to a set of n *sdof* systems

$$\ddot{z}_i + \omega_i^2 z_i = F_i(t); i = 1,2,\cdots, n.$$

…(A.21)

Solution of these set of equations is order of magnitude simpler than solution of equation A.19. In fact, this indeed, is the advantage of introducing the transformation $x = \Phi z$. To

solve equation A.19 we would need the initial conditions in the new z-coordinate system. These can be determined by noting that

$$x(0) = \Phi z(0)$$
$$\Rightarrow \Phi^t M x(0) = \Phi^t M \Phi z(0)$$

…(A.22)

This would mean that

$$z(0) = \Phi^t M x(0) \;\&\; \dot{z}(0) = \Phi^t M \dot{x}(0)$$

…(A.23)

It may be noted that the above method for finding the initial conditions avoids the need to invert the modal matrix Φ.

A.4 Introduction of damping: will the modal matrix Φ also diagonalize C?

Now we consider the equation of motion A.1 and proceed with the transformation $x = \Phi z$. This would lead to the equation of motion

$$\Phi^t M \Phi \ddot{z} + \Phi^t C \Phi \dot{z} + \Phi^t K \Phi z = \Phi^t f = F(t)$$

…(A.24)

While we have shown that the matrices $\overline{M} = \Phi^t M \Phi$, & $\overline{K} = \Phi^t K \Phi$ are diagonal, there is no such property associated with the matrix $\Phi^t C \Phi$. This would mean that, even after transforming equation A.1 into the new form (A.24), the coordinates continue to be mutually coupled with the coupling taking place through the new non-diagonal damping matrix $\overline{C} = \Phi^t C \Phi$. Thus the effort expended in determining the undamped natural frequencies and mode shapes is wasted. This disappointment could be avoided if we demand that the damping matrix C be such that $\overline{C} = \Phi^t C \Phi$ is diagonal! If the damping matrix C indeed satisfies this condition, we say that the system is *classically* damped. For such systems, equation A.24 becomes equivalent to a set of uncoupled, damped sdof systems, given by

$$\ddot{z}_i + 2\eta_i \omega_i \dot{z}_i + \omega_i^2 z_i = F_i(t); i = 1,2,\cdots,n$$

…(A.25)

with initial conditions given as before by equation A.23. The quantity η_i is called the i^{th} modal damping constant. One of the popular models for classical damping is known as the Rayleigh damping model. Here one assumes that the damping matrix is linearly *proportional* to the mass and stiffness matrices as

$$C = \alpha M + \beta K$$

…(A.26)

Here α & β are scalar constants to be experimentally determined. In this case, it turns out that

$$2\eta_i\omega_i = \alpha + \beta\omega_i^2$$
$$\Rightarrow \eta_i = \frac{\alpha}{2\omega_i} + \frac{\beta\omega_i}{2}$$

…(A.27)

Thus, in an experimental determination of α & β, one could determine modal damping ratios η_i for at least two modes and use them in setting up two equations for the unknowns α & β. This implies that, with Rayleigh's damping model, we can specify damping ratio for only two modes and for all other modes, the damping ratios get automatically specified in terms of α & β. It is to be noted that classical damping matrices that are more general than the Rayleigh's damping model exists that permit specification of modal damping values for any set of $r \le n$ modes.

A.5 Classical damping matrix in terms of modal damping values

Here we consider the problem of determining the damping matrix C given $\eta_i, i = 1,2,\cdots,n.$ A direct approach to solve this problem is to note that,

$$diag[2\eta_i\omega_i] = \Phi^t C \Phi$$

…(A.28)

and get

$$C = \left[\Phi^t\right]^{-1} diag[2\eta_i\omega_i]\Phi^{-1}$$

…(A.29)

This way of finding C thus involves inverting the modal matrix and its transpose and, therefore, appears to be very inefficient from a computational perspective. To remedy this situation we note that

$$\Phi^t M \Phi = I$$
$$\Rightarrow \left[\Phi^t\right]^{-1}\Phi^t M\Phi = \left[\Phi^t\right]^{-1}$$
$$\Rightarrow \left[\Phi^t\right]^{-1} = M\Phi$$

…(A.30)

Similarly, it follows that

$$\Phi^{-1} = \Phi^t M$$

…(A.31)

Combining equations A.30 and A.31 with A.29 we get

$$C = M\Phi diag[2\eta_i\omega_i]\Phi^t M$$

…(A.32)

Clearly, this equation does not involve the inversion of modal matrix and its transpose.

A.6 Solution of equation A.1 without coordinate transformation

It is possible to solve equation A.1 without having to uncouple the equation of motion. For instance, one could use numerical integration procedures such as Runge-Kutta methods or the predictor-corrector methods to achieve this. Alternatively, one could use integral transform techniques, such as, Laplace transforms, to solve the problem. For the special case in which the excitation is harmonic, that is, $f(t) = f_0 \exp(i\lambda t)$, and, interest is focused on steady state behavior, it can be noted that solution of equation A.1 can be sought in the form

$$x(t) = X \exp(i\lambda t) \qquad \ldots(A.33)$$

Here X is the unknown vector of amplitude of response to be determined. Substituting this in equation A.1, one gets,

$$[-\lambda^2 M + i\lambda C + K]X = f_0$$
$$\Rightarrow X = \left[-\lambda^2 M + i\lambda C + K\right]^{-1} f_0 \qquad \ldots(A.34)$$

The matrix $D(\lambda) = -\lambda^2 M + i\lambda C + K$ can be called as the dynamic stiffness matrix. This matrix is a complex valued symmetric matrix that is dependent upon the driving frequency λ.